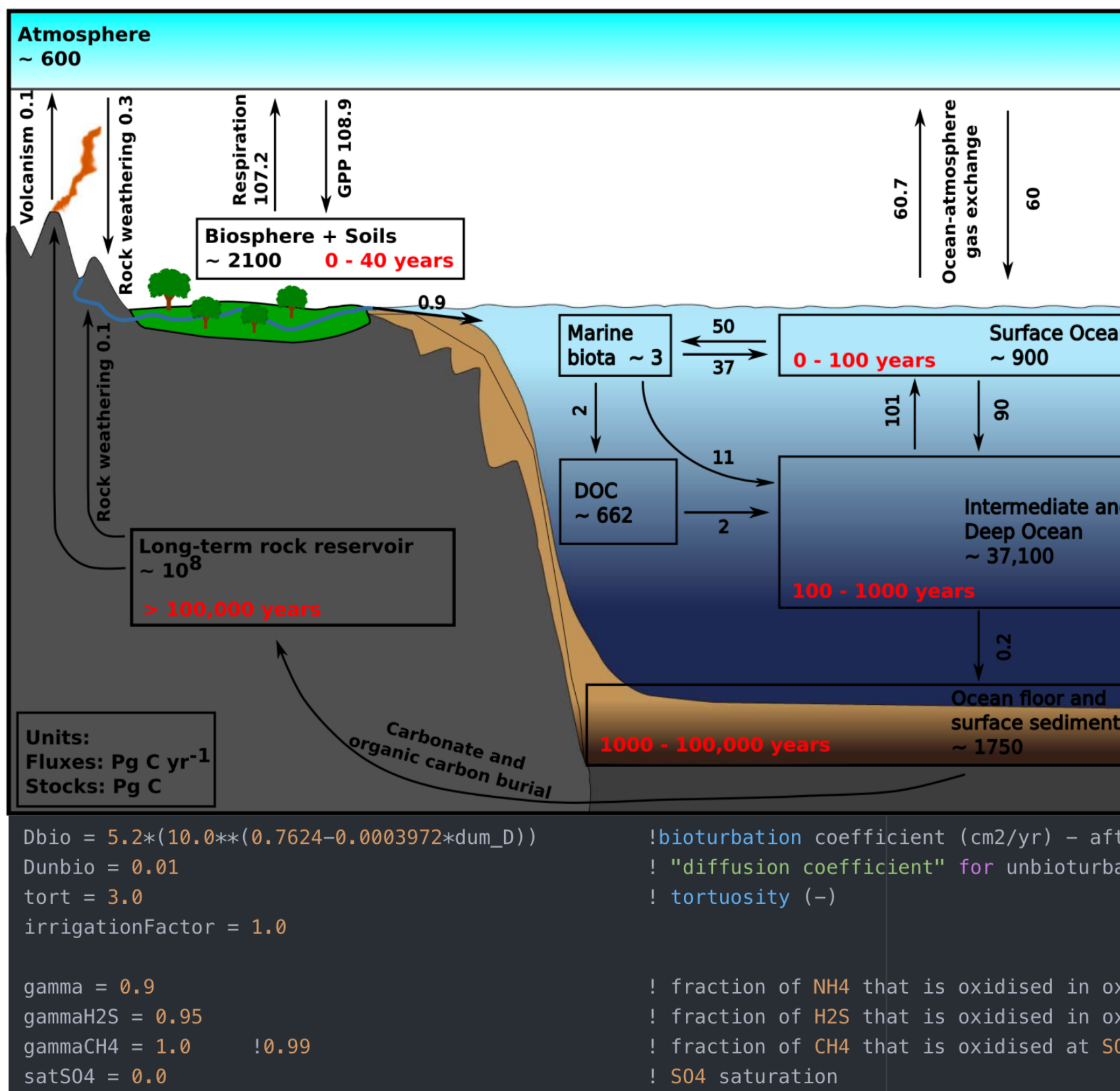
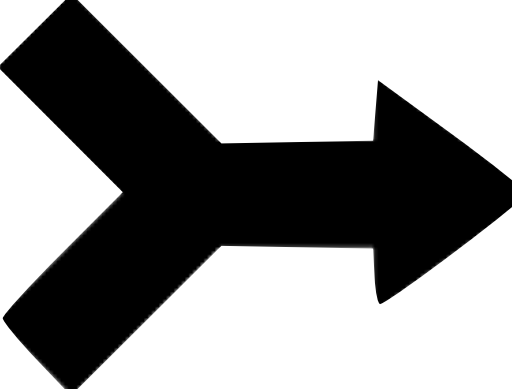


COSMOS: Curation Of Scientific MOdels of the Earth system from publications

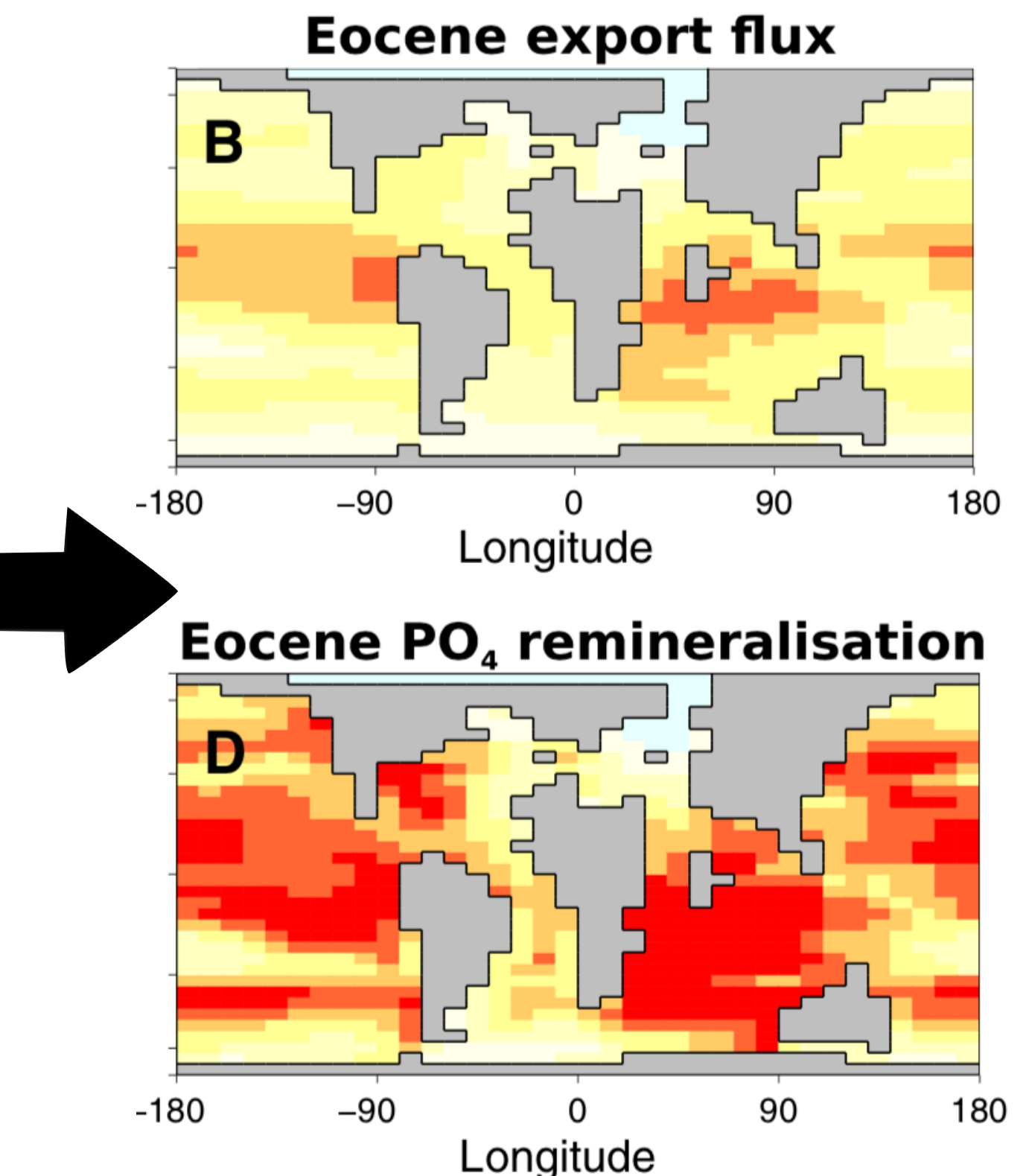
Theo Rekatsinas, Shanan Peters, Miron Livny
University of Wisconsin-Madison

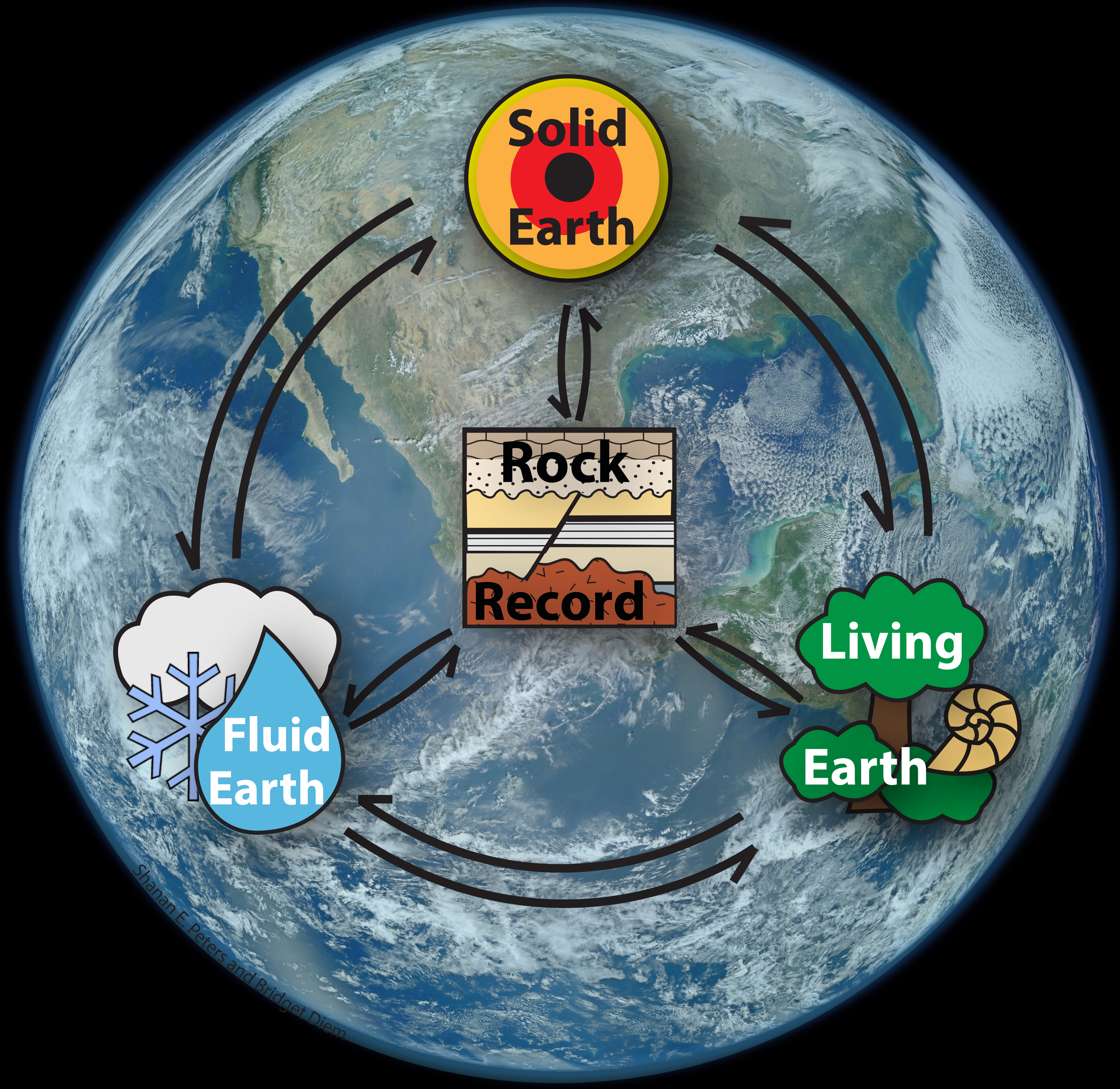
$$F_{\text{CaCO}_3} = F_{\text{CaCO}_3,0} \left(1 + k_{\text{Ca}} (T - T_0)\right) \frac{R}{R_0} \frac{P}{P_0}$$

$$F_{\text{CaSiO}_3} = F_{\text{CaSiO}_3,0} e^{\frac{1000E_a}{RT_0}(T-T_0)} \left(\frac{R}{R_0}\right)^{\beta} \frac{P}{P_0}$$

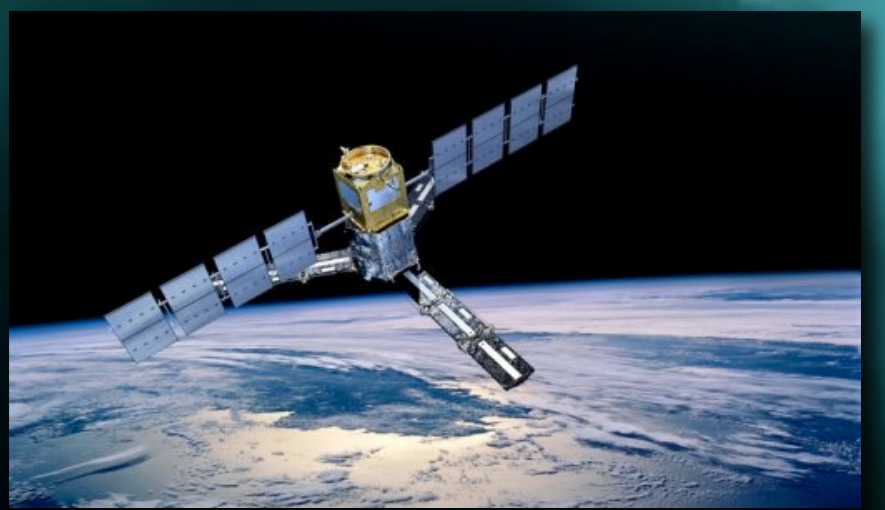
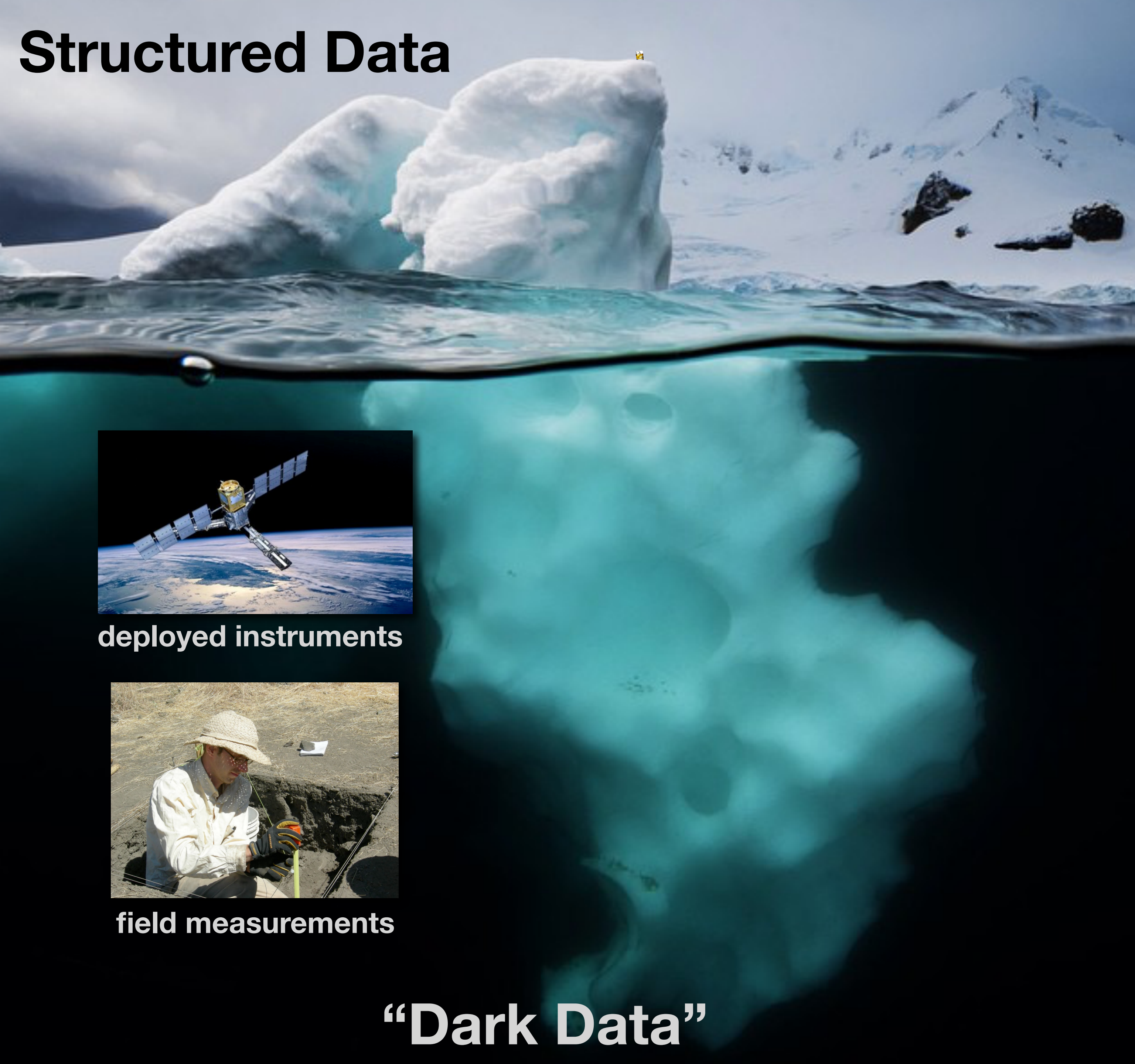


GENIE:
Grid ENabled Integrated Earth system model





Structured Data



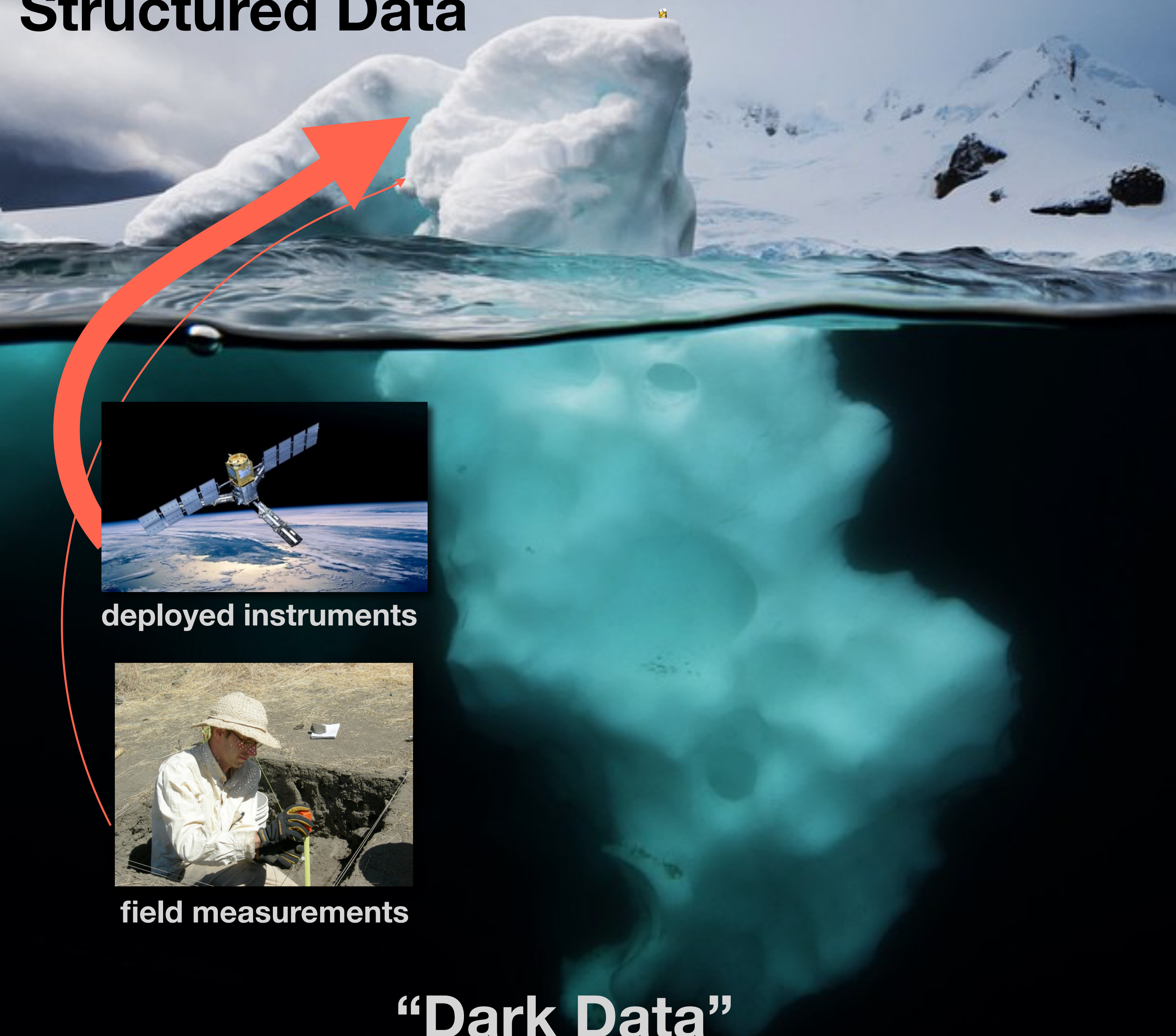
deployed instruments



field measurements

“Dark Data”

Structured Data



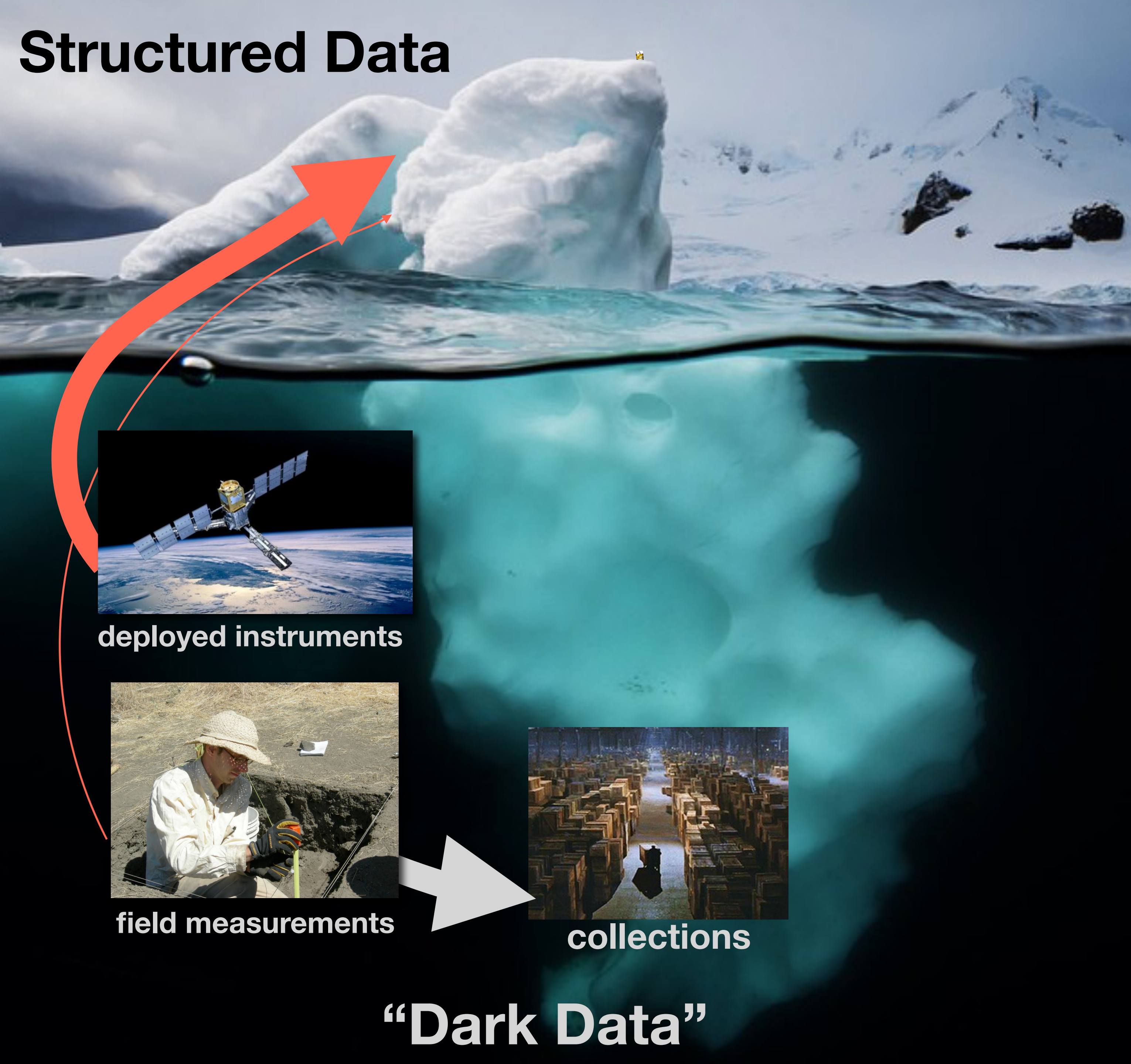
deployed instruments



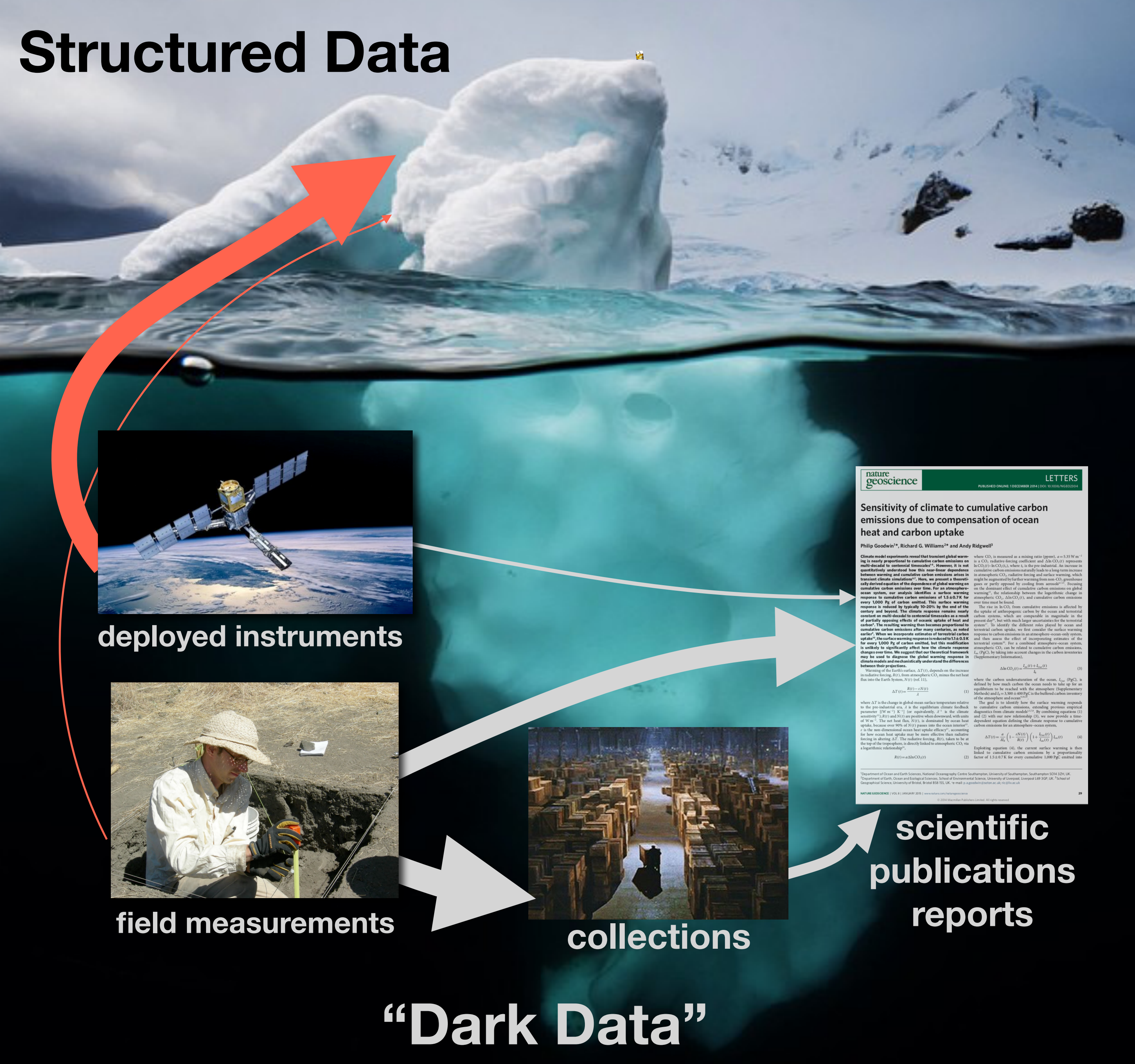
field measurements

“Dark Data”

Structured Data



Structured Data



Structured Data



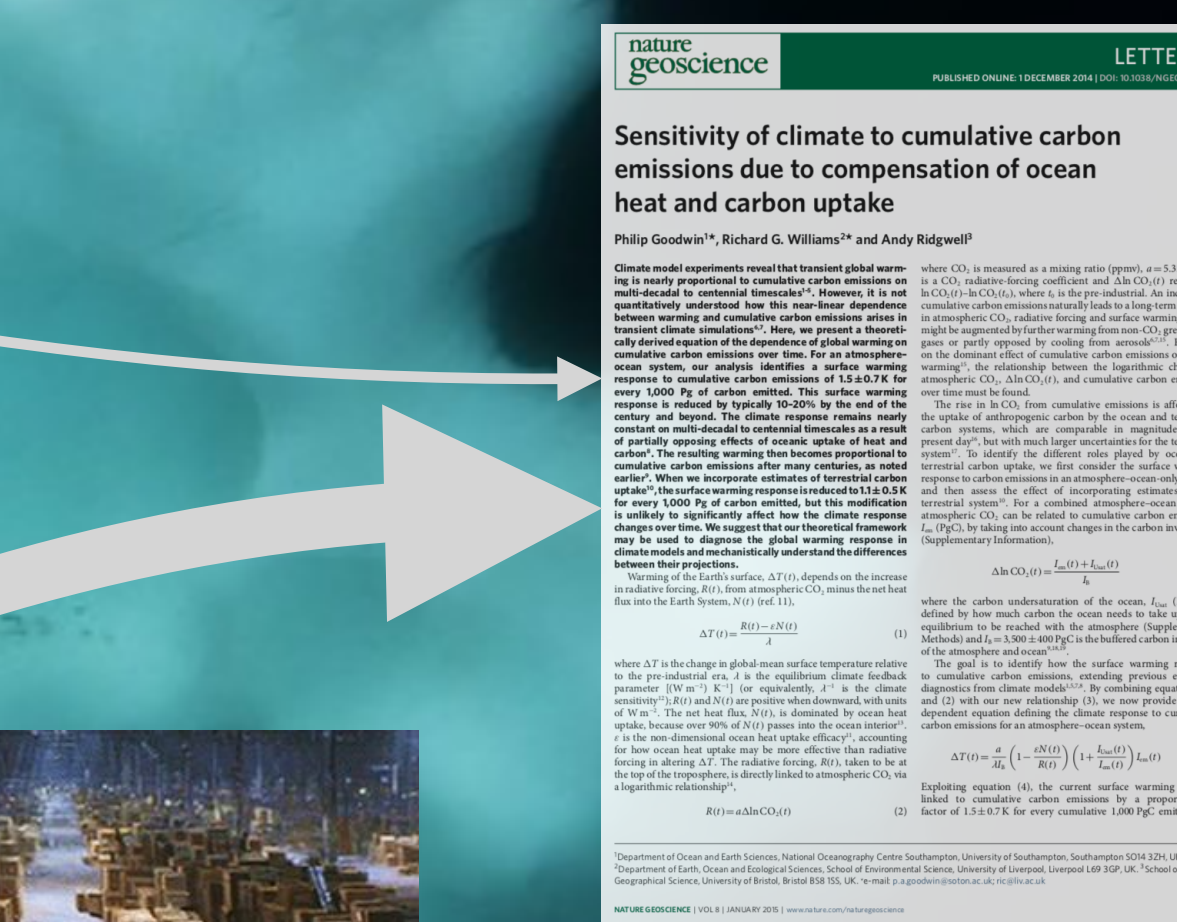
deployed instruments



field measurements



collections



scientific publications
reports

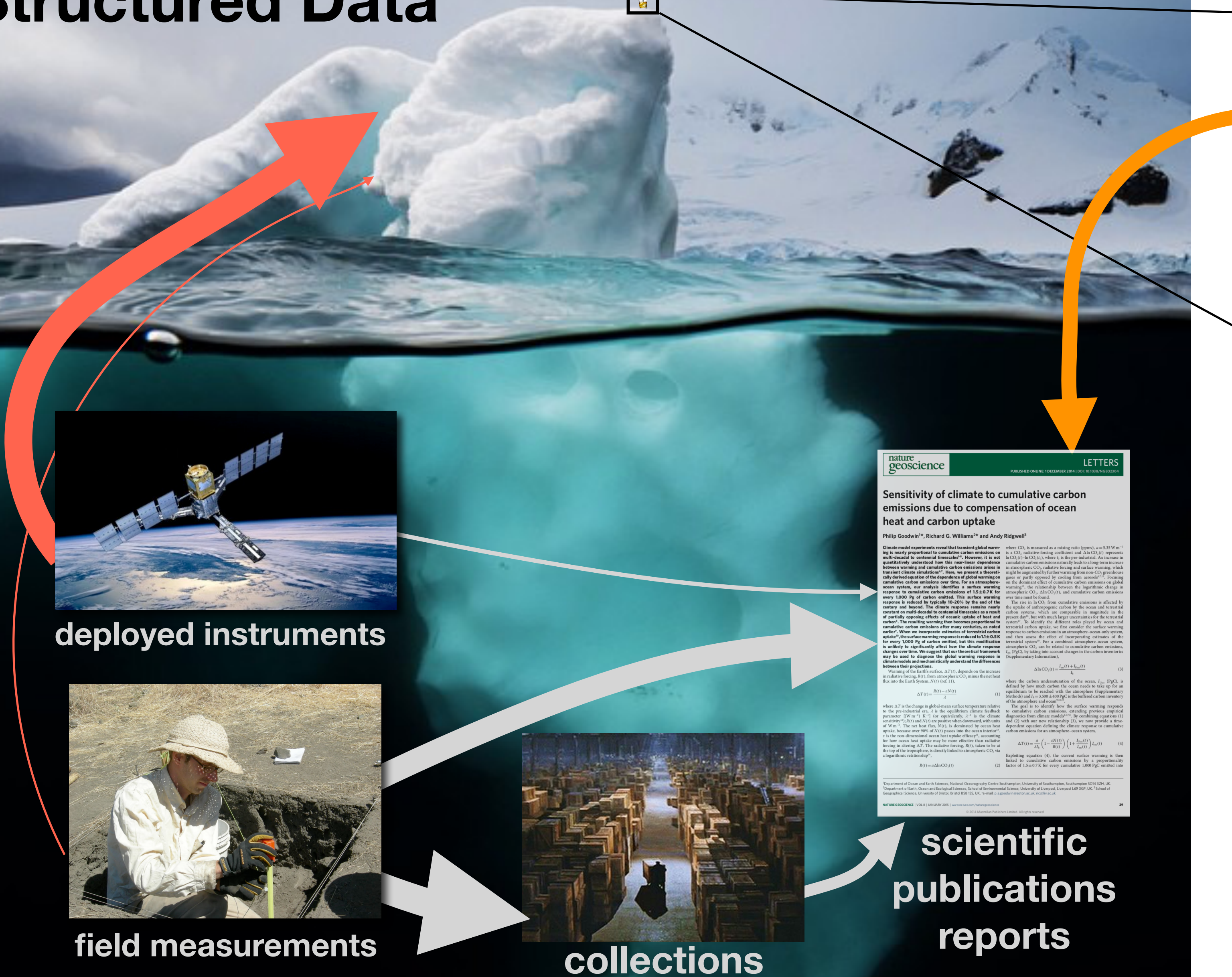
“Dark Data”

Scientific Models



$$\frac{\partial c}{\partial t} = \nabla \cdot (D \nabla c) - \nabla \cdot (\mathbf{v}c) + R$$

Structured Data



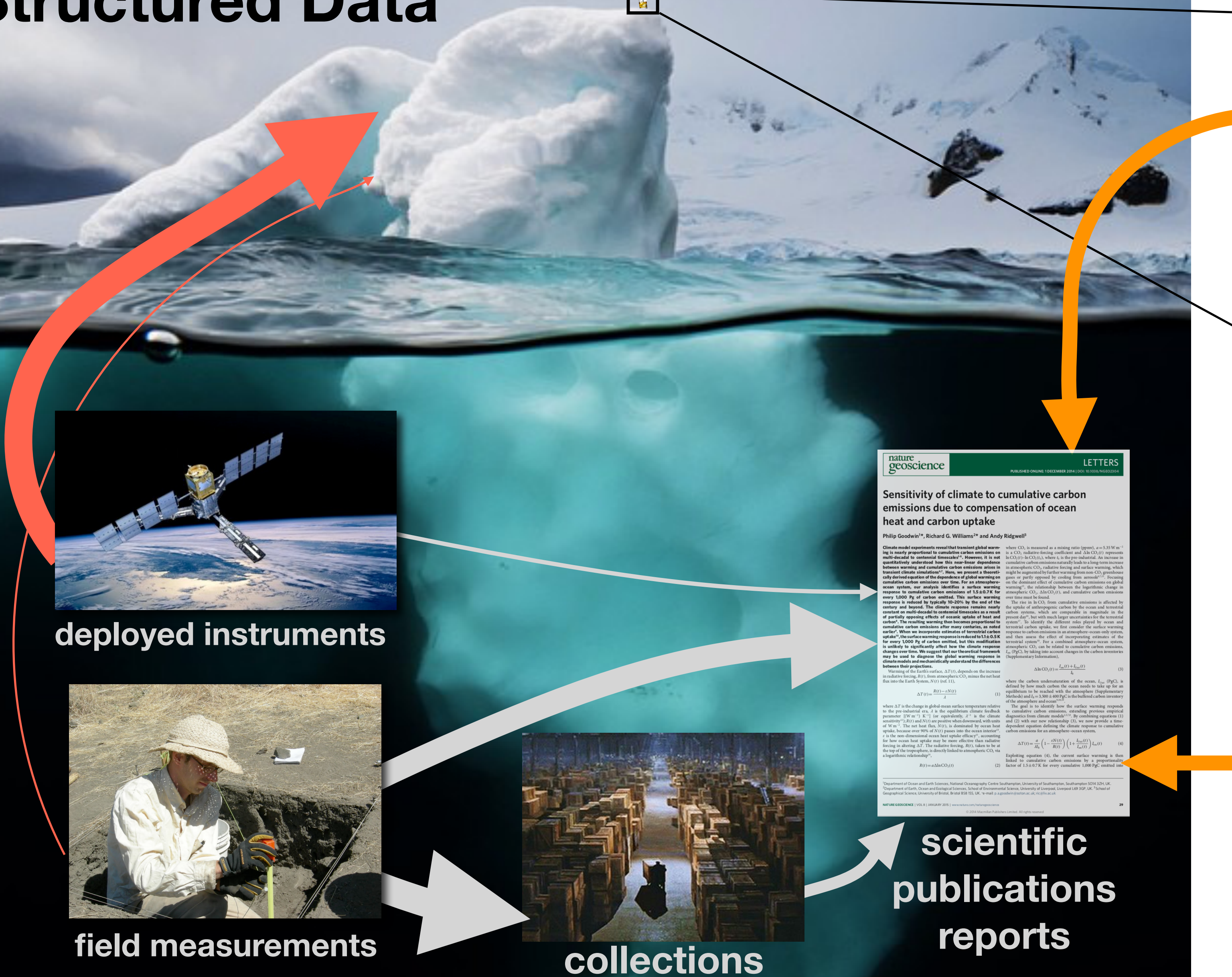
Scientific Models



$$\frac{\partial c}{\partial t} = \nabla \cdot (D \nabla c) - \nabla \cdot (\mathbf{v}c) + R$$

“Dark Data”

Structured Data



“Dark Data”

Scientific Models



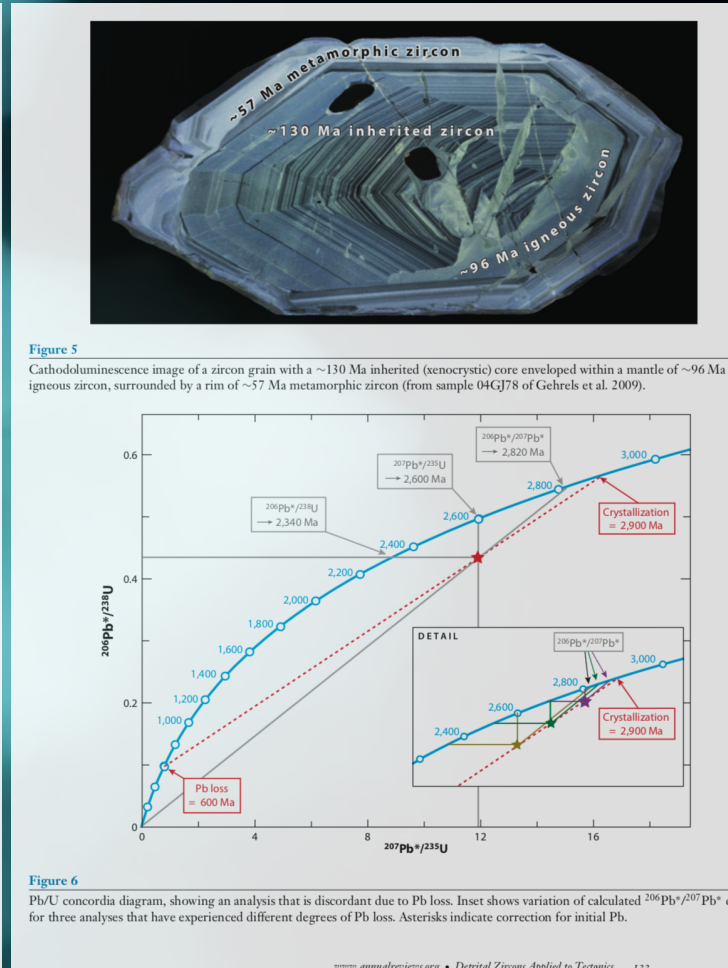
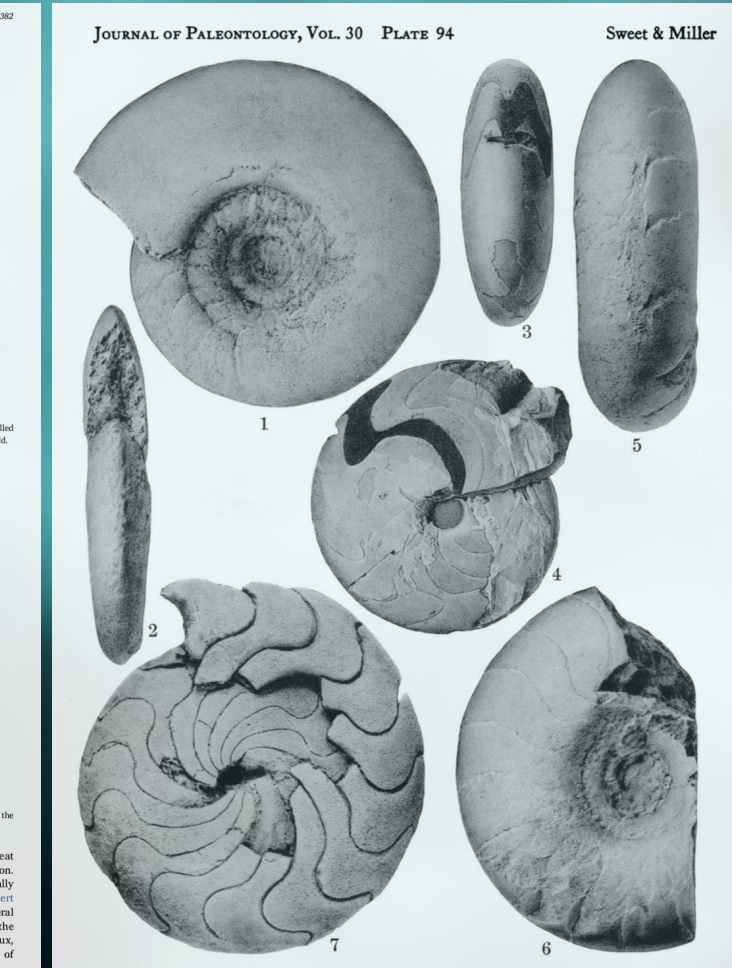
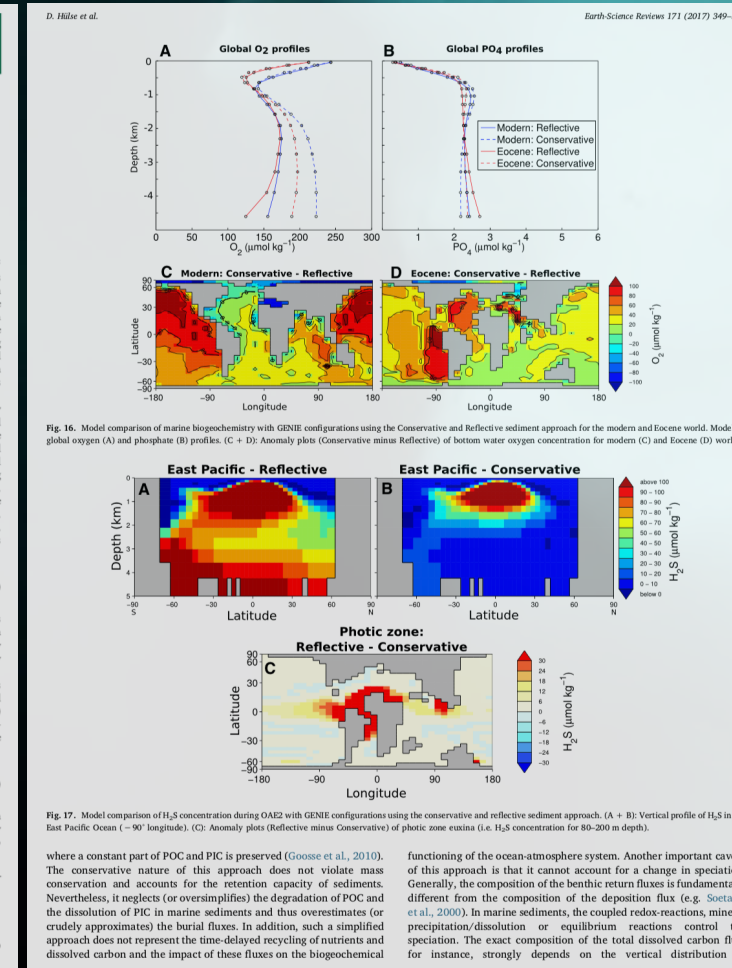
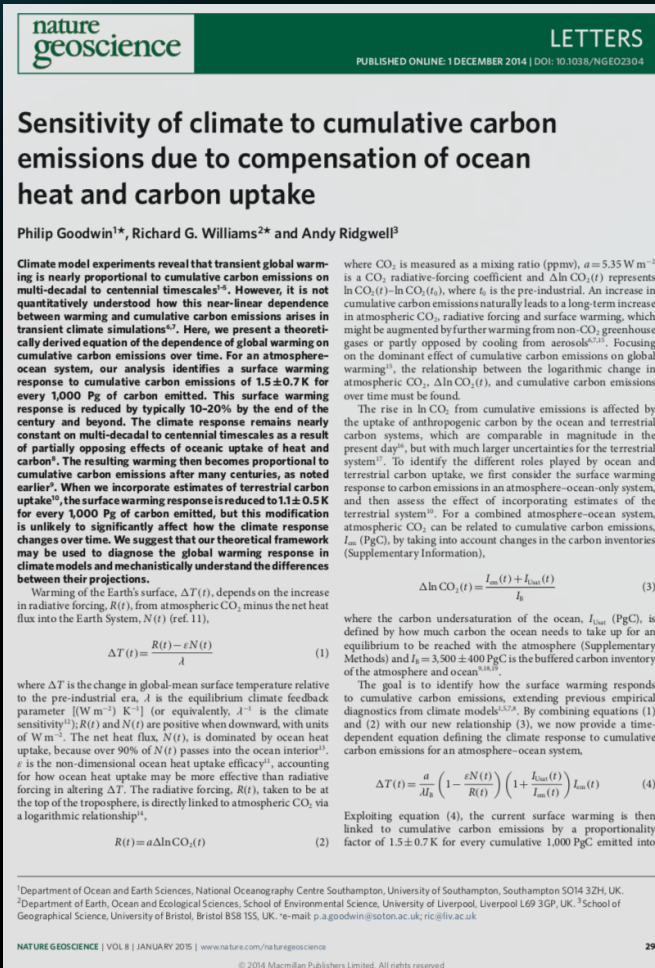
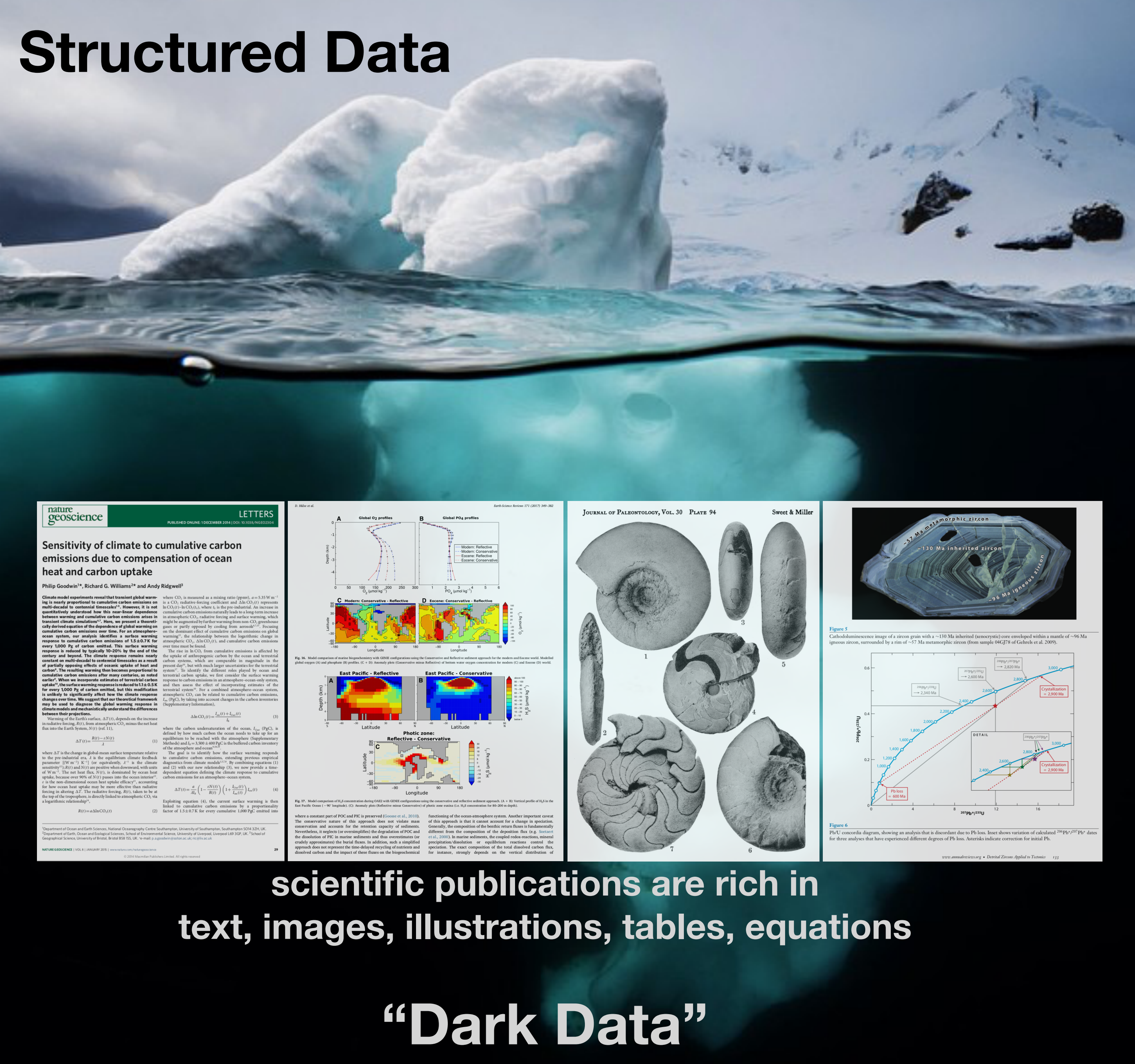
$$\frac{\partial c}{\partial t} = \nabla \cdot (D \nabla c) - \nabla \cdot (\mathbf{v}c) + R$$



Model Predictions

scientific
publications
reports

Structured Data



scientific publications are rich in
text, images, illustrations, tables, equations

“Dark Data”

January 7, 2016

Structured Data



nature
geoscience

LETTERS

PUBLISHED ONLINE 1 DECEMBER 2014 | DOI: 10.1038/NGEO2094

Sensitivity of climate to cumulative carbon emissions due to compensation of ocean heat and carbon uptake

Philip Goodwin¹, Richard G. Williams^{2*} and Andy Ridgwell¹

Climate model experiments reveal that transient global warming is nearly proportional to cumulative carbon emissions on multi-decadal to centennial timescales^{1–4}. However, it is not quantified whether the transient warming response is linear or non-linear between warming and cumulative carbon emissions arises in transient climate simulations^{1–4}. Here, we present a theoretical analysis of the sensitivity of the transient warming response to cumulative carbon emissions over time. For an atmosphere-ocean system, our results show that the logarithmic change in atmospheric CO₂ (Δln(CO₂)) and cumulative carbon emissions over time must be equal to the cumulative carbon emissions of 1.5 ± 0.7 K for every 1,000 Pg of carbon emitted. The surface warming response to cumulative carbon emissions is therefore constant over a century and beyond. The climate response remains nearly constant on multi-decadal to centennial timescales as a result of partial compensating effects of ocean uptake of atmospheric carbon¹. The resulting warming then becomes proportional to cumulative carbon emissions, with a slope that is steeper than earlier¹. When we incorporate estimates of terrestrial carbon uptake⁵, the surface warming response is reduced to 1.1 ± 0.5 K for every 1,000 Pg of carbon emitted. The effect of ocean uptake is unlikely to significantly affect how the climate response changes over time, as long as the ocean uptake of atmospheric carbon may be used to diagnose the global warming response in climate models and mechanically understand responses in climate models.

Warning of the Earth's surface, $\Delta T(t)$, depends on the increase in radiative forcing, $R(t)$, and atmospheric CO₂ minus the net heat flux into the Earth System, $N(t)$ (ref. 11).

$$\Delta T(t) = \frac{R(t) - N(t)}{J} \quad (1)$$

where ΔT is the change in global-mean surface temperature relative to the pre-industrial era, J is the equilibrium radiative forcing parameter, $R(t)$ and $N(t)$ are positive when downward, with units of W m⁻². The net heat flux, $N(t)$, is dominated by ocean heat uptake, which is proportional to the non-dimensional ocean heat uptake sensitivity¹, $R(t)$, and $N(t)$ are positive when downward, with units of W m⁻². The net heat flux, $N(t)$, is dominated by ocean heat uptake, which is proportional to the non-dimensional ocean heat uptake sensitivity¹, $R(t)$, and $N(t)$ are positive when downward, with units of W m⁻². The net heat flux, $N(t)$, is dominated by ocean heat uptake, which is proportional to the non-dimensional ocean heat uptake sensitivity¹, $R(t)$, and $N(t)$ are positive when downward, with units of W m⁻². The net heat flux, $N(t)$, is dominated by ocean heat uptake, which is proportional to the non-dimensional ocean heat uptake sensitivity¹, $R(t)$, and $N(t)$ are positive when downward, with units of W m⁻².

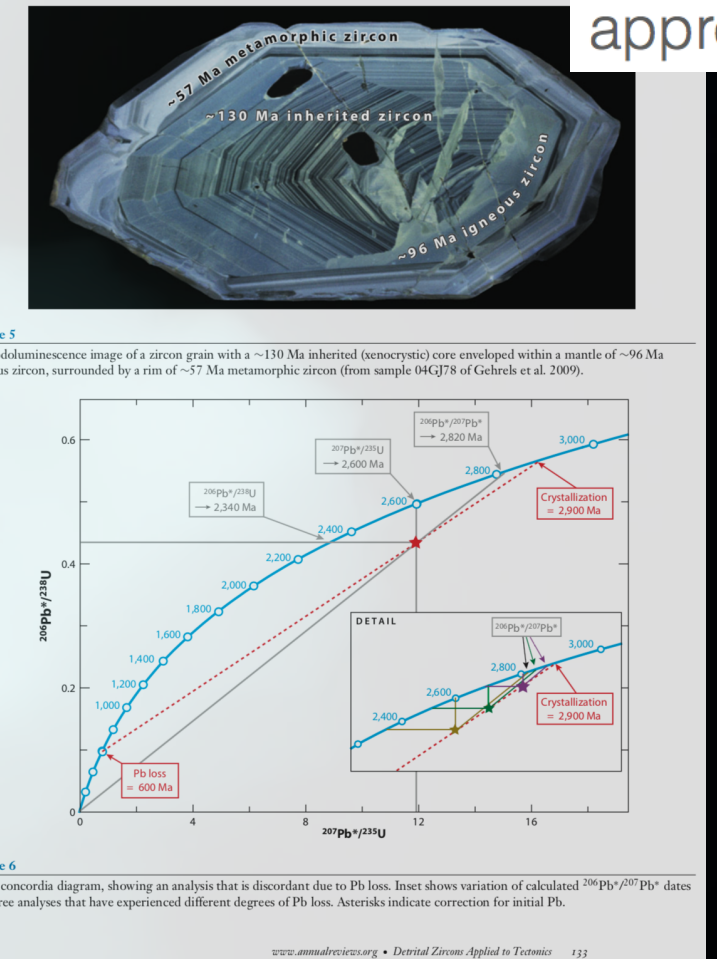
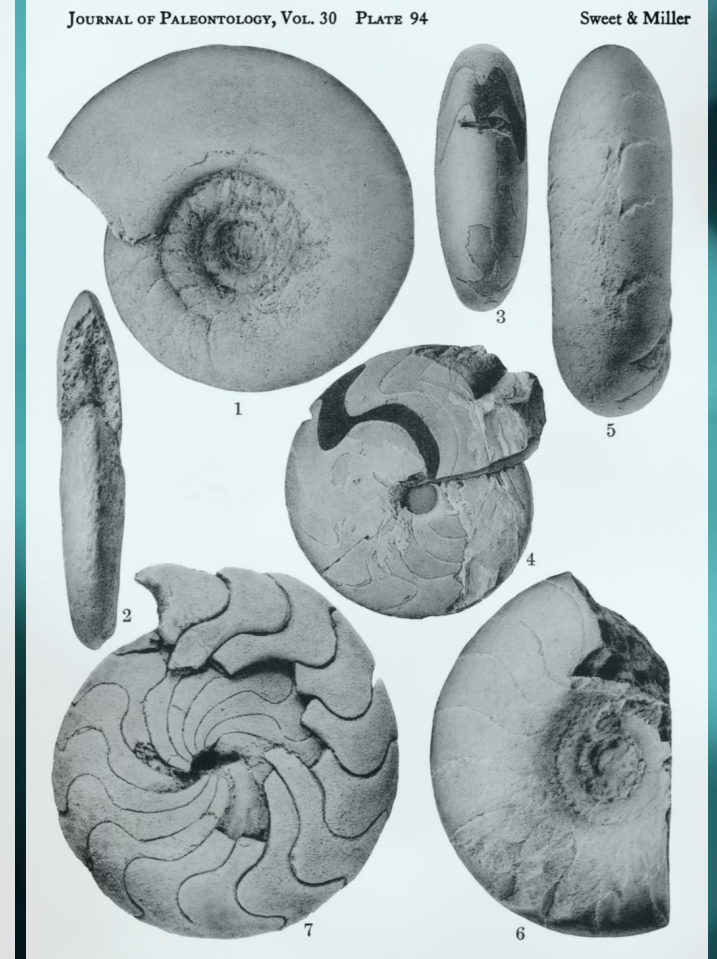
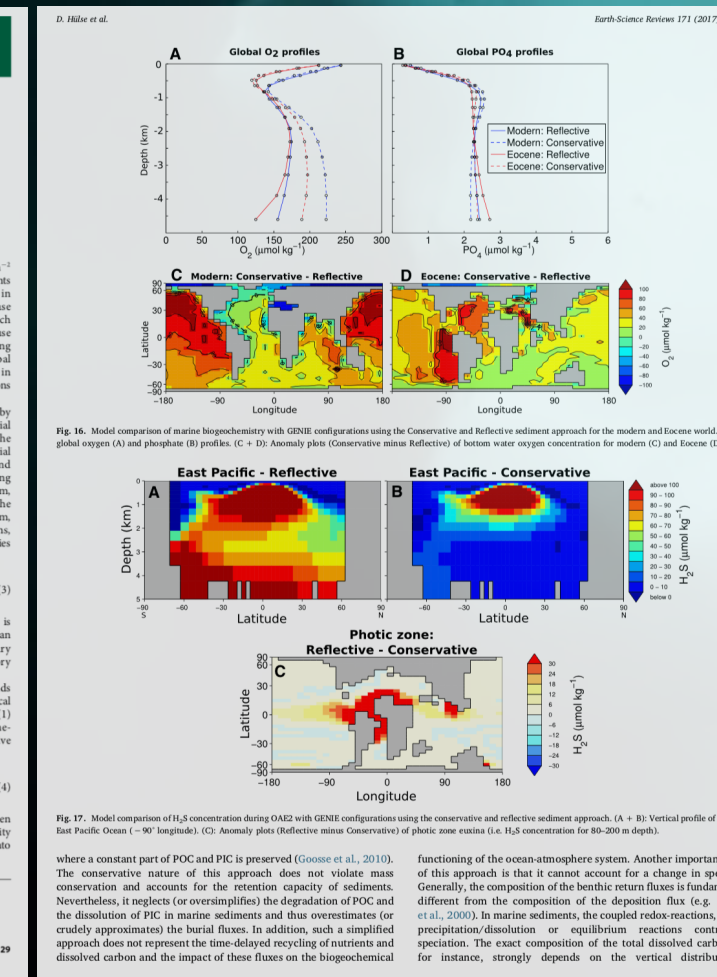
$$R(t) = \alpha \Delta \ln(\text{CO}_2(t)) \quad (2)$$

Explaining equation (4), the current surface warming is then linked to cumulative carbon emissions by a proportionality factor of 1.5 ± 0.7 K for every cumulative 1,000 Pg C emitted into the atmosphere¹.

$$R(t) = \alpha \Delta \ln(\text{CO}_2(t)) \quad (3)$$

¹Department of Ocean and Earth Sciences, National Oceanography Centre Southampton, University of Southampton, Southampton SO14 3ZH, UK. ²Department of Earth Sciences, Lancaster University, Lancaster LA1 4YQ, UK. *e-mail: r.g.williams@lancaster.ac.uk. ³Centre of Geophysical Sciences, University of Bristol, Bristol BS8 5SS, UK. ⁴e-mail: r.g.williams@bris.ac.uk. ⁵See online supplementary information for details.

NATURE GEOSCIENCE | VOL 8 | JANUARY 2015 | www.nature.com/geoscience/ 29

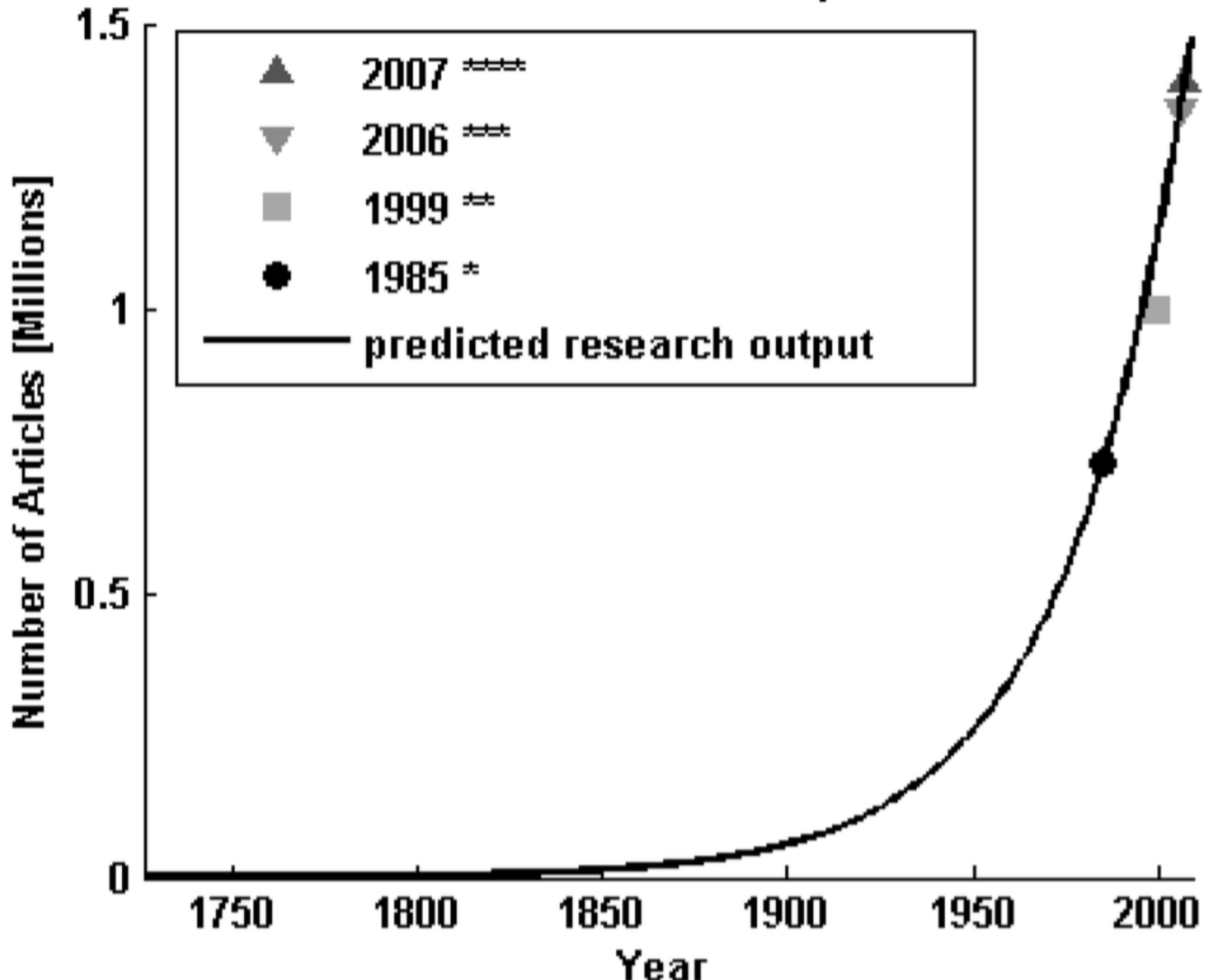


By Sarah Boon, PhD

Do you feel overwhelmed by the number of research papers in your field? Do you wonder if you're missing key ideas that could be critical for your research program? Does it feel like the deluge is only getting worse?

You're not imagining things. According to research from the University of Ottawa, in 2009 we passed the 50 million mark in terms of the total number of science papers published since 1665, and approximately 2.5 million new scientific papers are published each year.

Annual Global Research Output 1726-2009



scientific publications are rich in text, images, illustrations, tables, equations

“Dark Data”

COSMOS: overview of objectives

Biogeosciences, 4, 87–104, 2007
www.biogeosciences.net/4/87/2007/
© Author(s) 2007. This work is licensed
under a Creative Commons License.



Biogeosciences

Marine geochemical data assimilation in an efficient Earth System Model of global biogeochemical cycling

A. Ridgwell¹, J. C. Hargreaves², N. R. Edwards³, J. D. Annan², T. M. Lenton⁴, R. Marsh⁵, A. Yool⁵, and A. Watson⁴

¹School of Geographical Sciences, University of Bristol, Bristol, UK

Table 1. EnKF calibrated biogeochemical parameters in the GENIE-1 model.

Name	Prior assumptions (mean and range ^a)	Posterior mean ^b	Description
$u_0^{\text{PO}_4}$	$1.65 \mu\text{mol kg}^{-1} \text{ yr}^{-1}$ (0.3–3.0)	$1.91 \mu\text{mol kg}^{-1} \text{ yr}^{-1}$	maximum PO_4 uptake (removal) rate (Eq. 3)
K^{PO_4}	$0.2 \mu\text{mol kg}^{-1}$ (0.1–0.3)	$0.21 \mu\text{mol kg}^{-1}$	PO_4 Michaelis-Menton half-saturation concentration (Eq. 3)
r^{POC}	0.05 (0.02–0.08)	0.055	initial proportion of POC export as fraction #2 (Eq. 6)
l^{POC}	600 m (200–1000)	556 m	e -folding remineralization depth of POC fraction #1 (Eq. 6)
$r_0^{\text{CaCO}_3:\text{POC}}$	0.036 (0.015–0.088) ^c	0.022 ^d	$\text{CaCO}_3:\text{POC}$: export rain ratio scalar (Eq. 8)
η	1.5 (1.0–2.0)	1.28	thermodynamic calcification rate power (Eq. 9)
r^{CaCO_3}	0.4 (0.2–0.6)	0.489	initial proportion of CaCO_3 export as fraction #2 (Eq. 11)
l^{CaCO_3}	600 m (200–1000)	1055	e -folding remineralization depth of CaCO_3 fraction #1 (Eq. 11)

^a the range is quoted as 1 standard deviation either side of the mean

addition of calcium carbonate preservation in
ments and its role in regulating atmospheric CO_2
elsewhere (Ridgwell and Hargreaves, 2007).

We have calibrated the model parameters
ocean carbon cycling in GENIE-1 by assimilating
national datasets of phosphate and alkalinity using
the Kalman filter method. The calibrated (me-
dicts a global export production of particulate

particulate organic phosphorus ($F_{z=h_e}^{\text{POP}}$, in units of mol PO_4
 $\text{m}^{-2} \text{ yr}^{-1}$) is equated directly with PO_4 uptake (Eq. 1):

$$F_{z=h_e}^{\text{POP}} = \int_{h_e}^0 \rho \cdot (1 - \nu) \cdot \Gamma dz \quad (4)$$

where ρ is the density of seawater and h_e the thickness of
the euphotic zone (175 m in the 8-level version of this ocean
model).

COSMOS: overview of objectives

1. Automate knowledge base construction (KBC) for equations, parameterizations, and descriptions of scientific models expressed in the published literature.

Biogeosciences, 4, 87–104, 2007
www.biogeosciences.net/4/87/2007/
© Author(s) 2007. This work is licensed under a Creative Commons License.



Biogeosciences

Marine geochemical data assimilation in an efficient Earth System Model of global biogeochemical cycling

A. Ridgwell¹, J. C. Hargreaves², N. R. Edwards³, J. D. Annan², T. M. Lenton⁴, R. Marsh⁵, A. Yool⁵, and A. Watson⁴

¹School of Geographical Sciences, University of Bristol, Bristol, UK

Table 1. EnKF calibrated biogeochemical parameters in the GENIE-1 model.

Name	Prior assumptions (mean and range ^a)	Posterior mean ^b	Description
$u_0^{\text{PO}_4}$	$1.65 \mu\text{mol kg}^{-1} \text{ yr}^{-1}$ (0.3–3.0)	$1.91 \mu\text{mol kg}^{-1} \text{ yr}^{-1}$	maximum PO_4 uptake (removal) rate (Eq. 3)
K^{PO_4}	$0.2 \mu\text{mol kg}^{-1}$ (0.1–0.3)	$0.21 \mu\text{mol kg}^{-1}$	PO_4 Michaelis-Menton half-saturation concentration (Eq. 3)
r^{POC}	0.05 (0.02–0.08)	0.055	initial proportion of POC export as fraction #2 (Eq. 6)
l^{POC}	600 m (200–1000)	556 m	e -folding remineralization depth of POC fraction #1 (Eq. 6)
$r_0^{\text{CaCO}_3:\text{POC}}$	0.036 (0.015–0.088) ^c	0.022 ^d	$\text{CaCO}_3:\text{POC}$: export rain ratio scalar (Eq. 8)
η	1.5 (1.0–2.0)	1.28	thermodynamic calcification rate power (Eq. 9)
r^{CaCO_3}	0.4 (0.2–0.6)	0.489	initial proportion of CaCO_3 export as fraction #2 (Eq. 11)
l^{CaCO_3}	600 m (200–1000)	1055	e -folding remineralization depth of CaCO_3 fraction #1 (Eq. 11)

^a the range is quoted as 1 standard deviation either side of the mean

addition of calcium carbonate preservation in
ments and its role in regulating atmospheric CO_2
elsewhere (Ridgwell and Hargreaves, 2007).

We have calibrated the model parameters
ocean carbon cycling in GENIE-1 by assimilating
national datasets of phosphate and alkalinity using
the Kalman filter method. The calibrated (me-
dicts a global export production of particulate

particulate organic phosphorus ($F_{z=h_e}^{\text{POP}}$, in units of mol PO_4
 $\text{m}^{-2} \text{ yr}^{-1}$) is equated directly with PO_4 uptake (Eq. 1):

$$F_{z=h_e}^{\text{POP}} = \int_{h_e}^0 \rho \cdot (1 - \nu) \cdot \Gamma dz \quad (4)$$

where ρ is the density of seawater and h_e the thickness of
the euphotic zone (175 m in the 8-level version of this ocean
model).

COSMOS: overview of objectives

1. Automate knowledge base construction (KBC) for equations, parameterizations, and descriptions of scientific models expressed in the published literature.

2. Automate KBC for empirical/experimental data and observations in publications that are semantically related to model inputs and predictions.

Biogeosciences, 4, 87–104, 2007
www.biogeosciences.net/4/87/2007/
© Author(s) 2007. This work is licensed under a Creative Commons License.



Biogeosciences

Marine geochemical data assimilation in an efficient Earth System Model of global biogeochemical cycling

A. Ridgwell¹, J. C. Hargreaves², N. R. Edwards³, J. D. Annan², T. M. Lenton⁴, R. Marsh⁵, A. Yool⁵, and A. Watson⁴

¹School of Geographical Sciences, University of Bristol, Bristol, UK

Table 1. EnKF calibrated biogeochemical parameters in the GENIE-1 model.

Name	Prior assumptions (mean and range ^a)	Posterior mean ^b	Description
$u_0^{\text{PO}_4}$	$1.65 \mu\text{mol kg}^{-1} \text{ yr}^{-1}$ (0.3–3.0)	$1.91 \mu\text{mol kg}^{-1} \text{ yr}^{-1}$	maximum PO_4 uptake (removal) rate (Eq. 3)
K^{PO_4}	$0.2 \mu\text{mol kg}^{-1}$ (0.1–0.3)	$0.21 \mu\text{mol kg}^{-1}$	PO_4 Michaelis-Menton half-saturation concentration (Eq. 3)
r^{POC}	0.05 (0.02–0.08)	0.055	initial proportion of POC export as fraction #2 (Eq. 6)
l^{POC}	600 m (200–1000)	556 m	e -folding remineralization depth of POC fraction #1 (Eq. 6)
$r_0^{\text{CaCO}_3:\text{POC}}$	0.036 (0.015–0.088) ^c	0.022 ^d	$\text{CaCO}_3:\text{POC}$: export rain ratio scalar (Eq. 8)
η	1.5 (1.0–2.0)	1.28	thermodynamic calcification rate power (Eq. 9)
r^{CaCO_3}	0.4 (0.2–0.6)	0.489	initial proportion of CaCO_3 export as fraction #2 (Eq. 11)
l^{CaCO_3}	600 m (200–1000)	1055	e -folding remineralization depth of CaCO_3 fraction #1 (Eq. 11)

^a the range is quoted as 1 standard deviation either side of the mean

addition of calcium carbonate preservation in
ments and its role in regulating atmospheric CO_2
elsewhere (Ridgwell and Hargreaves, 2007).

We have calibrated the model parameters
ocean carbon cycling in GENIE-1 by assimilating
national datasets of phosphate and alkalinity using
the Kalman filter method. The calibrated (me-
dicts a global export production of particulate

particulate organic phosphorus ($F_{z=h_e}^{\text{POP}}$, in units of mol PO_4
 $\text{m}^{-2} \text{ yr}^{-1}$) is equated directly with PO_4 uptake (Eq. 1):

$$F_{z=h_e}^{\text{POP}} = \int_{h_e}^0 \rho \cdot (1 - \nu) \cdot \Gamma dz \quad (4)$$

where ρ is the density of seawater and h_e the thickness of
the euphotic zone (175 m in the 8-level version of this ocean
model).

COSMOS: overview of objectives

1. Automate knowledge base construction (KBC) for equations, parameterizations, and descriptions of scientific models expressed in the published literature.
2. Automate KBC for empirical/experimental data and observations in publications that are semantically related to model inputs and predictions.
3. Remove major pain-point in model-data integration and tangibly improve pace/completeness of model assessment and refinement, advance science.

Biogeosciences, 4, 87–104, 2007
www.biogeosciences.net/4/87/2007/
© Author(s) 2007. This work is licensed under a Creative Commons License.



Biogeosciences

Marine geochemical data assimilation in an efficient Earth System Model of global biogeochemical cycling

A. Ridgwell¹, J. C. Hargreaves², N. R. Edwards³, J. D. Annan², T. M. Lenton⁴, R. Marsh⁵, A. Yool⁵, and A. Watson⁴

¹School of Geographical Sciences, University of Bristol, Bristol, UK

Table 1. EnKF calibrated biogeochemical parameters in the GENIE-1 model.

Name	Prior assumptions (mean and range ^a)	Posterior mean ^b	Description
$u_0^{\text{PO}_4}$	$1.65 \mu\text{mol kg}^{-1} \text{ yr}^{-1}$ (0.3–3.0)	$1.91 \mu\text{mol kg}^{-1} \text{ yr}^{-1}$	maximum PO_4 uptake (removal) rate (Eq. 3)
K^{PO_4}	$0.2 \mu\text{mol kg}^{-1}$ (0.1–0.3)	$0.21 \mu\text{mol kg}^{-1}$	PO_4 Michaelis-Menton half-saturation concentration (Eq. 3)
r^{POC}	0.05 (0.02–0.08)	0.055	initial proportion of POC export as fraction #2 (Eq. 6)
l^{POC}	600 m (200–1000)	556 m	e -folding remineralization depth of POC fraction #1 (Eq. 6)
$r_0^{\text{CaCO}_3:\text{POC}}$	0.036 (0.015–0.088) ^c	0.022 ^d	$\text{CaCO}_3:\text{POC}$: export rain ratio scalar (Eq. 8)
η	1.5 (1.0–2.0)	1.28	thermodynamic calcification rate power (Eq. 9)
r^{CaCO_3}	0.4 (0.2–0.6)	0.489	initial proportion of CaCO_3 export as fraction #2 (Eq. 11)
l^{CaCO_3}	600 m (200–1000)	1055	e -folding remineralization depth of CaCO_3 fraction #1 (Eq. 11)

^a the range is quoted as 1 standard deviation either side of the mean

addition of calcium carbonate preservation in
ments and its role in regulating atmospheric CO_2
elsewhere (Ridgwell and Hargreaves, 2007).

We have calibrated the model parameters
ocean carbon cycling in GENIE-1 by assimilating
national datasets of phosphate and alkalinity using
the Kalman filter method. The calibrated (me-
dicts a global export production of particulate

particulate organic phosphorus ($F_{z=h_e}^{\text{POP}}$, in units of mol PO_4
 $\text{m}^{-2} \text{ yr}^{-1}$) is equated directly with PO_4 uptake (Eq. 1):

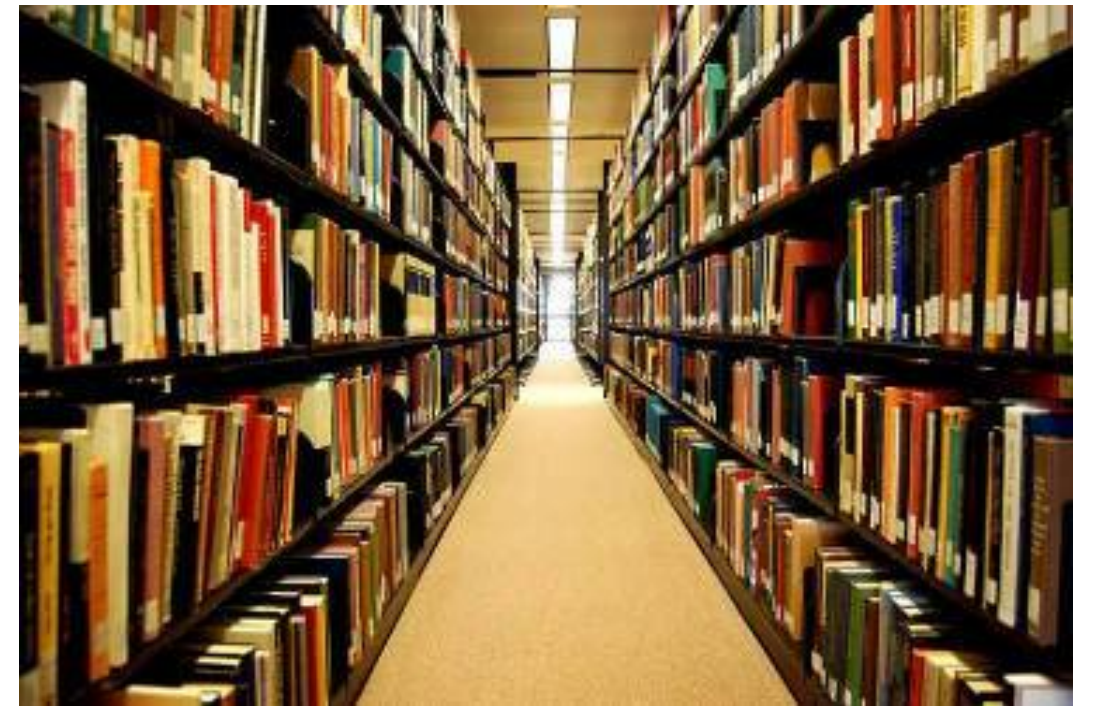
$$F_{z=h_e}^{\text{POP}} = \int_{h_e}^0 \rho \cdot (1 - \nu) \cdot \Gamma dz \quad (4)$$

where ρ is the density of seawater and h_e the thickness of
the euphotic zone (175 m in the 8-level version of this ocean
model).

COSMOS: required components

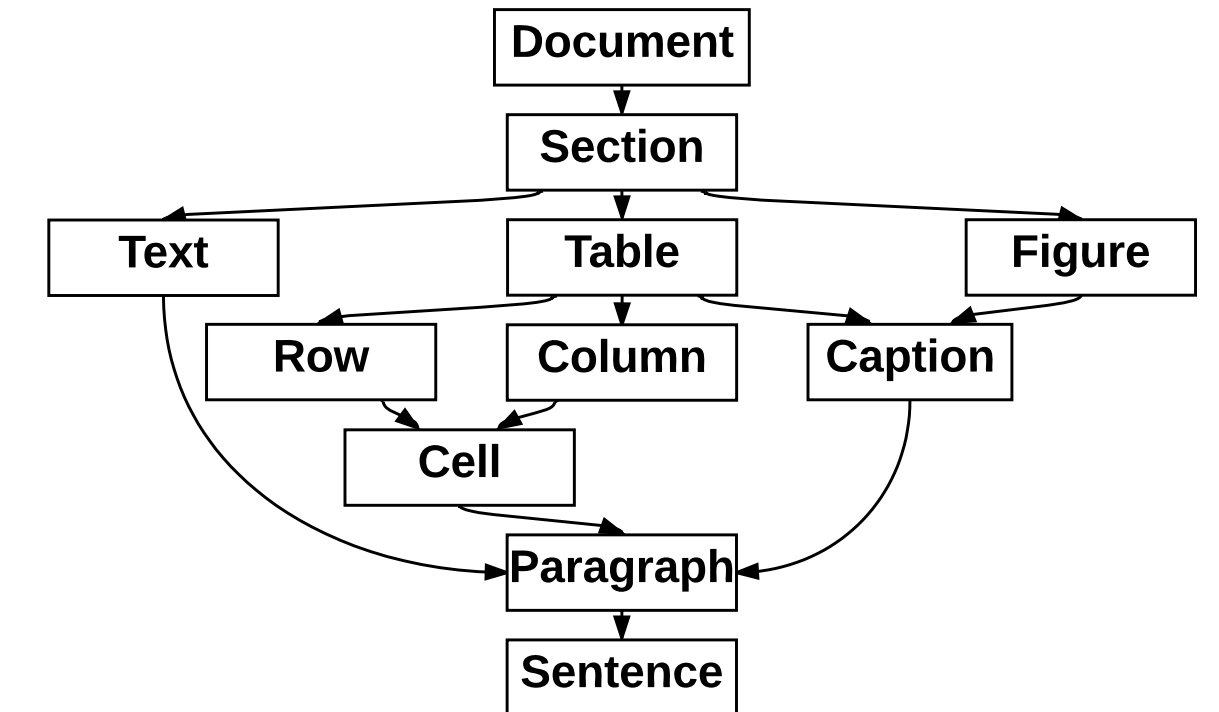
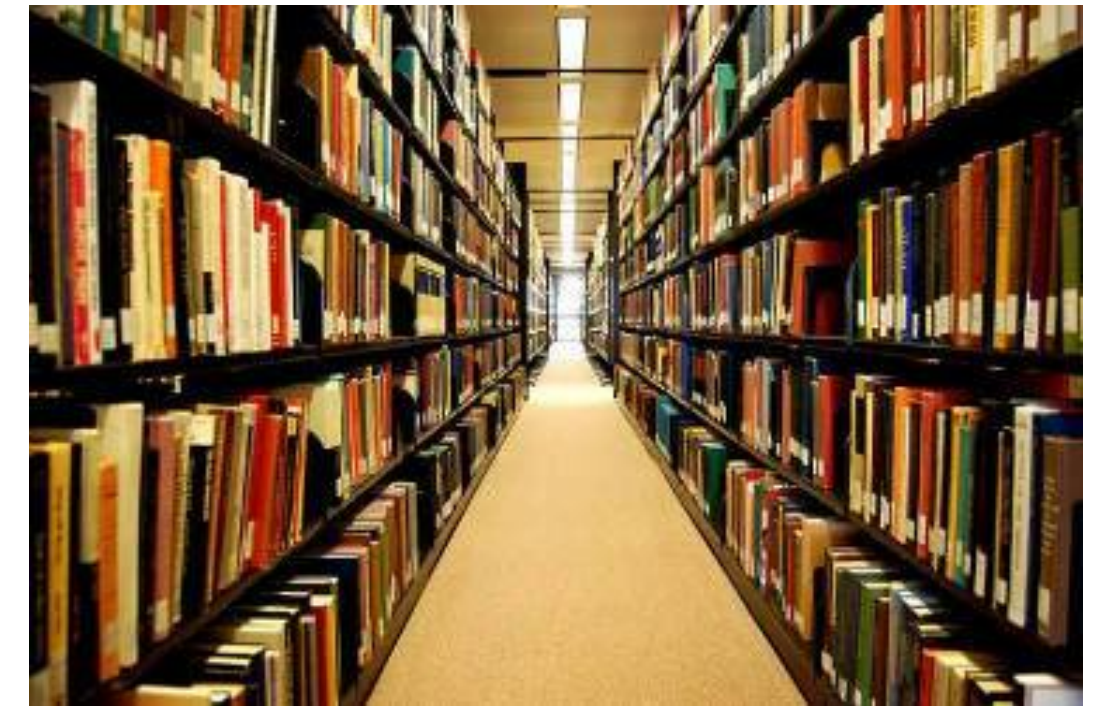
COSMOS: required components

1. Principled, automated access to scientific publications and the computing capacity and infrastructure required to repeatedly analyze them.



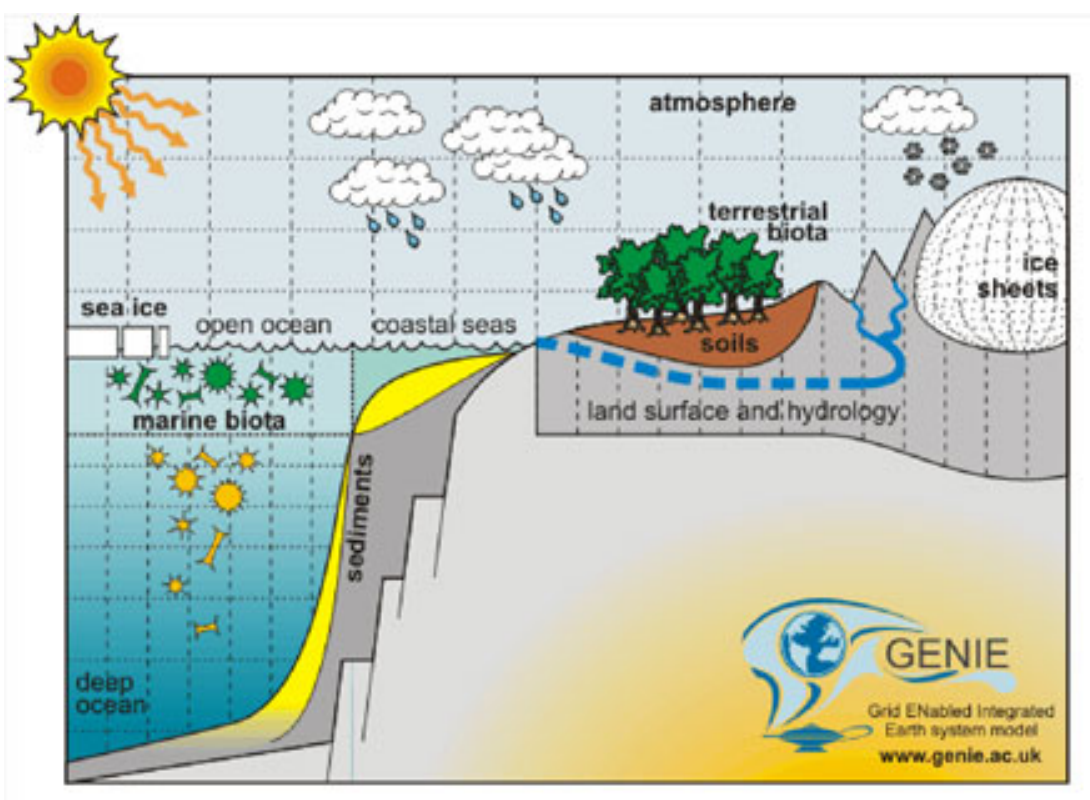
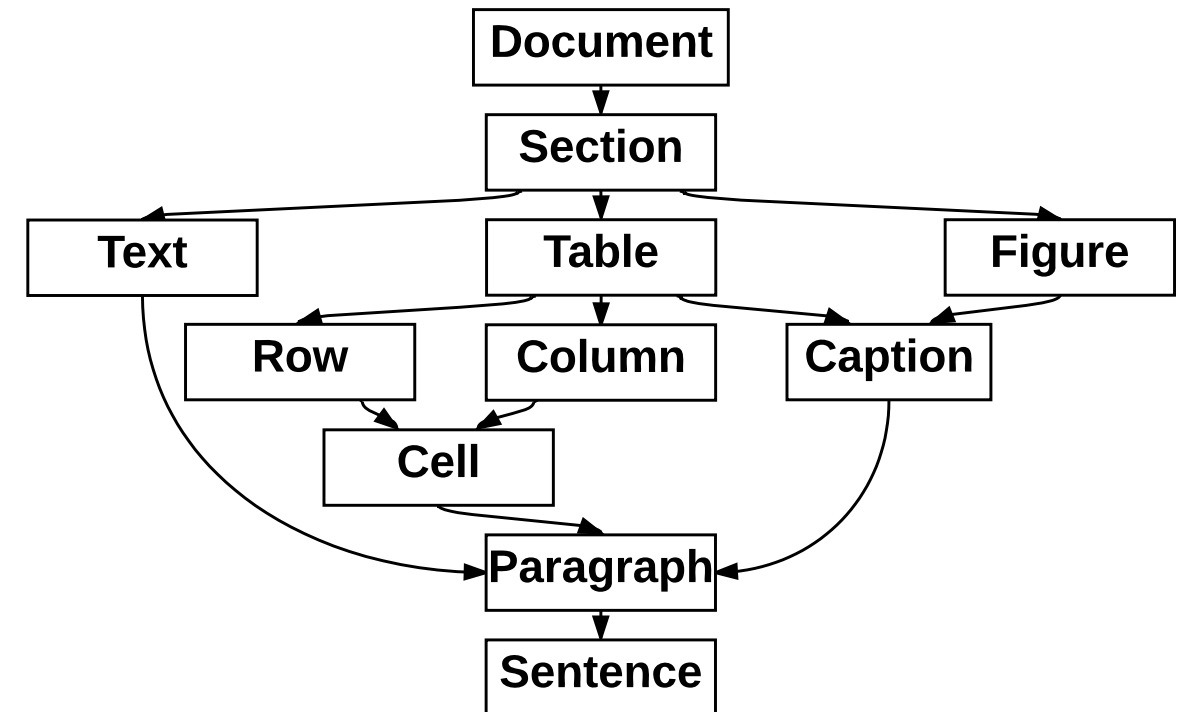
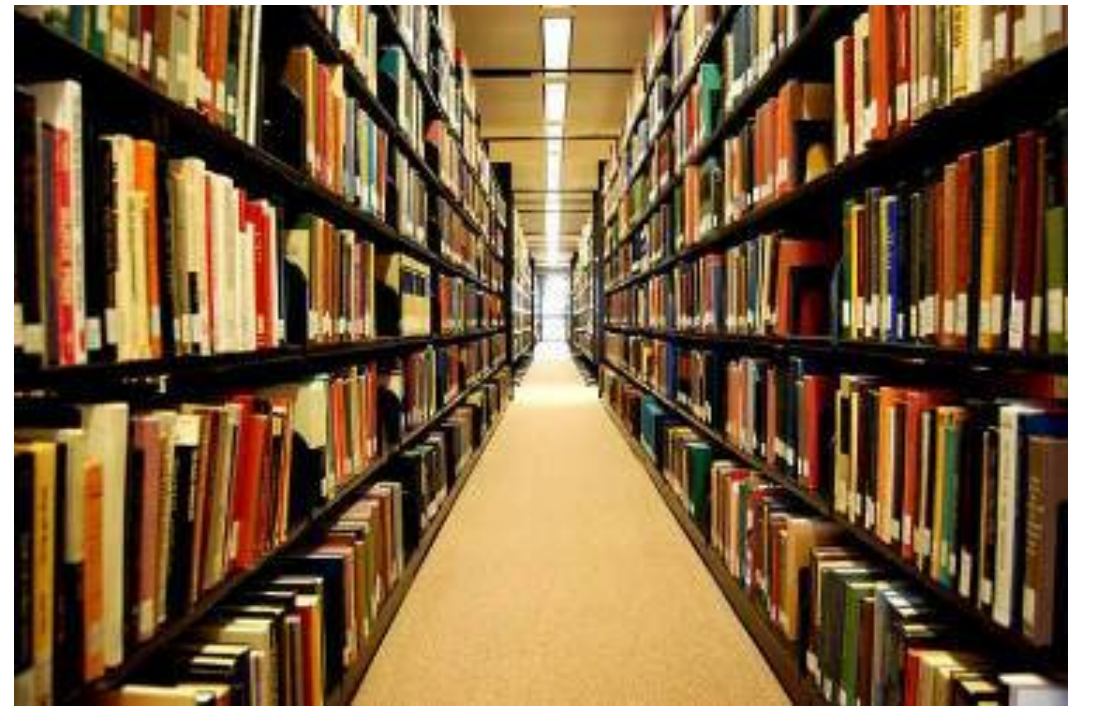
COSMOS: required components

1. Principled, automated access to scientific publications and the computing capacity and infrastructure required to repeatedly analyze them.
2. Models and techniques to represent and capture multi-modal data within publications.



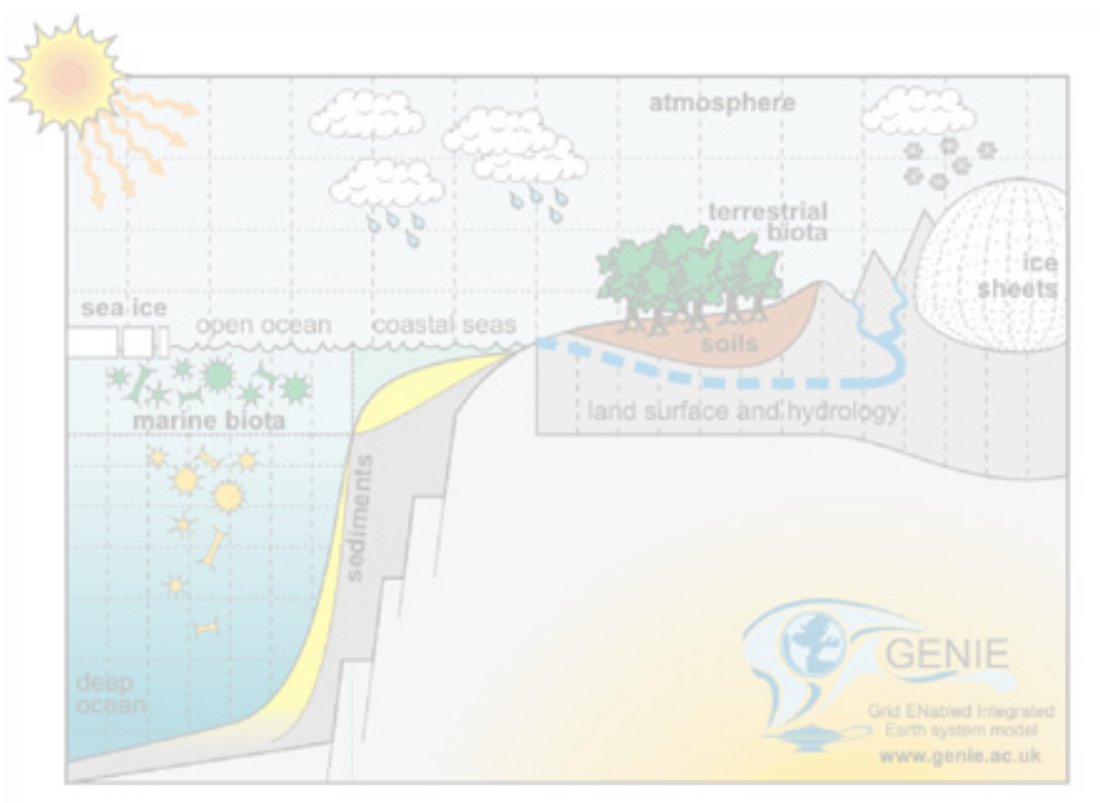
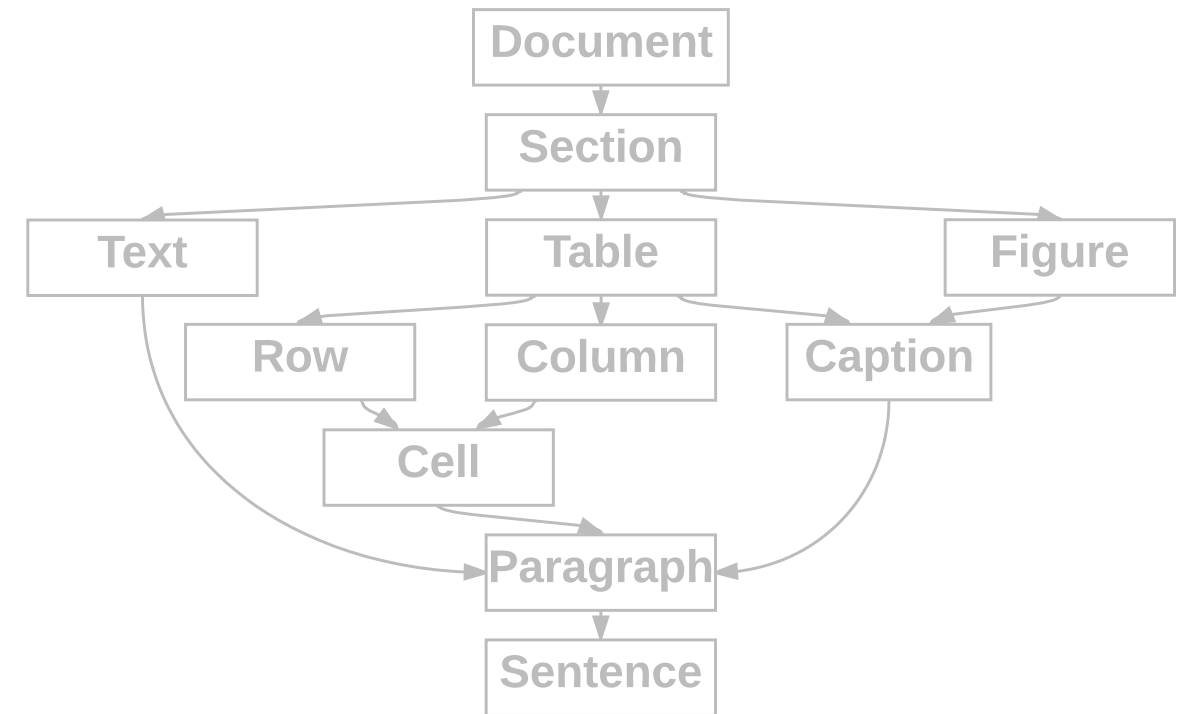
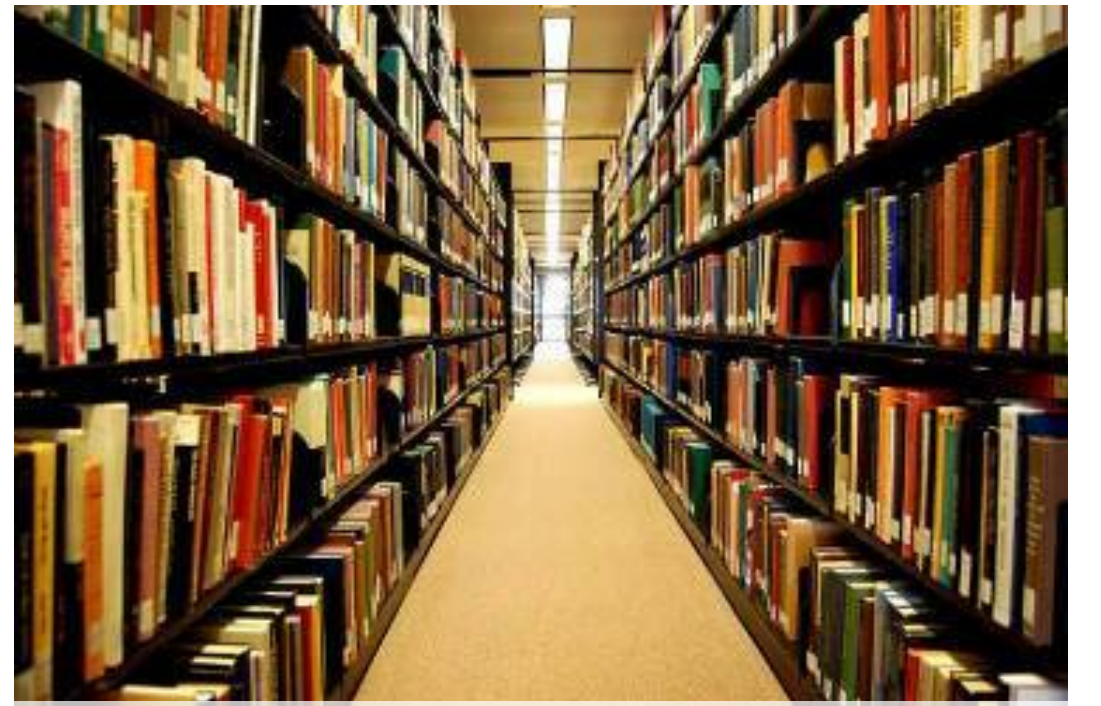
COSMOS: required components

1. Principled, automated access to scientific publications and the computing capacity and infrastructure required to repeatedly analyze them.
2. Models and techniques to represent and capture multi-modal data within publications.
3. Earth system model with parameterizations and predictions that overlap with many different types of empirical data and observations in publications.



COSMOS: required components

1. Principled, automated access to scientific publications and the computing capacity and infrastructure required to repeatedly analyze them.
2. Models and techniques to represent and capture multi-modal data within publications.
3. Earth system model with parameterizations and predictions that overlap with many different types of empirical data and observations in publications.



GeoDeepDive

(aka: xDD)

8.3M published documents coupled to
and readable by a computing infrastructure

GeoDeepDive Infrastructure Overview

ScienceDirect

Journals Books

PDF Purchase Export Search ScienceDirect Advanced search

 ELSEVIER

Cretaceous Research

Volume 29, Issues 5–6, October–December 2008, Pages 1008–1023

7th International Symposium on the Cretaceous



Organic carbon deposition and phosphorus accumulation during Oceanic Anoxic Event 2 in Tarfaya, Morocco

Haydon P. Mort^a, Thierry Adatte^{a, 2}, Gerta Keller^b, David Bartels^b, Karl B. Föllmi^{a, 2}, Philipp Steinmann^{a, 2}, Zsolt Berner^c, E.H. Chellai^d

+ Show more

<https://doi.org/10.1016/j.cretres.2008.05.026> Get rights and content

publisher agreements



PLOS
ONE



GeoDeepDive Infrastructure Overview

ScienceDirect

Journals Books

PDF Purchase Export Search ScienceDirect Advanced search

 Cretaceous Research

Volume 29, Issues 5–6, October–December 2008, Pages 1008–1023

7th International Symposium on the Cretaceous



Organic carbon deposition and phosphorus accumulation during Oceanic Anoxic Event 2 in Tarfaya, Morocco

Haydon P. Mort^a, Thierry Adatte^{a, 2}, Gerta Keller^b, David Bartels^b, Karl B. Föllmi^{a, 2}, Philipp Steinmann^{a, 2}, Zsolt Berner^c, E.H. Chellai^d

+ Show more

<https://doi.org/10.1016/j.cretres.2008.05.026>

Get rights and content

Cretaceous Research 29 (2008) 1008–1023

Contents lists available at ScienceDirect
Cretaceous Research
journal homepage: www.elsevier.com/locate/CretRes

Organic carbon deposition and phosphorus accumulation during Oceanic Anoxic Event 2 in Tarfaya, Morocco

Haydon P. Mort^{a,*}, Thierry Adatte^{a, 2}, Gerta Keller^b, David Bartels^b, Karl B. Föllmi^{a, 2}, Philipp Steinmann^{a, 2}, Zsolt Berner^c, E.H. Chellai^d

^aRue Emile Argand 11, Institute of Geology, University of Neuchâtel, Case postale 158, CH-2009 Neuchâtel, Switzerland
^bDepartment of Geosciences, Princeton University, Guyot Hall, Princeton, NJ 08544-1003, USA
^cInstitut für Mineralogie und Geochemie, Universität Karlsruhe, 76128 Karlsruhe, Germany
^dUniversity Cadi Ayyad, Faculty of Sciences Semlalia, Marrakech, Morocco

ARTICLE INFO

Article history:
Received 23 September 2006
Accepted in revised form 4 May 2008
Available online 28 June 2008

Keywords:
Anoxia
Phosphorus burial
Organic carbon
Morocco
Cenomanian-Turonian

ABSTRACT

With a multi-proxy approach, an attempt was made to constrain productivity and bottom-water redox conditions and their effects on the phosphorus accumulation rate at the Mohammed el-Pege section on the Tarfaya coast, Morocco, during the Cenomanian-Turonian Anoxic Event (OAE 2). A distinct $\delta^{34}\text{C}_{\text{org}}$ isotope excursion of $\sim 2.5\text{\textperthousand}$ occurs close to the top of the section. The unusually abrupt shift of the isotope excursion and disappearance of several planktonic foraminiferal species (e.g. *Rotalipora cushmani* and *Rotatlipora greenhornensis*) in this level suggests a hiatus of between 40–60 kyr at the excursion onset. Nevertheless, it was possible to determine both the long-term environmental history as well as the processes that took place immediately prior to and during OAE 2. TOC values increase gradually from the start of the section ($\sim 2.5\text{\textperthousand}$) to the top of the section ($\sim 3.5\text{\textperthousand}$). This reflects a long-term eustatic sea-level rise and subsidence causing the encroachment of less toxic waters into the Tarfaya Basin. Similarly a reduction in the mineralogically constructed ‘detrital index’ can be explained by the decrease in the continental flux of terrigenous material due to a relative sea-level rise. A speciation of phosphorus in the upper part of the section, which spans the start and mid-stages of OAE 2, shows overall higher abundances of P_{reactive} mass accumulation rates before the isotope excursion onset and lower values during the plateau. Due to the probable short hiatus, the onset of the decrease in phosphorus content relative to the isotope excursion is uncertain, although the excursion plateau already contains lower concentrations. The $\text{CaCO}_3/\text{Total}$ and V/I ratios suggest that this reduction was mostly likely caused by a decrease in the availability of oxygenated conditions (primarily as a result of reduced productivity) and a corresponding fall in the phosphorus retention ability of the sediment. Productivity appears to have remained high during the isotope plateau possibly due to a combination of ocean-surface fertilisation via increased aridity (increased K/I and T/U ratios) and/or higher dissolved inorganic phosphorus content in the water column as a result of the decrease in sediment P retention. The evidence for decreased P-burial has been observed in many other palaeoenvironments during OAE 2. Tarfaya’s unique upwelling paleosituation provides strong evidence that the nutrient recycling was a global phenomenon and therefore a critical factor in starting and sustaining OAE 2.

© 2008 Elsevier Ltd. All rights reserved.

1. Introduction

At least seven so-called ‘anoxic events’ punctuated various intervals in the Cretaceous of which one occurred in the latest Cenomanian (Bonarelli Level) dated around 93.5 Ma. Generally these events are characterized by enhanced organic-rich shale deposition and positive $\delta^{13}\text{C}$ excursions (Schlanger and Jenkyns, 1976; Jenkyns, 1980). Although the fundamental causal mechanisms have remained enigmatic, there have been no shortages of ideas that have, at least in part, helped to explain these events. The causal nature of each OAE is likely to be subtly different given the differing sea-level positions, tectonic and paleogeographic situations (Haq et al., 1987; Jenkyns, 1991; Hallam and Wignall, 1999; Aguilera-Franco et al., 2001) and ocean chemistry at each point in time. In terms of the amount and rate of organic carbon sequestration OAE 2 was probably the largest of the anoxic events that punctuated the Cretaceous. Often the debate has centred on the role of preservation and productivity in producing the characteristic positive $\delta^{13}\text{C}$

* Corresponding author.
E-mail address: h.mort@geo.uu.nl (H.P. Mort).

¹ Present address: Department of Earth Sciences – Geochemistry, Faculty of Geosciences, Utrecht University, PO Box 80.021, 3508 CD Utrecht, The Netherlands.

² Present address: Institut de Géologie et de Paléontologie, IGP, Université de Lausanne, Anthropole, CH-1015 Lausanne, Switzerland.

0165-6673/\$ – see front matter © 2008 Elsevier Ltd. All rights reserved.
doi:10.1016/j.cretres.2008.05.026

publisher agreements



doc. fetching/storage



8-12k/day

GeoDeepDive Infrastructure Overview

ScienceDirect

Journals Books

Purchase Export Search ScienceDirect Advanced search

Cretaceous Research

Volume 29, Issues 5–6, October–December 2008, Pages 1008–1023

7th International Symposium on the Cretaceous

Organic carbon deposition and phosphorus accumulation during Oceanic Anoxic Event 2 in Tarfaya, Morocco

Haydon P. Mort^a, Thierry Adatte^{a, 2}, Gerta Keller^b, David Bartels^b, Karl B. Föllmi^{a, 2}, Philipp Steinmann^{a, 2}, Zsolt Berner^c, E.H. Chellai^d

[+ Show more](#)

<https://doi.org/10.1016/j.cretres.2008.05.026>

Get rights and content

Cretaceous Research 29 (2008) 1008–1023

Contents lists available at ScienceDirect
Cretaceous Research journal homepage: www.elsevier.com/locate/CretRes

Organic carbon deposition and phosphorus accumulation during Oceanic Anoxic Event 2 in Tarfaya, Morocco

Haydon P. Mort^{a,*}, Thierry Adatte^{a, 2}, Gerta Keller^b, David Bartels^b, Karl B. Föllmi^{a, 2}, Philipp Steinmann^{a, 2}, Zsolt Berner^c, E.H. Chellai^d

^aRue Emile Argand 11, Institute of Geology, University of Neuchâtel, Case postale 158, CH-2009 Neuchâtel, Switzerland
^bDepartment of Geosciences, Princeton University, Guyot Hall, Princeton, NJ 08544-1003, USA
^cInstitut für Mineralogie und Geochemie, Universität Karlsruhe, 76128 Karlsruhe, Germany
^dUniversity Cadi Ayyad, Faculty of Sciences Semlalia, Marrakech, Morocco

ARTICLE INFO

Article history:
Received 23 September 2006
Accepted in revised form 4 May 2008
Available online 28 June 2008

Keywords:
Anoxia
Phosphorus burial
Organic carbon
Morocco
Cenomanian-Turonian

ABSTRACT

With a multi-proxy approach, an attempt was made to constrain productivity and bottom-water redox conditions and their effects on the phosphorus accumulation rate at the Mohammed Pâge section on the Tarfaya coast, Morocco, during the Cenomanian-Turonian Anoxic Event (OAE 2). A distinct $\delta^{34}\text{C}_{\text{org}}$ isotope excursion of $\sim 2.5\text{\textperthousand}$ occurs close to the top of the section. The unusually abrupt shift of the isotope excursion and disappearance of several planktonic foraminiferal species (e.g. *Rotalipora cushmani* and *Rotalipora greenhornensis*) in this level suggests a hiatus of between 40–60 kyr at the excursion onset. Nevertheless, it was possible to determine both the long-term environmental history as well as the processes that took place immediately prior to and during OAE 2. TOC C values increase gradually from the base of the section (from $\sim 2.5\text{\textperthousand}$ to $\sim 3.5\text{\textperthousand}$) due to a combination of long-term eustatic sea-level rise and subsidence causing the encroachment of less toxic waters into the Tarfaya Basin. Similarly a reduction in the mineralogically constructed ‘detrital index’ can be explained by the decrease in the continental flux of terrigenous material due to a relative sea-level rise. A speciation of phosphorus in the upper part of the section, which spans the start and mid-stages of OAE 2, shows overall higher abundances of $\text{P}_{\text{reactive}}$ mass accumulation rates before the isotope excursion onset and lower values during the plateau. Due to the probable short hiatus, the onset of the decrease in phosphorus content relative to the isotope excursion is uncertain, although the excursion plateau already contains lower concentrations. The $\text{CaCO}_3/\text{Total}$ and V/Al ratios suggest that this reduction was mostly caused by a decreasing CaCO_3 availability being taken up (primarily as a result of increased productivity) and a corresponding fall in the phosphorus retention ability of the system. Productivity appears to have remained high during the isotope plateau possibly due to a combination of ocean-surface fertilisation via increased aridity (increased K/Al and Ti/Al ratios) and/or higher dissolved inorganic phosphorus content in the water column as a result of the decrease in sediment P retention. The evidence for decreased P-burial has been observed in many other palaeoenvironments during OAE 2. Tarfaya’s unique upwelling paleosituation provides strong evidence that the nutrient recycling was a global phenomenon and therefore a critical factor in starting and sustaining OAE 2.

© 2008 Elsevier Ltd. All rights reserved.

1. Introduction

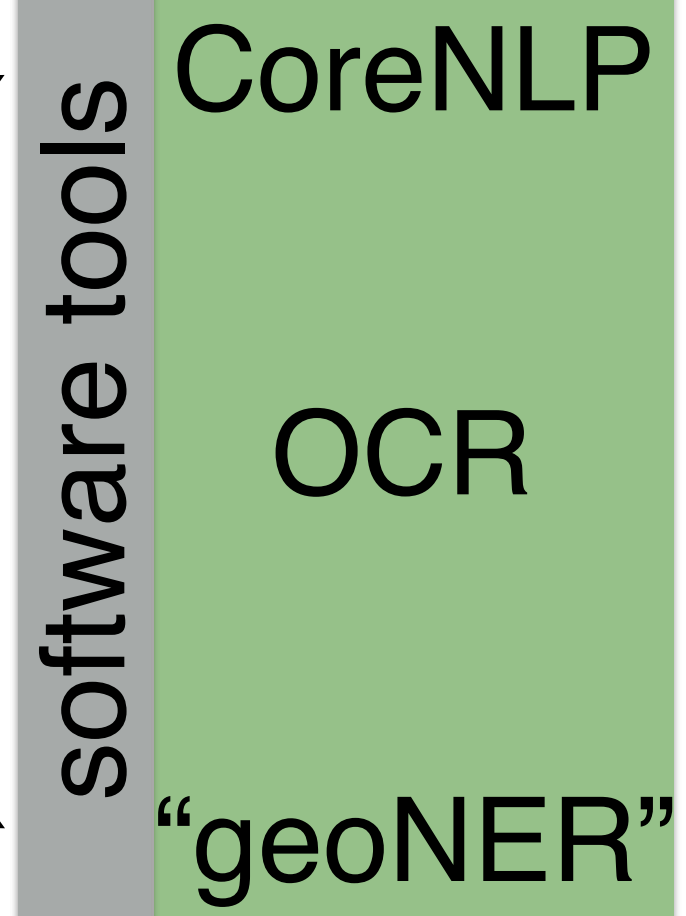
At least seven so-called ‘anoxic events’ punctuated various intervals in the Cretaceous of which one occurred in the latest Cenomanian (Bonarelli Level) dated around 93.5 Ma. Generally these events are characterized by enhanced organic-rich shale deposition and positive $\delta^{13}\text{C}$ excursions (Schlanger and Jenkyns, 1976; Jenkyns, 1980). Although the fundamental causal mechanisms have remained enigmatic, there have been no shortages of ideas that have, at least in part, helped to explain these events. The causal nature of each OAE is likely to be subtly different given the differing sea-level positions, tectonic and paleogeographic situations (Haq et al., 1987; Jenkyns, 1991; Hallam and Wignall, 1999; Aguirre-Franco et al., 2001) and ocean chemistry at each point in time. In terms of the amount and rate of organic carbon sequestration OAE 2 was probably the largest of the anoxic events that punctuated the Cretaceous. Often the debate has centred on the role of preservation and productivity in producing the characteristic positive $\delta^{13}\text{C}$

* Corresponding author.
E-mail address: h.mort@geo.uu.nl (H.P. Mort).

¹ Present address: Department of Earth Sciences – Geochemistry, Faculty of Geosciences, Utrecht University, PO Box 80.021, 3508 CD Utrecht, The Netherlands.

² Present address: Institut de Géologie et de Paléontologie, IGP, Université de Lausanne, Anthropole, CH-1015 Lausanne, Switzerland.

0165-6673/\$ – see front matter © 2008 Elsevier Ltd. All rights reserved.
doi:10.1016/j.cretres.2008.05.026



publisher agreements



doc. fetching/storage



8-12k/day

parsing, annotation, labeling

GeoDeepDive Infrastructure Overview

ScienceDirect

Journals Books

Purchase Export Search ScienceDirect Advanced search

Cretaceous Research

Volume 29, Issues 5–6, October–December 2008, Pages 1008–1023

7th International Symposium on the Cretaceous

Organic carbon deposition and phosphorus accumulation during Oceanic Anoxic Event 2 in Tarfaya, Morocco

Haydon P. Mort^a, Thierry Adatte^{a, 2}, Gerta Keller^b, David Bartels^b, Karl B. Föllmi^{a, 2}, Philipp Steinmann^{a, 2}, Zsolt Berner^c, E.H. Chellai^d

+ Show more

<https://doi.org/10.1016/j.cretres.2008.05.026>

Get rights and content

Cretaceous Research 29 (2008) 1008–1023

Contents lists available at ScienceDirect
Cretaceous Research
journal homepage: www.elsevier.com/locate/CretRes

Organic carbon deposition and phosphorus accumulation during Oceanic Anoxic Event 2 in Tarfaya, Morocco

Haydon P. Mort^{a,*}, Thierry Adatte^{a, 2}, Gerta Keller^b, David Bartels^b, Karl B. Föllmi^{a, 2}, Philipp Steinmann^{a, 2}, Zsolt Berner^c, E.H. Chellai^d

* Rue Emile Argand 11, Institute of Geology, University of Neuchâtel, Case postale 158, CH-2009 Neuchâtel, Switzerland
^a Department of Geosciences, Princeton University, Guyot Hall, Princeton, NJ 08544-1003, USA
^b Institut für Mineralogie und Geochemie, Universität Karlsruhe, 76128 Karlsruhe, Germany
^c University Cadi Ayyad, Faculty of Sciences Semlalia, Marrakech, Morocco

ARTICLE INFO

Received 23 September 2006
Accepted in revised form 4 May 2008
Available online 28 June 2008

Keywords: Anoxia Phosphorus burial Organic carbon Morocco Cenomanian-Turonian

ABSTRACT

With a multi-proxy approach, an attempt was made to constrain productivity and bottom-water redox conditions and their effects on the phosphorus accumulation rate at the Mohammed el-Pege section on the Tarfaya coast, Morocco, during the Cenomanian-Turonian Anoxic Event (OAE 2). A distinct $\delta^{34}\text{C}_{\text{org}}$ isotope excursion of $\sim 2.5\text{\textperthousand}$ occurs close to the top of the section. The unusually abrupt shift of the isotope excursion and disappearance of several planktonic foraminiferal species (e.g. *Rotalipora cushmani* and *Rotalipora greenhornensis*) in this level suggests a hiatus of between 40–60 kyr at the excursion onset. Nevertheless, it was possible to determine both the long-term environmental history as well as the processes that took place immediately prior to and during OAE 2. TOC% values increase gradually from the base of the section (from $\sim 2.5\text{\textperthousand}$ to $\sim 4.5\text{\textperthousand}$) and then decrease during the long-term eustatic sea-level rise and subsidence causing the encroachment of lessoxic waters into the Tarfaya Basin. Similarly a reduction in the mineralogically constructed ‘detrital index’ can be explained by the decrease in the continental flux of terrigenous material due to a relative sea-level rise. A speciation of phosphorus in the upper part of the section, which spans the start and mid-stages of OAE 2, shows overall higher abundances of $\text{P}_{\text{reactive}}$ mass accumulation rates before the isotope excursion onset and lower values during the plateau. Due to the probable short hiatus, the onset of the decrease in phosphorus content relative to the isotope excursion is uncertain, although the excursion plateau already contains lower concentrations. The $\text{CaCO}_3/\text{Total}$ and V/Al ratios suggest that this reduction was mostly caused by a decreasing fall in the phosphorus release ability of the sediment. Productivity appears to have remained high during the isotope plateau possibly due to a combination of ocean-surface fertilisation via increased aridity (increased K/Al and Ti/Al ratios) and/or higher dissolved inorganic phosphorus content in the water column as a result of the decrease in sediment P retention. The evidence for decreased P-burial has been observed in many other palaeoenvironments during OAE 2. Tarfaya’s unique upwelling paleosituation provides strong evidence that the nutrient recycling was a global phenomenon and therefore a critical factor in starting and sustaining OAE 2.

© 2008 Elsevier Ltd. All rights reserved.

1. Introduction

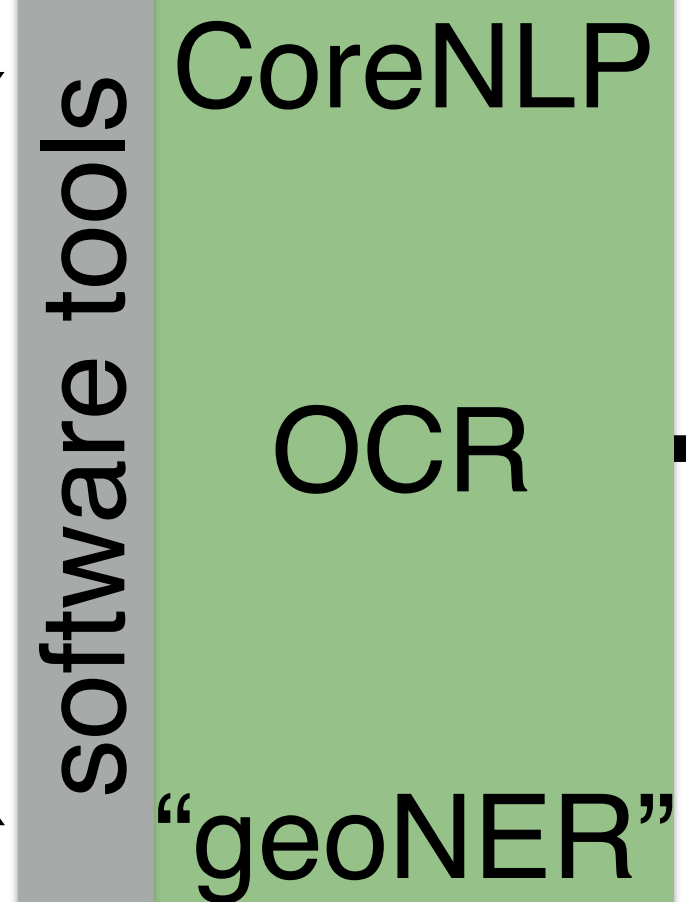
At least seven so-called ‘anoxic events’ punctuated various intervals in the Cretaceous of which one occurred in the latest Cenomanian (Bonarelli Level) dated around 93.5 Ma. Generally these events are characterized by enhanced organic-rich shale deposition

* Corresponding author.
E-mail address: h.mort@geo.uu.nl (H.P. Mort).

¹ Present address: Department of Earth Sciences – Geochemistry, Faculty of Geosciences, Utrecht University, PO Box 80.021, 3508 CD Utrecht, The Netherlands.

² Present address: Institut de Géologie et de Paléontologie, IGP, Université de Lausanne, Anthropole, CH-1015 Lausanne, Switzerland.

0165-6070/\$ - see front matter © 2008 Elsevier Ltd. All rights reserved.
doi:10.1016/j.cretres.2008.05.026



publisher agreements



doc. fetching/storage



8-12k/day

parsing, annotation, labeling

GeoDeepDive Infrastructure Overview

ScienceDirect

Journals Books

Purchase Export Search ScienceDirect Advanced search

Cretaceous Research

Volume 29, Issues 5–6, October–December 2008, Pages 1008–1023

7th International Symposium on the Cretaceous

Organic carbon deposition and phosphorus accumulation during Oceanic Anoxic Event 2 in Tarfaya, Morocco

Haydon P. Mort^a, Thierry Adatte^{a, 2}, Gerta Keller^b, David Bartels^b, Karl B. Föllmi^{a, 2}, Philipp Steinmann^{a, 2}, Zsolt Berner^c, E.H. Chellai^d

+ Show more

<https://doi.org/10.1016/j.cretres.2008.05.026>

Get rights and content

Cretaceous Research 29 (2008) 1008–1023

Contents lists available at ScienceDirect
Cretaceous Research
journal homepage: www.elsevier.com/locate/CretRes

Organic carbon deposition and phosphorus accumulation during Oceanic Anoxic Event 2 in Tarfaya, Morocco

Haydon P. Mort^{a,*}, Thierry Adatte^{a, 2}, Gerta Keller^b, David Bartels^b, Karl B. Föllmi^{a, 2}, Philipp Steinmann^{a, 2}, Zsolt Berner^c, E.H. Chellai^d

* Rue Emile Argand 11, Institute of Geology, University of Neuchâtel, Case postale 158, CH-2009 Neuchâtel, Switzerland
^a Department of Geosciences, Princeton University, Guyot Hall, Princeton, NJ 08544-1003, USA
^b Institut für Mineralogie und Geochemie, Universität Karlsruhe, 76128 Karlsruhe, Germany
^c University Cadi Ayyad, Faculty of Sciences Semlalia, Marrakech, Morocco

ARTICLE INFO

Received 23 September 2006
Accepted in revised form 4 May 2008
Available online 28 June 2008

Keywords: Anoxia Phosphorus burial Organic carbon Morocco Cenomanian-Turonian

ABSTRACT

With a multi-proxy approach, an attempt was made to constrain productivity and bottom-water redox conditions and their effects on the phosphorus accumulation rate at the Mohammed el-Pege section on the Tarfaya coast, Morocco, during the Cenomanian-Turonian Anoxic Event (OAE 2). A distinct $\delta^{34}\text{C}_{\text{org}}$ isotope excursion of $\sim 2.5\text{\textperthousand}$ occurs close to the top of the section. The unusually abrupt shift of the isotope excursion and disappearance of several planktonic foraminiferal species (e.g. *Rotalipora cushmani* and *Rotalipora greenhornensis*) in this level suggests a hiatus of between 40–60 kyr at the excursion onset. Nevertheless, it was possible to determine both the long-term environmental history as well as the processes that took place immediately prior to and during OAE 2. TOC values increase gradually from the base of the section (from $\sim 2.5\text{\textperthousand}$ to $\sim 3.5\text{\textperthousand}$) and then decrease again during the long-term eustatic sea-level rise and subsidence causing the encroachment of lessoxic waters into the Tarfaya Basin. Similarly a reduction in the mineralogically constructed ‘detrital index’ can be explained by the decrease in the continental flux of terrigenous material due to a relative sea-level rise. A speciation of phosphorus in the upper part of the section, which spans the start and mid-stages of OAE 2, shows overall higher abundances of $\text{P}_{\text{reactive}}$ mass accumulation rates before the isotope excursion onset and lower values during the plateau. Due to the probable short hiatus, the onset of the decrease in phosphorus content relative to the isotope excursion is uncertain, although the excursion plateau already contains lower concentrations. The $\text{CaCO}_3/\text{Total}$ and V/Al ratios suggest that this reduction was mostly caused by a decreasing fall in the phosphorus release ability of the sediment. Productivity appears to have remained high during the isotope plateau possibly due to a combination of ocean-surface fertilisation via increased aridity (increased K/Al and Ti/Al ratios) and/or higher dissolved inorganic phosphorus content in the water column as a result of the decrease in sediment P retention. The evidence for decreased P-burial has been observed in many other palaeoenvironments during OAE 2. Tarfaya’s unique upwelling paleosituation provides strong evidence that the nutrient recycling was a global phenomenon and therefore a critical factor in starting and sustaining OAE 2.

© 2008 Elsevier Ltd. All rights reserved.

1. Introduction

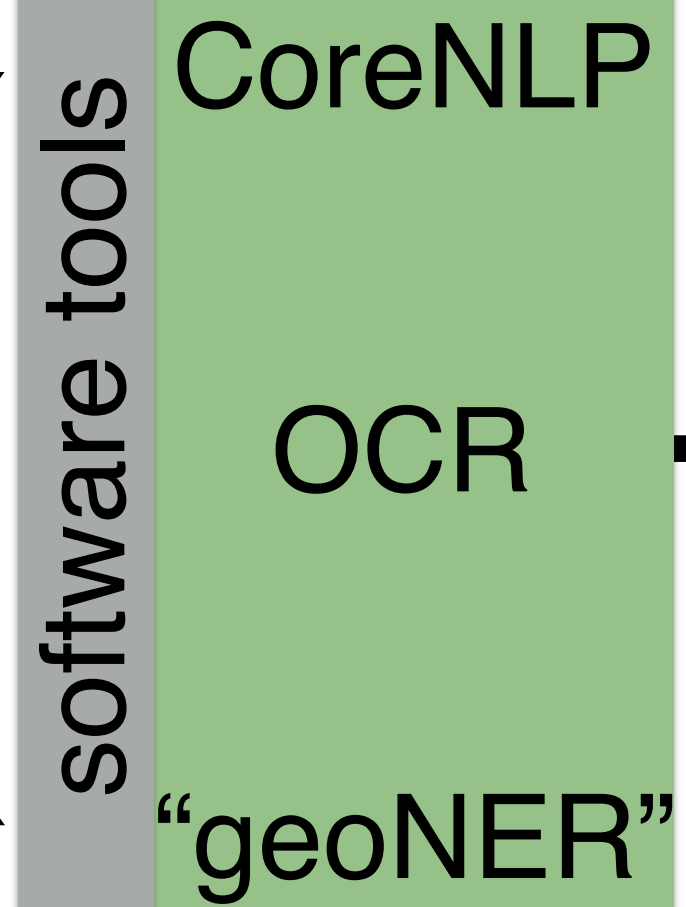
At least seven so-called ‘anoxic events’ punctuated various intervals in the Cretaceous of which one occurred in the latest Cenomanian (Bonarelli Level) dated around 93.5 Ma. Generally these events are characterized by enhanced organic-rich shale deposition

* Corresponding author.
E-mail address: h.mort@geo.uu.nl (H.P. Mort).

¹ Present address: Department of Earth Sciences – Geochemistry, Faculty of Geosciences, Utrecht University, PO Box 80.021, 3508 CD Utrecht, The Netherlands.

² Present address: Institut de Géologie et de Paléontologie, IGP, Université de Lausanne, Anthropole, CH-1015 Lausanne, Switzerland.

0165-6070/\$ – see front matter © 2008 Elsevier Ltd. All rights reserved.
doi:10.1016/j.cretres.2008.05.026



publisher agreements



doc. fetching/storage



8-12k/day

parsing,
annotation,
labeling

COSMOS

GeoDeepDive Infrastructure Overview

ScienceDirect

Journals Books

Purchase Export Search ScienceDirect Advanced search

Cretaceous Research
Volume 29, Issues 5–6, October–December 2008, Pages 1008–1023
7th International Symposium on the Cretaceous

Organic carbon deposition and phosphorus accumulation during Oceanic Anoxic Event 2 in Tarfaya, Morocco

Haydon P. Mort^a, Thierry Adatte^{a, 2}, Gerta Keller^b, David Bartels^b, Karl B. Föllmi^{a, 2}, Philipp Steinmann^{a, 2}, Zsolt Berner^c, E.H. Chellai^d

[+ Show more](#)

<https://doi.org/10.1016/j.cretres.2008.05.026>

Get rights and content

Cretaceous Research 29 (2008) 1008–1023
Contents lists available at ScienceDirect
Cretaceous Research
journal homepage: www.elsevier.com/locate/CretRes

Organic carbon deposition and phosphorus accumulation during Oceanic Anoxic Event 2 in Tarfaya, Morocco

Haydon P. Mort^{a,*}, Thierry Adatte^{a, 2}, Gerta Keller^b, David Bartels^b, Karl B. Föllmi^{a, 2}, Philipp Steinmann^{a, 2}, Zsolt Berner^c, E.H. Chellai^d

* Rue Emile Argand 11, Institute of Geology, University of Neuchâtel, Case postale 158, CH-2009 Neuchâtel, Switzerland
^a Department of Geosciences, Princeton University, Guyot Hall, Princeton, NJ 08544-1003, USA
^b Institut für Mineralogie und Geochemie, Universität Karlsruhe, 76128 Karlsruhe, Germany
^c University Cadi Ayyad, Faculty of Sciences Semlalia, Marrakech, Morocco

ARTICLE INFO

Received 23 September 2006
Accepted in revised form 4 May 2008
Available online 28 June 2008

Keywords: Anoxia Phosphorus burial Organic carbon Morocco Cenomanian-Turonian

ABSTRACT

With a multi-proxy approach, an attempt was made to constrain productivity and bottom-water redox conditions and their effects on the phosphorus accumulation rate at the Mohammed Isgane section on the Tarfaya coast, Morocco, during the Cenomanian-Turonian Anoxic Event (OAE 2). A distinct $\delta^{34}\text{C}_{\text{org}}$ isotope excursion of $+2.5\text{\textperthousand}$ occurs close to the top of the section. The unusually abrupt shift of the isotope excursion and disappearance of several planktonic foraminiferal species (e.g. *Rotalipora cushmani* and *Rotalipora greenhornensis*) in this level suggests a hiatus of between 40–60 kyr at the excursion onset. Nevertheless, it was possible to determine both the long-term environmental history as well as the processes that took place immediately prior to and during OAE 2. TOC_x values increase gradually from the base of the section (from c. 2.5% to c. 4.5%) and then decrease again towards the top of the section. This pattern is interpreted as reflecting a long-term eustatic sea-level rise and subsidence causing the encroachment of lessoxic waters into the Tarfaya Basin. Similarly a reduction in the mineralogically constructed ‘detrital index’ can be explained by the decrease in the continental flux of terrigenous material due to a relative sea-level rise. A speciation of phosphorus in the upper part of the section, which spans the start and mid-stages of OAE 2, shows overall higher abundances of $\text{P}_{\text{reactive}}$ mass accumulation rates before the isotope excursion onset and lower values during the plateau. Due to the probable short hiatus, the onset of the decrease in phosphorus content relative to the isotope excursion is uncertain, although the excursion plateau already contains lower concentrations. The $\text{CaCO}_3/\text{Total}$ and V/I ratios suggest that this reduction was mostly caused by a decrease in the availability of oxygenated calcareous (primarily as a result of reduced productivity) and a corresponding fall in the phosphorus retention ability of the system. Productivity appears to have remained high during the isotope plateau possibly due to a combination of ocean-surface fertilisation via increased aridity (increased K/I and T/U ratios) and/or higher dissolved inorganic phosphorus content in the water column as a result of the decrease in sediment P retention. The evidence for decreased P-burial has been observed in many other palaeoenvironments during OAE 2. Tarfaya’s unique upwelling paleosituation provides strong evidence that the nutrient recycling was a global phenomenon and therefore a critical factor in starting and sustaining OAE 2.

© 2008 Elsevier Ltd. All rights reserved.

1. Introduction

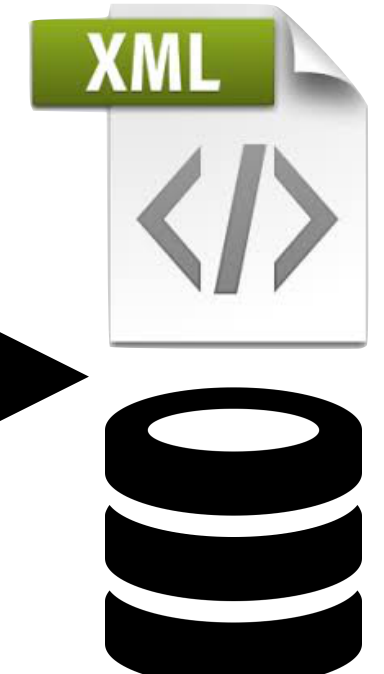
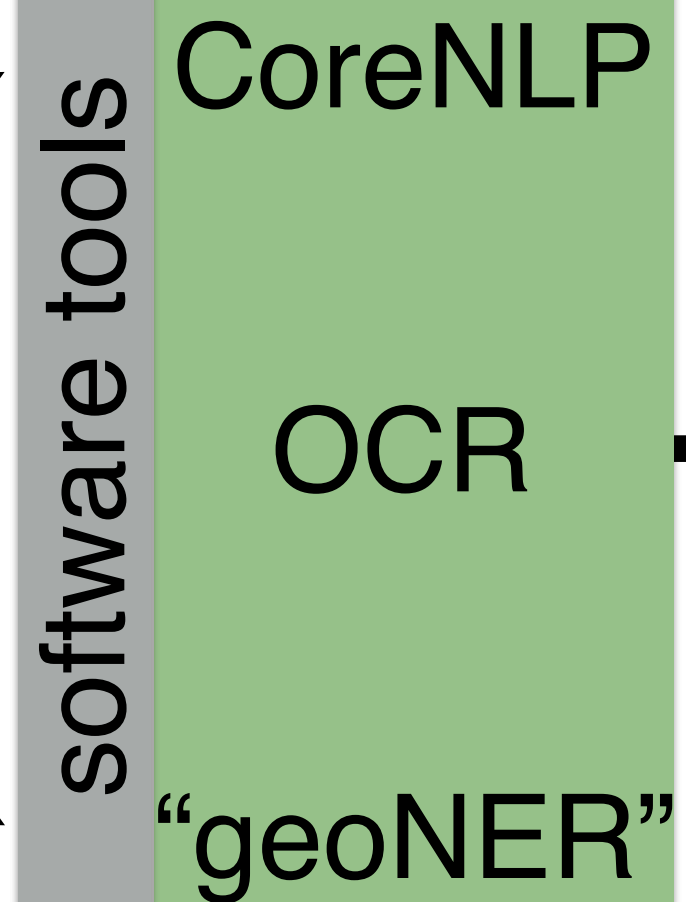
At least seven so-called ‘anoxic events’ punctuated various intervals in the Cretaceous of which one occurred in the latest Cenomanian (Bonarelli Level) dated around 93.5 Ma. Generally these events are characterized by enhanced organic-rich shale deposition

* Corresponding author.
E-mail address: h.mort@geo.uu.nl (H.P. Mort).

¹ Present address: Department of Earth Sciences – Geochemistry, Faculty of Geosciences, Utrecht University, PO Box 80021, 3508 CD Utrecht, The Netherlands.

² Present address: Institut de Géologie et de Paléontologie, IGP, Université de Lausanne, Anthropole, CH-1015 Lausanne, Switzerland.

0165-6070/\$ – see front matter © 2008 Elsevier Ltd. All rights reserved.
doi:10.1016/j.cretres.2008.05.026



publisher agreements



doc. fetching/storage



8-12k/day

Science!

parsing,
annotation,
labeling

COSMOS

GeoDeepDive Infrastructure Overview

ScienceDirect

Journals Books

Purchase Export Search ScienceDirect Advanced search

Cretaceous Research
Volume 29, Issues 5–6, October–December 2008, Pages 1008–1023
7th International Symposium on the Cretaceous

Organic carbon deposition and phosphorus accumulation during Oceanic Anoxic Event 2 in Tarfaya, Morocco

Haydon P. Mort^a, Thierry Adatte^{a, 2}, Gerta Keller^b, David Bartels^b, Karl B. Föllmi^{a, 2}, Philipp Steinmann^{a, 2}, Zsolt Berner^c, E.H. Chellai^d

[+ Show more](#)

<https://doi.org/10.1016/j.cretres.2008.05.026>

Get rights and content

Cretaceous Research 29 (2008) 1008–1023
Contents lists available at ScienceDirect
Cretaceous Research
journal homepage: www.elsevier.com/locate/CretRes

Organic carbon deposition and phosphorus accumulation during Oceanic Anoxic Event 2 in Tarfaya, Morocco

Haydon P. Mort^{a,*}, Thierry Adatte^{a, 2}, Gerta Keller^b, David Bartels^b, Karl B. Föllmi^{a, 2}, Philipp Steinmann^{a, 2}, Zsolt Berner^c, E.H. Chellai^d

* Rue Emile Argand 11, Institute of Geology, University of Neuchâtel, Case postale 158, CH-2009 Neuchâtel, Switzerland
^a Department of Geosciences, Princeton University, Guyot Hall, Princeton, NJ 08544-1003, USA
^b Institut für Mineralogie und Geochemie, Universität Karlsruhe, 76128 Karlsruhe, Germany
^c University Cadi Ayyad, Faculty of Sciences Semlalia, Marrakech, Morocco

ARTICLE INFO

Received 23 September 2006
Accepted in revised form 4 May 2008
Available online 28 June 2008

Keywords: Anoxia Phosphorus burial Organic carbon Morocco Cenomanian-Turonian

ABSTRACT

With a multi-proxy approach, an attempt was made to constrain productivity and bottom-water redox conditions and their effects on the phosphorus accumulation rate at the Mohammed Isgane section on the Tarfaya coast, Morocco, during the Cenomanian-Turonian Anoxic Event (OAE 2). A distinct $\delta^{34}\text{C}_{\text{org}}$ isotope excursion of $+2.5\text{\textperthousand}$ occurs close to the top of the section. The unusually abrupt shift of the isotope excursion and disappearance of several planktonic foraminiferal species (e.g. *Rotalipora cushmani* and *Rotalipora greenhornensis*) in this level suggests a hiatus of between 40–60 kyr at the excursion onset. Nevertheless, it was possible to determine both the long-term environmental history as well as the processes that took place immediately prior to and during OAE 2. TOC C values increase gradually from the base of the section (from $\sim 2.5\text{\textperthousand}$ to $\sim 4.5\text{\textperthousand}$) due to a combination of long-term eustatic sea-level rise and subsidence causing the encroachment of lessoxic waters into the Tarfaya Basin. Similarly a reduction in the mineralogically constructed ‘detrital index’ can be explained by the decrease in the continental flux of terrigenous material due to a relative sea-level rise. A speciation of phosphorus in the upper part of the section, which spans the start and mid-stages of OAE 2, shows overall higher abundances of $\text{P}_{\text{reactive}}$ mass accumulation rates before the isotope excursion onset and lower values during the plateau. Due to the probable short hiatus, the onset of the decrease in phosphorus content relative to the isotope excursion is uncertain, although the excursion plateau already contains lower concentrations. The $\text{CaCO}_3/\text{Total}$ and V/Al ratios suggest that this reduction was mostly caused by a decrease in average biological oxygen consumption (productivity as a measure of primary productivity) and a corresponding fall in the phosphorus retention ability of the system. Productivity appears to have remained high during the isotope plateau possibly due to a combination of ocean-surface fertilisation via increased aridity (increased K/Al and V/Al ratios) and/or higher dissolved inorganic phosphorus content in the water column as a result of the decrease in sediment P retention. The evidence for decreased P-burial has been observed in many other palaeoenvironments during OAE 2. Tarfaya’s unique upwelling paleosituation provides strong evidence that the nutrient recycling was a global phenomenon and therefore a critical factor in starting and sustaining OAE 2.

© 2008 Elsevier Ltd. All rights reserved.

1. Introduction

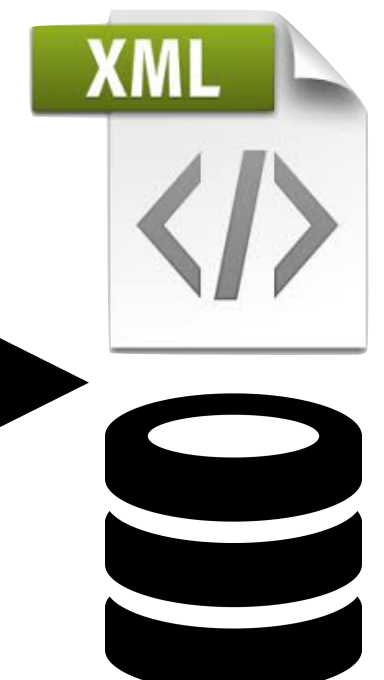
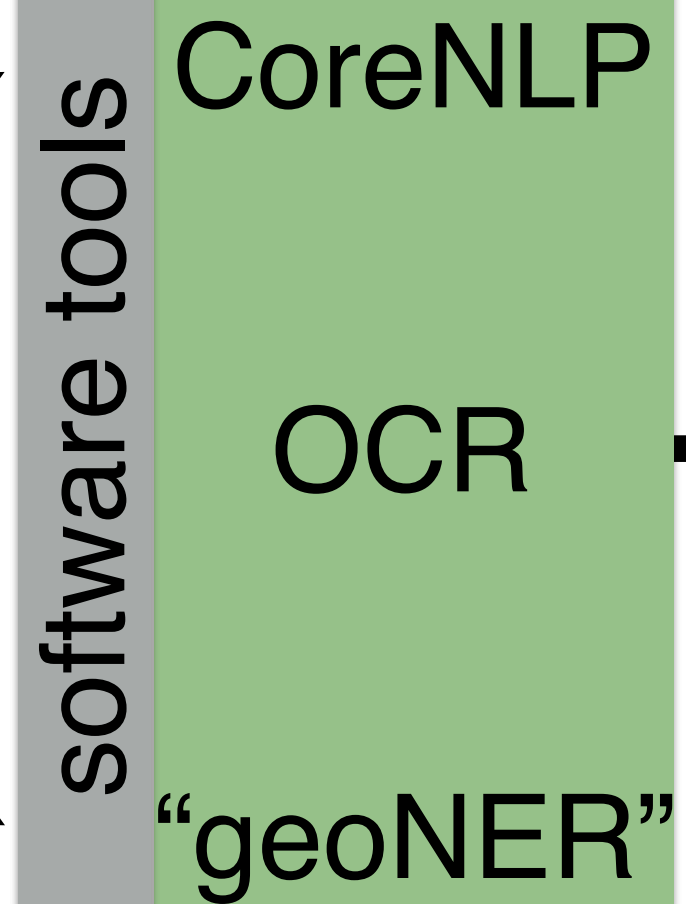
At least seven so-called ‘anoxic events’ punctuated various intervals in the Cretaceous of which one occurred in the latest Cenomanian (Bonarelli Level) dated around 93.5 Ma. Generally these events are characterized by enhanced organic-rich shale deposition

* Corresponding author.
E-mail address: h.mort@geo.uu.nl (H.P. Mort).

¹ Present address: Department of Earth Sciences – Geochemistry, Faculty of Geosciences, Utrecht University, PO Box 80.021, 3508 CD Utrecht, The Netherlands.

² Present address: Institut de Géologie et de Paléontologie, IGP, Université de Lausanne, Anthropole, CH-1015 Lausanne, Switzerland.

0165-6673/\$ – see front matter © 2008 Elsevier Ltd. All rights reserved.
doi:10.1016/j.cretres.2008.05.026



publisher agreements



doc. fetching/storage



8-12k/day

parsing, annotation, labeling

Science!

COSMOS

Original document data and metadata curation



```
<doi_record>
<journal_metadata language="en">
<full_title>Annals of the New York Academy of
Sciences</full_title>
</journal_metadata>
<journal_issue>
<publication_date media_type="print">
    <month>03</month>
    <year>1956</year>
</publication_date>
<journal_volume>
<volume>63</volume>
<doi_data>
<doi>10.1111/nyas.1956.63.issue-6</doi>
</doi_data>
<titles>
<title>TOPOLOGICAL CYTOCHEMISTRY</title>
</titles>
<contributors>
<person_name contributor_role="author"
sequence="first">
<given_name>M. J.</given_name>
<surname>Kopac</surname>
</person_name>
</contributors>
<first_page>1219</first_page>
<last_page>1235</last_page>
</pages>
```



Original PDFs



ELSEVIER

```
{u'dc:title': u'Editorial Board',
 u'prism:coverDate': [{u'$':
u'2011-01-01', u'@_fa':
u'true'}],
 u'prism:coverDisplayDate':
u'January\u2013June 2011',
 u'prism:doi': u'10.1016/
S0753-3969(11)00046-2',
 u'prism:publicationName':
u'Annales de Pal\xe9ontologie',
 u'prism:startingPage': u'i',
 u'prism:volume': u'97'}
```

Original document data and metadata curation



```
<doi_record>
<journal_metadata language="en">
<full_title>Annals of the New York Academy of
Sciences</full_title>
</journal_metadata>
<journal_issue>
<publication_date media_type="print">
    <month>03</month>
    <year>1956</year>
</publication_date>
<journal_volume>
<volume>63</volume>
<doi_data>
<doi>10.1111/nyas.1956.63.issue-6</doi>
</doi_data>
<titles>
<title>TOPOLOGICAL CYTOCHEMISTRY</title>
</titles>
<contributors>
<person_name contributor_role="author"
sequence="first">
<given_name>M. J.</given_name>
<surname>Kopac</surname>
</person_name>
</contributors>
<first_page>1219</first_page>
<last_page>1235</last_page>
</pages>
```



Original PDFs

Fetched by GDD



```
{u'dc:title': u'Editorial Board',
 u'prism:coverDate': [{u'$':
u'2011-01-01', u'@_fa':
u'true'}],
 u'prism:coverDisplayDate':
u'January\u2013June 2011',
 u'prism:doi': u'10.1016/
S0753-3969(11)00046-2',
 u'prism:publicationName':
u'Annales de Pal\xe9ontologie',
 u'prism:startingPage': u'i',
 u'prism:volume': u'97'}
```

Harmonized Document Metadata (bibJSON files + mongoDB)

```
{
  "authors": "Kopac, M. J.",
  "coverDate": "March 1956",
  "publication_date": {"month": 3, "year": 1956},
  "publisher": "Wiley-Blackwell",
  "pubname": "Annals of the New York Academy of Sciences",
  "sha1": "01b2fcc8a94a2bfbe785812aab28e45fcbe02d3f",
  "startingPage": "1219",
  "time": ["2016-03-17T08:39:22.532-05:00"],
  "title": "TOPOLOGICAL CYTOCHEMISTRY",
  "vol": "63",
  "doi": "10.1111/j.1749-6632.1956.tb32132.x",
  "url": "http://doi.wiley.com/10.1111/j.
1749-6632.1956.tb32132.x"
}

{
  "coverDate": "January–June 2011",
  "publication_date": {"month": 6, "year": 2011},
  "publisher": "Elsevier",
  "pubname": "Annales de Paléontologie",
  "sha1": "6ee25a57571021e45faa1b545a5c59b9748ada7b",
  "startingPage": "i",
  "time": "2015-07-09T15:00:17.875-05:00",
  "title": "Editorial Board",
  "vol": "97",
  "doi": "10.1016/S0753-3969(11)00046-2",
  "url": "http://www.sciencedirect.com/science/article/pii/
S0753396911000462"
}
```

Vocabulary ingestion and labeling

geodeepdive.org/api/dictionaries

curated lists of terms
with hierarchy/context:



The Paleobiology Database
revealing the history of life



mindat.org



6k
mineral names/
chemistry



45k
stratigraphic names/
hierarchy, rock types

GDD-supplied full text
and citation info.

Pyritization of soft-bodied fossils: Beecher's Trilobite Bed, Upper Ordovician, New York State

Derek E.G. Briggs
Department of Geology, University of Bristol, Wills Memorial Building, Queen's Road
Bristol BS8 1RJ, England
Simon H. Bottrell, Robert Raiswell
Department of Earth Sciences, University of Leeds, Leeds LS2 9JT, England

ABSTRACT
Although pyrite is ubiquitous in fine-grained, organic, carbon-bearing marine sediments, it is only rarely involved in the preservation of soft-bodied organisms. Beecher's Trilobite Bed in Upper Ordovician strata of New York State is an exception—it is a classic locality for trilobites having appendages and other soft tissues preserved in pyrite. The relative timing and duration of the formation of pyrite associated with the fossils and their host sediments were determined by use of sulfur isotope ratios. The exoskeleton and appendages of the trilobites show relatively light sulfur isotope values in contrast to the enclosing sediment, which is characterized by a substantial excursion to heavy isotope values. Preservation of soft parts requires rapid burial of carcasses in sediments otherwise low in metabolizable organic matter. In these circumstances, pyrite formation within the sediments is suppressed; thus, concentrations of sulfate and reactive iron are initially high enough to promote early, rapid, and extensive pyritization of nonmineralized tissue.

INTRODUCTION
Fossils that preserve soft tissues provide critical evidence of the morphology and paleobiology of extinct organisms—in contrast to normal shelly fossil assemblages, which yield only limited information. Soft tissues (i.e., those lacking any mineral component in life) may be preserved in a variety of ways. Those that are particularly decay resistant (cuticles composed of lignin, sporopollenin, cutan, sclerotized chitin, for example) may become fossilized as stable kerogen compounds in certain environments (Tegelaar et al., 1989; Jeram et al., 1990). Tissues more susceptible to bacterial breakdown (e.g., muscles, internal organs, thin cuticles) survive only where they are replicated by very early authigenic mineralization (Allison, 1988b). This normally involves one of three groups of diagenetic minerals: phosphate, carbonate, or pyrite. Pyrite is commonly a component of fine-grained, organic-rich marine sediments, forming by reactions between detrital iron minerals and the H₂S generated by anaerobic sulfate-reducing bacteria (Goldhaber and Kaplan, 1974). In marine sediments, iron and seawater sulfate are normally present in abundance, and pyrite formation is apparently controlled by the concentration of metabolizable organic carbon (Berner, 1970, 1984).

Although pyrite is widespread in marine sediments, and commonly is found in association with fossils, these are usually the remains of mineralized (Hudson, 1982), or at least refractory, tissues (e.g., in plants; Kenrick and Edwards, 1988). Beecher's Trilobite Bed (named after the Yale paleontologist who worked extensively on the trilobites in the 1890s) is one of the very rare examples where pyrite formed early enough to contribute to the preservation of soft tissues. Only the Devonian (lower Emsian) Hunsrückschiefer of western Germany (Stürmer et al., 1980; Kott and Wuttke, 1987; Bartels and Brassel, 1990), which preserves the soft tissues of trilobites (Stürmer and Bergström, 1973), cephalopods (Stürmer, 1985), and ctenophores (Stanley and Stürmer, 1987), for example, is comparable.

Figure 1. *Triarthus eatoni*, ~30 mm long, from Beecher's Trilobite Bed (photograph by J. E. Almond, provided by H. B. Whittington).

Beecher's Bed is additionally important as the only major occurrence of soft-bodied organisms (Konservat-Lagerstätte) known from the Ordovician (Allison and Briggs, 1991). In this paper we analyze the mineralization of the trilobites in Beecher's Bed and present a model for the pyritization of soft tissues in the fossil record.

GEOLOGY, v. 19, p. 1221–1224, December 1991

1221

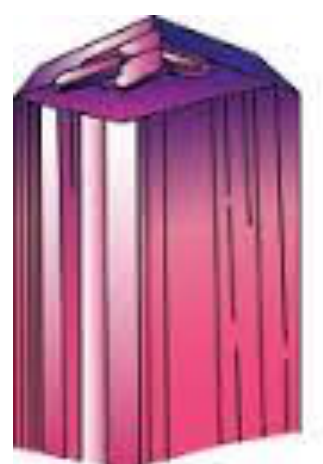
Vocabulary ingestion and labeling

geodeepdive.org/api/dictionaries

curated lists of terms
with hierarchy/context:



The Paleobiology Database
revealing the history of life



mindat.org

→ 350k
taxonomic names/
bio classification



→ 45k
stratigraphic names/
hierarchy, rock types

GDD-supplied full text
and citation info.

Pyritization of soft-bodied fossils: Beecher's Trilobite Bed, Upper Ordovician, New York State

Derek E.G. Briggs
Department of Geology, University of Bristol, Wills Memorial Building, Queen's Road
Bristol BS8 1RJ, England
Simon H. Bottrell, Robert Raiswell
Department of Earth Sciences, University of Leeds, Leeds LS2 9JT, England

ABSTRACT
Although pyrite is ubiquitous in fine-grained, organic, carbon-bearing marine sediments, it is only rarely involved in the preservation of soft-bodied organisms. Beecher's Trilobite Bed in Upper Ordovician strata of New York State is an exception—it is a classic locality for trilobites having appendages and other soft tissues preserved in pyrite. The relative timing and duration of the formation of pyrite associated with the fossils and their host sediments were determined by use of sulfur isotope ratios. The exoskeleton and appendages of the trilobites show relatively light sulfur isotope values in contrast to the enclosing sediment, which is characterized by a substantial excursion to heavy isotope values. Preservation of soft parts requires rapid burial of carcasses in sediments otherwise low in metabolizable organic matter. In these circumstances, pyrite formation within the sediments is suppressed; thus, concentrations of sulfate and reactive iron are initially high enough to promote early, rapid, and extensive pyritization of nonmineralized tissue.

INTRODUCTION
Fossils that preserve soft tissues provide critical evidence of the morphology and paleobiology of extinct organisms—in contrast to normal shelly fossil assemblages, which yield only limited information. Soft tissues (i.e., those lacking any mineral component in life) may be preserved in a variety of ways. Those that are particularly decay resistant (cuticles composed of lignin, sporopollenin, cutan, sclerotized chitin, for example) may become fossilized as stable kerogen compounds in certain environments (Tegelaar et al., 1989; Jeram et al., 1990). Tissues more susceptible to bacterial breakdown (e.g., muscles, internal organs, thin cuticles) survive only where they are replicated by very early authigenic mineralization (Allison, 1988b). This normally involves one of three groups of diagenetic minerals: phosphate, carbonate, or pyrite. Pyrite is commonly a component of fine-grained, organic-rich marine sediments, forming by reactions between detrital iron minerals and the H₂S generated by anaerobic sulfate-reducing bacteria (Goldhaber and Kaplan, 1974). In marine sediments, iron and seawater sulfate are normally present in abundance, and pyrite formation is apparently controlled by the concentration of metabolizable organic carbon (Berney, 1970, 1984).

Although pyrite is widespread in marine sediments, and commonly is found in association with fossils, these are usually the remains of mineralized (Hudson, 1982), or at least refractory, tissues (e.g., in plants; Kenrick and Edwards, 1988). Beecher's Trilobite Bed (named after the Yale paleontologist who worked extensively on the trilobites in the 1890s) is one of the very rare examples where pyrite formed early enough to contribute to the preservation of soft tissues. Only the Devonian (lower Emsian) Hunsrückschiefer of western Germany (Stürmer et al., 1980; Kott and Wuttke, 1987; Bartels and Brassel, 1990), which preserves the soft tissues of trilobites (Stürmer and Bergström, 1973), cephalopods (Stürmer, 1985), and ctenophores (Stanley and Stürmer, 1987), for example, is comparable.

Figure 1. *Triarthrus eatoni*, ~30 mm long, from Beecher's Trilobite Bed (photograph by J. E. Almond, provided by H. B. Whittington).

Beecher's Bed is additionally important as the only major occurrence of soft-bodied organisms (Konservat-Lagerstätte) known from the Ordovician (Allison and Briggs, 1991). In this paper we analyze the mineralization of the trilobites in Beecher's Bed and present a model for the pyritization of soft tissues in the fossil record.

1221

labeled
entities, tuples

[Trilobita](#)
[Triarthrus](#)
[Climacograptus](#)

[pyrite](#)

[Frankfort Shale](#)

exposed
via API

"term_hits": { ▼ 189470 properties, 6 MB

"Navajosuchus novomexicanus": 7,
"Ptilocolepidae": 2,
"Geotrupidae": 652,
"Macropoma lewesiensis": 11,
"Simia morio": 7,
"Anhanguera robustus": 4,
"Montipora verrilli": 36,
"Geffenina wangii": 6,
"Shuvosaurus": 198,
"Dryorhizopsidae": 1,
"Ostrea antarctica": 12,
"Pholidophorus dentatus": 10,
"Oochorista": 6,
"Sciurus arizonensis": 18,
"Probole biexcisa": 3,
"Toxopatagus": 271,
"Sulcavitus": 169,
"Brontops amplus": 2,
"Melonella": 1087,
"Bathrotomaria": 688,
"Placochelyanus": 64,
"Ilioichione": 555,
"Attenosaurus subulensis": 10,
"Miccylotyrans": 4,

"Deryeuma": 4,
"Chaetabraleus": 2,
"Cardinalis cardinalis": 1113,
"Odontaster": 2532,
"Coeloma": 384,
"Megatrema": 36,
"Xinjiangtitan": 4,
"Tephrodytes brassicarvalis": 74,
"Prolagus crusafonti": 42,
"Streblascopora germana": 2,
"Dichobunoidea": 11,
"Cetotherium hupschi": 1,
"Hauericeras (Gardeniceras) gardeni": 10,
"Parevania": 15,
"Histriobdellidae": 130,
"Berosus (Berosus)": 13,
"Dinornis elephantopus": 8,
"Sternoxi": 11,
"Bellimurina (Bellimurina)": 4,
"Raphignathoidea": 76,
"Cybelurus occidentalis": 4,



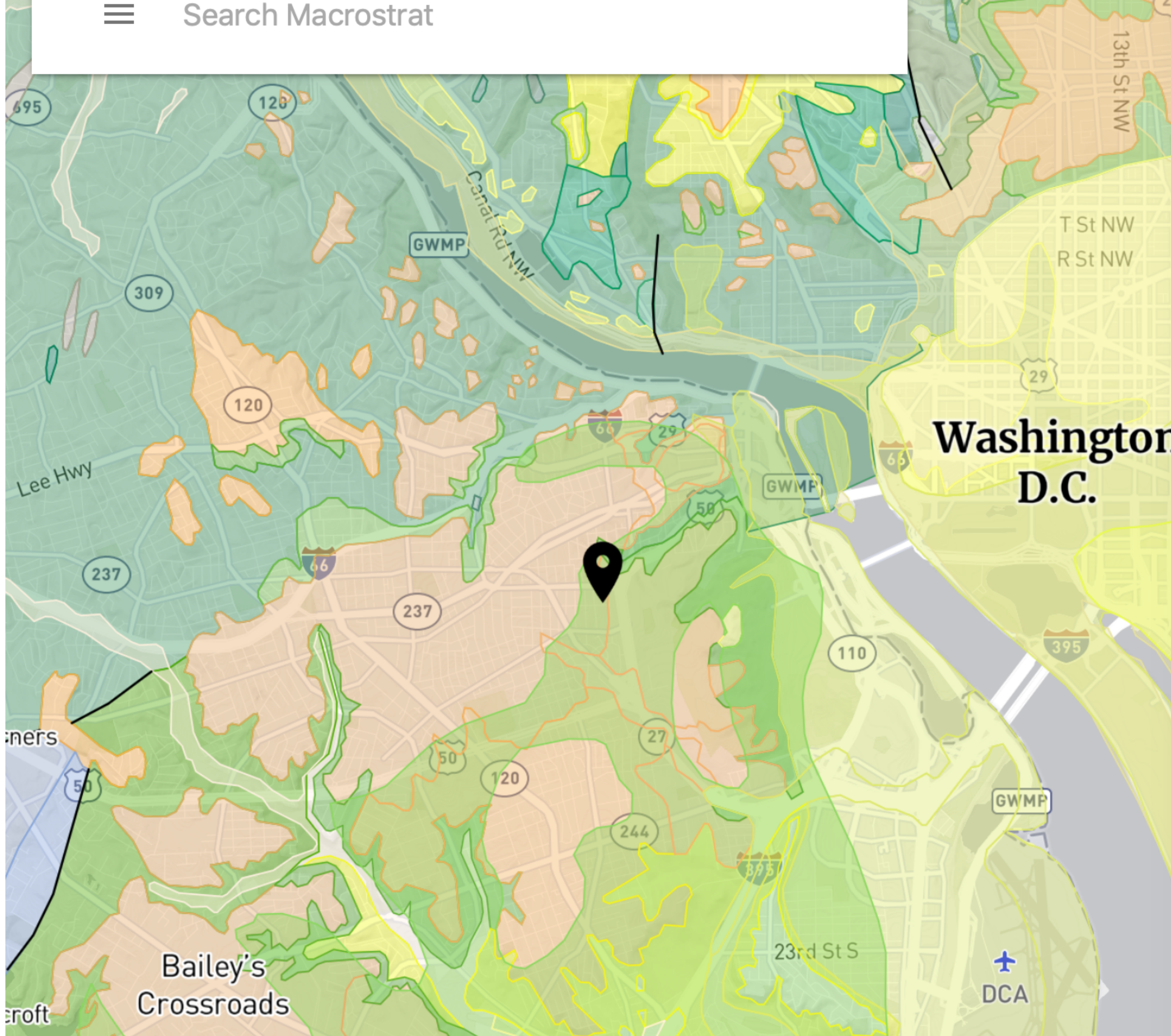
Define your own dictionaries:

https://github.com/UW-Deepdive-Infrastructure/dictionary_example

```
"term_hits": { ▼ 189470
  "Navajosuchus novomexicanus": 1,
  "Ptilocolepididae": 2,
  "Geotrupidae": 652,
  "Macropoma lewesiensis": 1,
  "Simia morio": 7,
  "Anhanguera robustus": 1,
  "Montipora verrilli": 1,
  "Geffenina wangi": 6,
  "Shuvosaurus": 198,
  "Dryorhizopsidae": 1,
  "Ostrea antarctica": 1,
  "Pholidophorus dentatus": 1,
  "Oochorista": 6,
  "Sciurus arizonensis": 1,
  "Prosbolus biexcisa": 3,
  "Toxopatagus": 271,
  "Sulcavitus": 169,
  "Brontops amplus": 2,
  "Melonella": 1087,
  "Bathrotomaria": 688,
  "Placochelyanus": 64,
  "Iliochione": 555,
  "Attenosaurus subulensis": 10,
  "Miccylyotyrans": 4,
  "pubname": "Earth-Science Reviews",
  "publisher": "Elsevier",
  "title": "The Cambrian palaeontological record of the Indian subcontinent",
  "coverDate": "Available online 11 June 2016",
  "URL": "http://www.sciencedirect.com/science/article/pii/S0012825216301179",
  "authors": "Hughes, Nigel C.",
  "hits": 4,
  "highlight": [ ▼ 4 items, 411 bytes
    " represented is the hyolithimorph Sulcavitus wynnei (Waagen, 1885) collected from several horizons within",
    ") Hy Sulcavitus wynnei (Waagen), dorsum, Khussak Formation, Salt Range, SH, GSI 4118 (CMCIP 71490",
    ",") Kruse and Hughes in press, fig. 5C, scale bar: 2.5 mm; T) Hy Sulcavitus wynnei (Waagen), venter",
    " 71490), Kruse and Hughes in press, fig. 5A, scale bar: 2.5 mm; U) Hy Sulcavitus wynnei (Waagen"
  ]
},
{ ▼ 8 properties, 431 bytes
  "pubname": "Alcheringa: An Australasian Journal of Palaeontology",
  "publisher": "Taylor and Francis",
  "title": "Biostratigraphic potential of Middle Cambrian hyoliths from the eastern Georgina Basin",
  "coverDate": "2002 01",
  "URL": "http://www.tandfonline.com/doi/abs/10.1080/03115510208619263",
  "authors": "Kruse, Peter D.",
  "hits": 1,
  "highlight": [ ▼ 1 item, 94 bytes
    ",it is noteworthy that Sulcavitus possesses a distinctive deep median sulcus on the dorsum"
  ]
}
```



Define your own dictionaries:
https://github.com/UW-Deepdive-Infrastructure/dictionary_example



Primary Literature via
GeoDeepDive

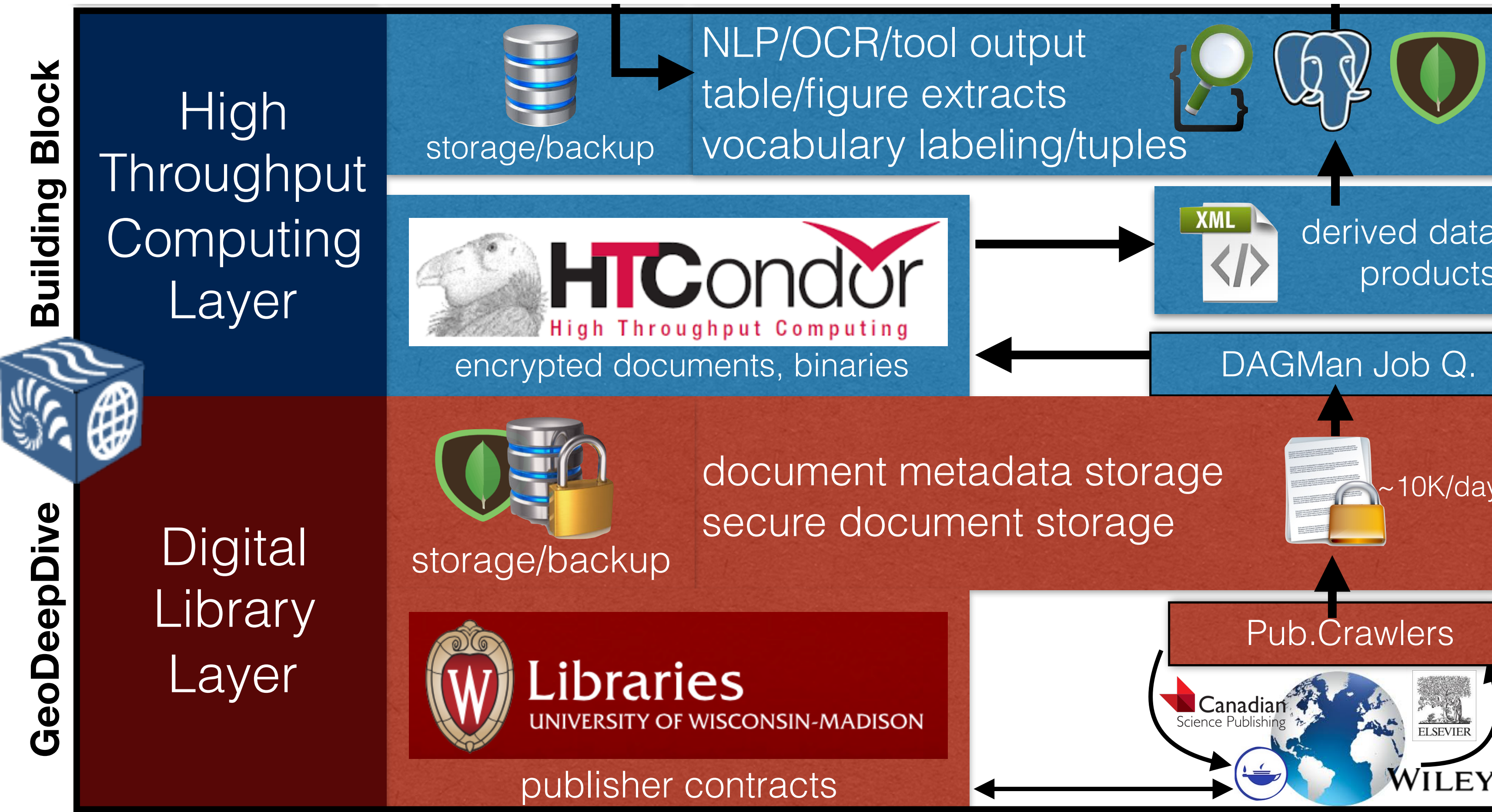
Palaeogeography, Palaeoclimatology, Palaeoecology Elsevier

Wolfe, Jack A., Upchurch, Garland R.,
1987. **North American nonmarine**
climates and vegetation during the
Late Cretaceous.

...First , toothed angiosperm leaves
appear by the Aptian (e.g. ,
Quercophyllum in Zone I of the **Potomac**
Group ; Hickey and Doyle , 1977) , and
virtually all other major physiognomic
types of dicotyledonous leaves appeared
by the early Cenomanian (Zone III of the
Potomac Group ; Upchurch and Wolfe
, 1987)

Uličný, David, Kvaček, Jiří, Svobodová,
Marcela, Špičáková, Lenka, 1997. High-
frequency sea-level fluctuations and
plant habitats in Cenomanian fluvial
depositional systems.

GeoDeepDive: key components

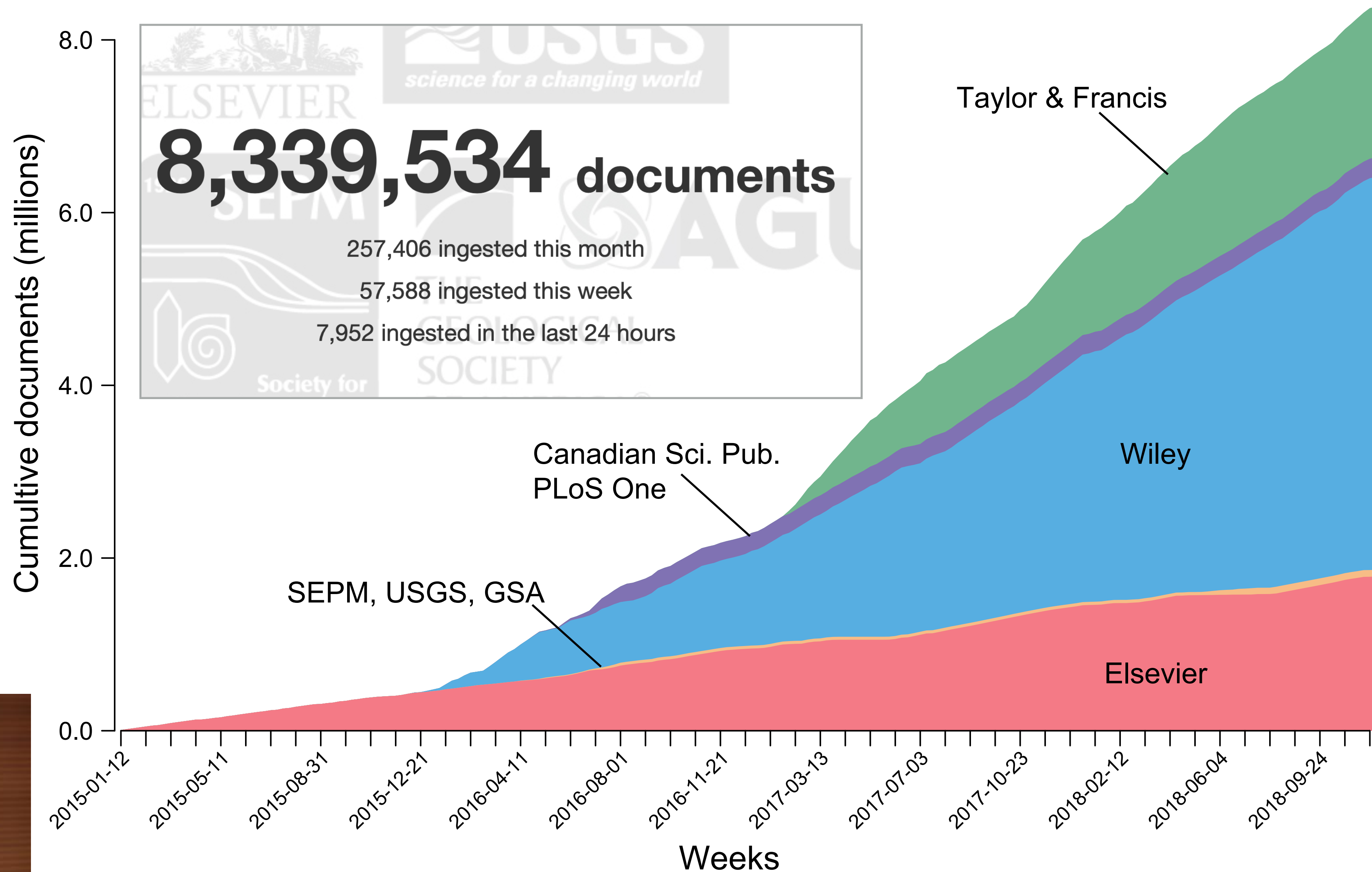


- Permissive, custom agreements with content owners that enable local storage, collaborative use.
- Automated system for acquiring documents and metadata from multiple providers.
- ElasticSearch for simple full-text word/phrase matching, cached results for large vocabularies.
- Harmonized document metadata for citation & linking to original content.
- Computing resources to rapidly re-analyze all documents.



support 2014-2018 by NSF-ICER 1343760
partial current support from USGS

✓ Principled access to scientific literature



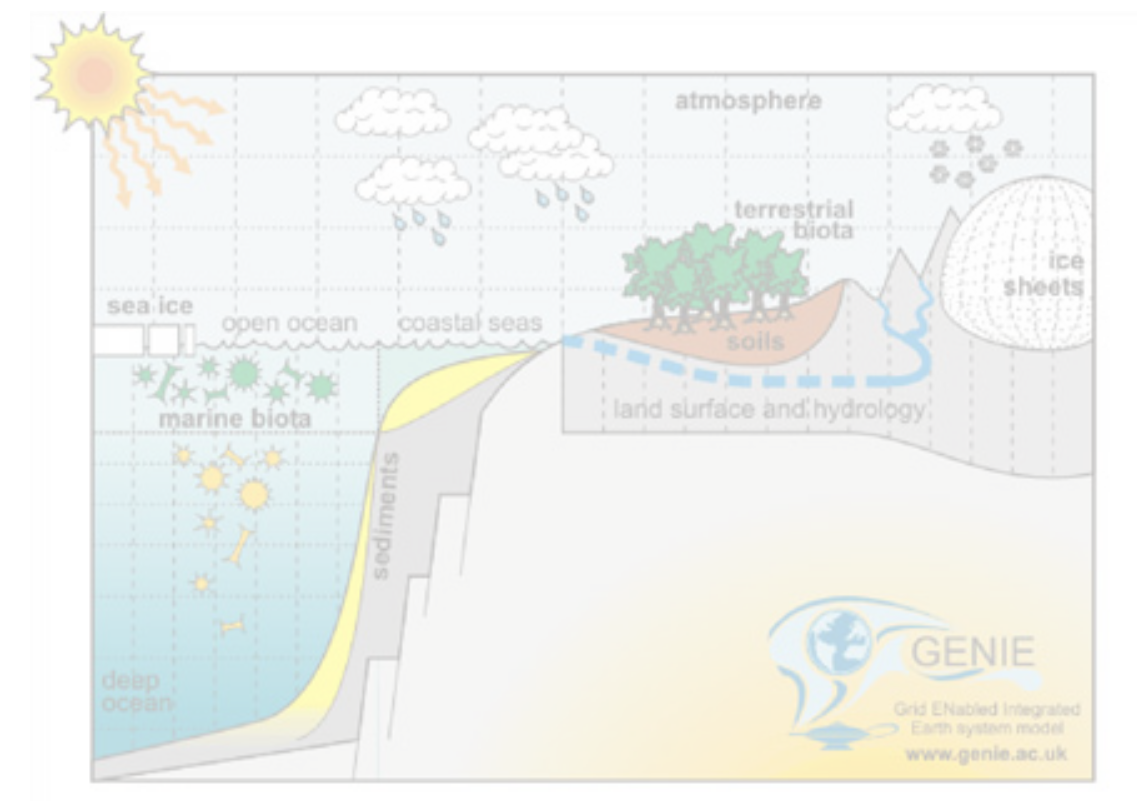
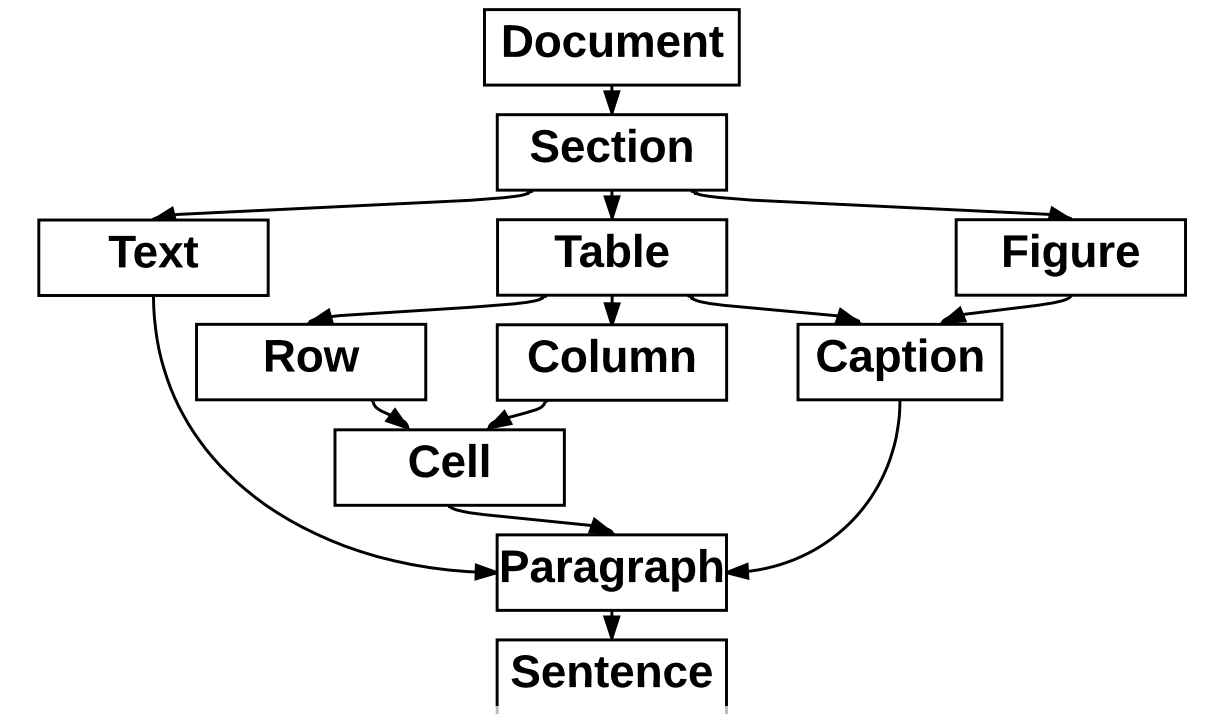
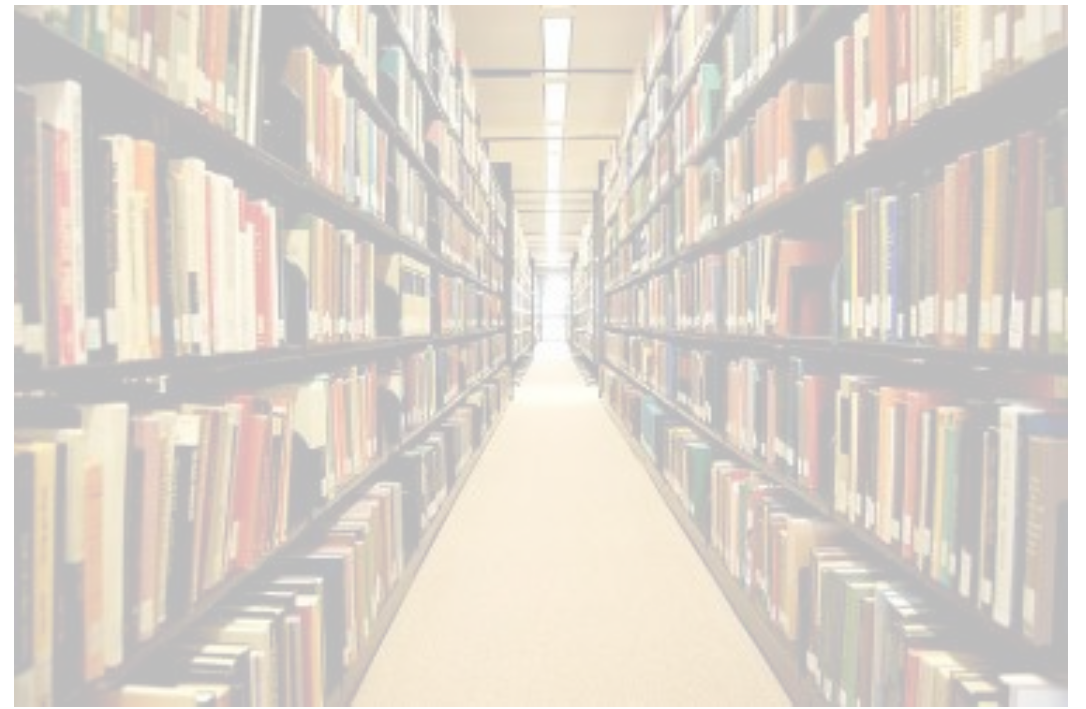
Miron Livny
Computer Sciences Dept.



Ian Ross
Computer Sciences Dept.

COSMOS: required components

1. Principled, automated access to scientific publications and the computing capacity and infrastructure required to repeatedly analyze them.
2. Models and techniques to represent and capture multi-modal data within publications.
3. Earth system model with parameterizations and predictions that overlap with many different types of empirical data and observations in publications.





FONDUE



Unstructured
Information



IBM Watson



Product Graph



KNOWLEDGE VAULT

Knowledge Base Construction



KNOWLEDGE VAULT



TextRunner/
ReVerb



NELL



Structured
Knowledge Base



And many more...



But, troves of "richly formatted" information remains untapped



Fonduer: Information Extraction over Richly Formatted Data

FONDUE

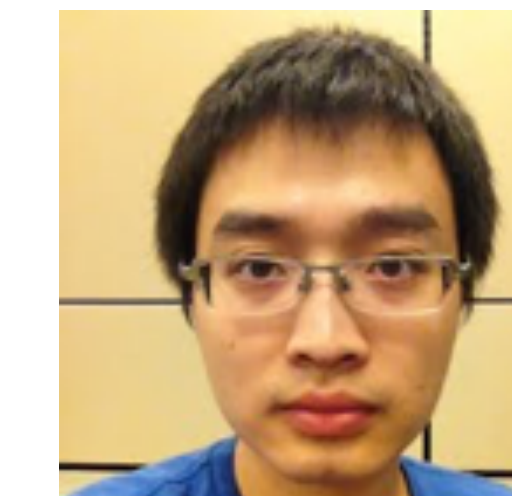
Our collaborators on Fonduer



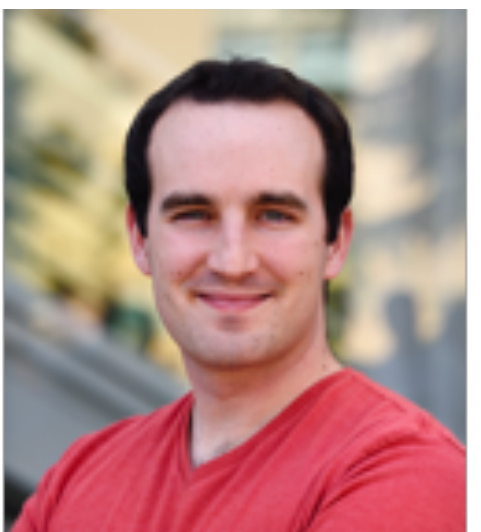
Sen Wu



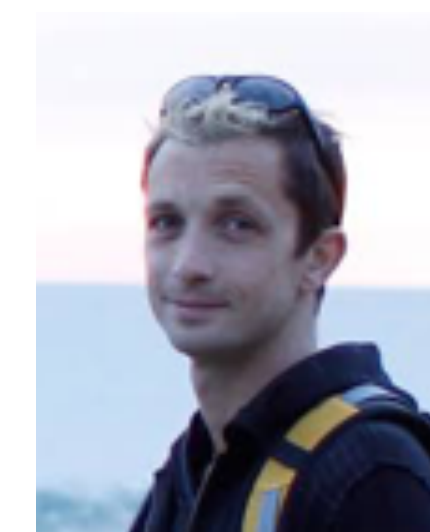
Luke Hsiao



Xiao Cheng



Braden Hancock



Philip Levis



Christopher Ré



Fonduer Users

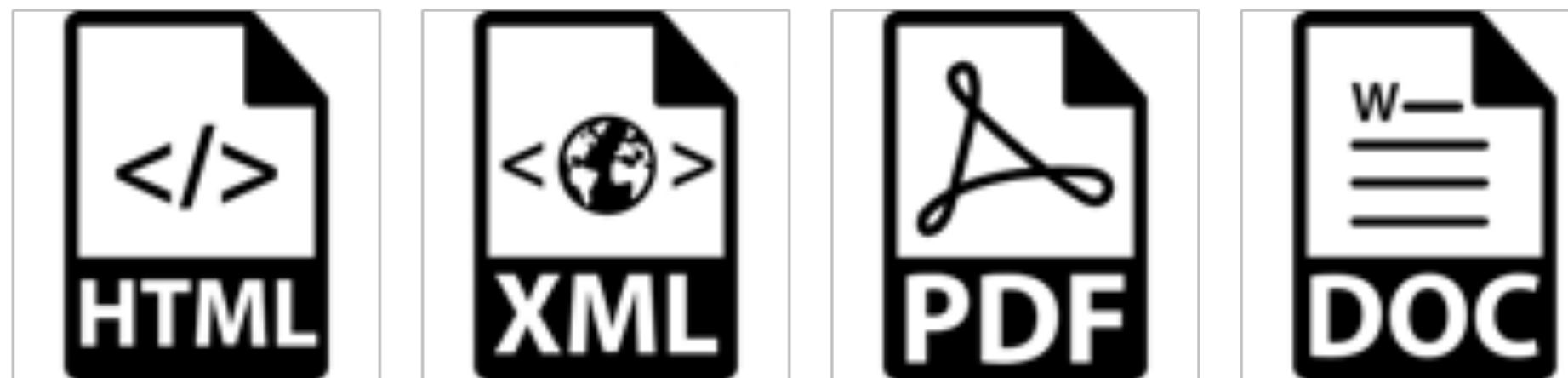




FONDUE

Richly formatted data

Richly formatted data: information is expressed via textual, structural, tabular, and visual cues.



Transistor Datasheet (PDF)

SMBT3904...MMBT3904

NPN Silicon Switching Transistors

- High DC current gain: 0.1 mA to 100 mA
- Low collector-emitter saturation voltage

Maximum Ratings

Parameter	Symbol	Value	Unit
Collector-emitter voltage	V_{CEO}	40	V
Collector-base voltage	V_{CBO}	60	
Emitter-base voltage	V_{EBO}	6	
Collector current	I_C	200	mA
Total power dissipation $T_S \leq 71^\circ\text{C}$ $T_S \leq 115^\circ\text{C}$	P_{tot}	330 s 250 s	mV
Junction temperature	T_j	150	°C
Storage temperature	T_{stg}	-65 ... 150	



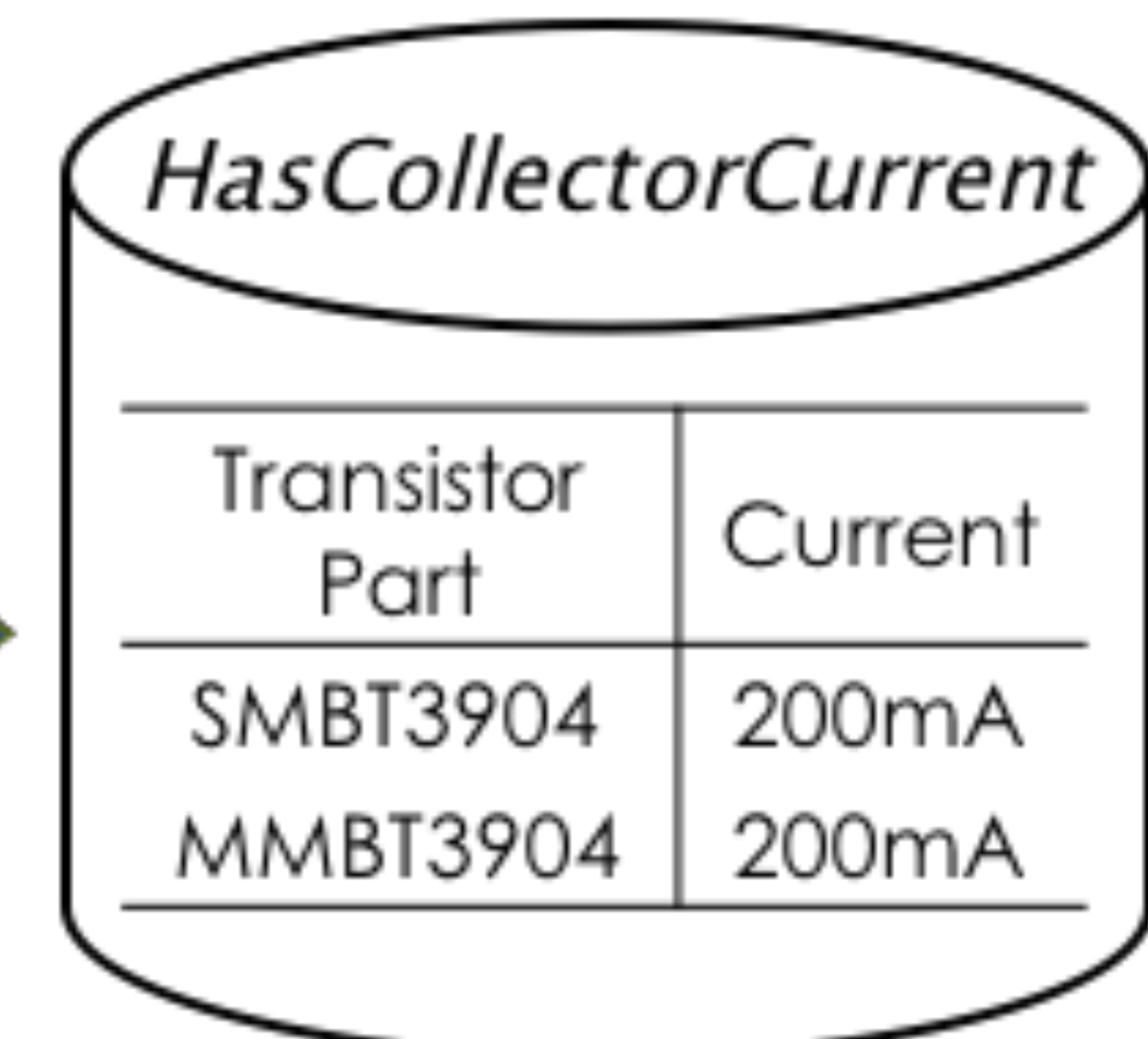
FONDUE

Knowledge base construction from richly formatted data

Goal: extract maximum collector current from transistor datasheets

Transistor Datasheet

SMBT3904..MMBT3904			
NPN Silicon Switching Transistors			
Parameter	Symbol	Value	Unit
Collector-emitter voltage	V_{CEO}	40	V
Collector-base voltage	V_{CBO}	60	
Emitter-base voltage	V_{EBO}	6	
Collector current	I_C	200	mA
Total power dissipation $T_S \leq 71^\circ\text{C}$	P_{tot}	330 250	mV
$T_S \leq 115^\circ\text{C}$			
Junction temperature	T_j	150	°C
Storage temperature	T_{stg}	-65 ... 150	



Knowledge Base



FONDER

Knowledge base construction from richly formatted data

Transistor Datasheet

Font: Arial; Size: 12; Style: Bold {SMBT3904..MMBT3904}

NPN Silicon Switching Transistors

- High DC current gain: 0.1 mA to 100 mA
- Low collector-emitter saturation voltage

Maximum Ratings

Parameter	Symbol	Value	Unit
Collector-emitter voltage	V_{CEO}	40	V
Collector-base voltage	V_{CBO}	Header: 'Value'; Row: 2; Column: 3	
Emitter-base voltage	V_{EBO}		
Collector current		200	mA
Total power dissipation $T_S \leq 71^\circ\text{C}$	P_{tot}	NER: Number 330	mV
$T_S \leq 115^\circ\text{C}$		250	
Junction temperature	T_j	150	°C
Storage temperature	T_{stg}	-65 ... 150	

In richly formatted data, semantics are expressed in textual, structural, tabular, and visual modalities throughout a document



FONDUE

Knowledge base construction from richly formatted data

Transistor Datasheet

SMBT3904...MMBT3904

NPN Silicon Switching Transistors

High DC current gain: 0.1 mA to 100 mA

Low collector-emitter saturation voltage

Maximum Ratings

Parameter	Symbol	Value	Unit
-----------	--------	-------	------

Collector-emitter voltage	VCEO	40	V
---------------------------	------	----	---

Collector-base voltage	VCBO	60	
------------------------	------	----	--

Emitter-base voltage	VEBO	6	
----------------------	------	---	--

Collector current	IC	200	mA
-------------------	----	-----	----

Total power dissipation	Ptot	mV	
-------------------------	------	----	--

TS \leq	71°C	330	
-----------	------	-----	--

TS \leq	115°C	250	
-----------	-------	-----	--

Junction temperature	Tj	150	°C
----------------------	----	-----	----

Storage temperature	Tstg	-65 ... 150	
---------------------	------	-------------	--

In richly formatted data, semantics are expressed in **textual**, **structural**, **tabular**, and **visual** modalities throughout a document

Conventional approach 1: Filter out other modalities besides unstructured text



FONDER

Knowledge base construction from richly formatted data

Transistor Datasheet

Header SMBT3904..MMBT3904			
NPN Silicon Switching Transistors			
<ul style="list-style-type: none">• High DC current gain: 0.1 mA to 100 mA• Low collector-emitter saturation voltage			
Maximum Ratings			
Parameter	Symbol	Value	Unit
Collector-emitter voltage	V_{CEO}	40	V
Collector-base voltage	V_{CBO}	60	
Emitter-base voltage	V_{EBO}	6	
Collector current	I_C	200	mA
Total power dissipation $T_S \leq 71^\circ\text{C}$	P_{tot}	330	mV
$T_S \leq 115^\circ\text{C}$		250	
Junction temperature	T_j	150	°C
Storage temperature	T_{stg}	-65 ... 150	

In richly formatted data, semantics are expressed in **textual**, **structural**, **tabular**, and **visual** modalities throughout a document

Conventional approach 1: Filter out other modalities besides unstructured text

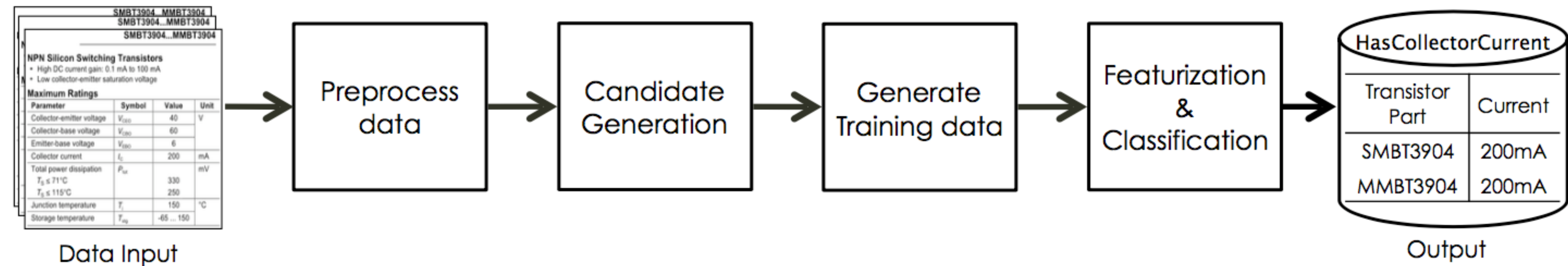
Conventional approach 2: Limit the context scope to sentences or tables.

Problem: Misses important relations if you neglect multimodal information



FONDWER

Fonduer's pipeline



Fonduer is a weakly supervised deep learning framework for knowledge base construction from richly formatted data



FONDUE

Multimodal weak supervision

Transistor Datasheet

SMBT3904..MMBT3904

NPN Silico Candidate 1 Transistors

- High DC current gain: 0.1 mA to 100 mA
- Low collector-emitter saturation voltage

Maximum Ratings

Parameter	Symbol	Value	Unit
Collector-emitter voltage	V_{CEO}	40	V
Collector-base voltage	V_{CBO}	60	
Emitter-base voltage	V_{EBO}		
Collector current	I_C	200	mA
Total power dissipation $T_S \leq 71^\circ\text{C}$	P_{tot}	330	mV
$T_S \leq 115^\circ\text{C}$		250	
Junction temperature	T_j	150	°C
Storage temperature	T_{stg}	-65 ... 150	

Candidate 2

A diagram showing arrows pointing from the 'Candidate 1' section of the datasheet to the 'SMBT3904' row in the 'Doc. level Candidates' table, and from the 'Candidate 2' section to the 'MMBT3904' row.

Doc. level Candidates	Supervision	
	Manual	Labeling function
SMBT3904	100	
MMBT3904	200	

Weak supervision: express any supervision signal via labeling functions to generate training data

```
# Check if current is in the same row with keyword 'collector'  
def in_the_same_row_with(candidate):  
    if 'collector' in  
        row_ngrams(candidate.current):  
            return 1  
    else: return -1
```



FONDUE

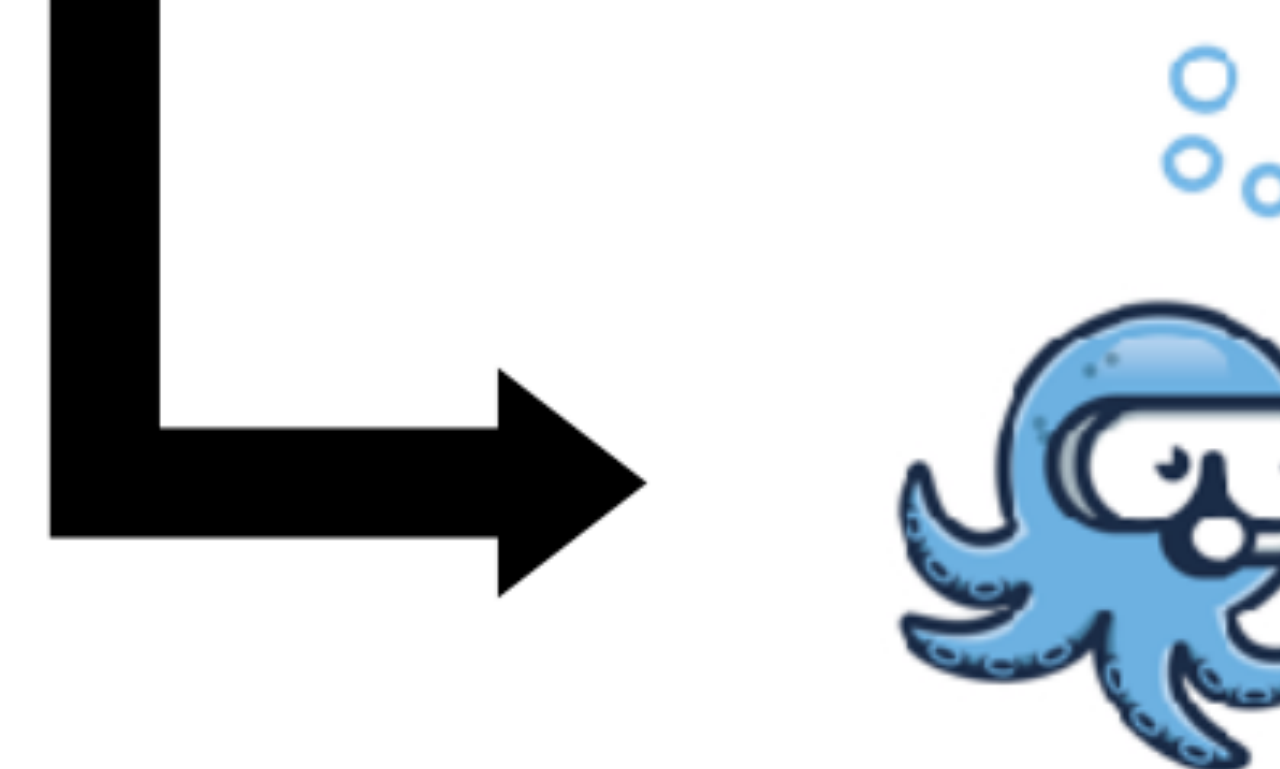
Multimodal weak supervision

Doc. level Candidates	Multimodal Supervision		
	Vertically aligned with 'Value'	Row ngrams contain 'mA'	'current' in sentence
SMBT3904 100	✗	∅	✓
SMBT3904 200	✓	✓	✗
SMBT3904 150	✓	✗	✗

∅=Abstain

Intuition: Use agreements / disagreements to learn the accuracy of LFs without ground truth

Output: Probabilistic Training Labels



Data programming/MeTal

SMBT3094 100 0.5

SMBT3094 200 0.85

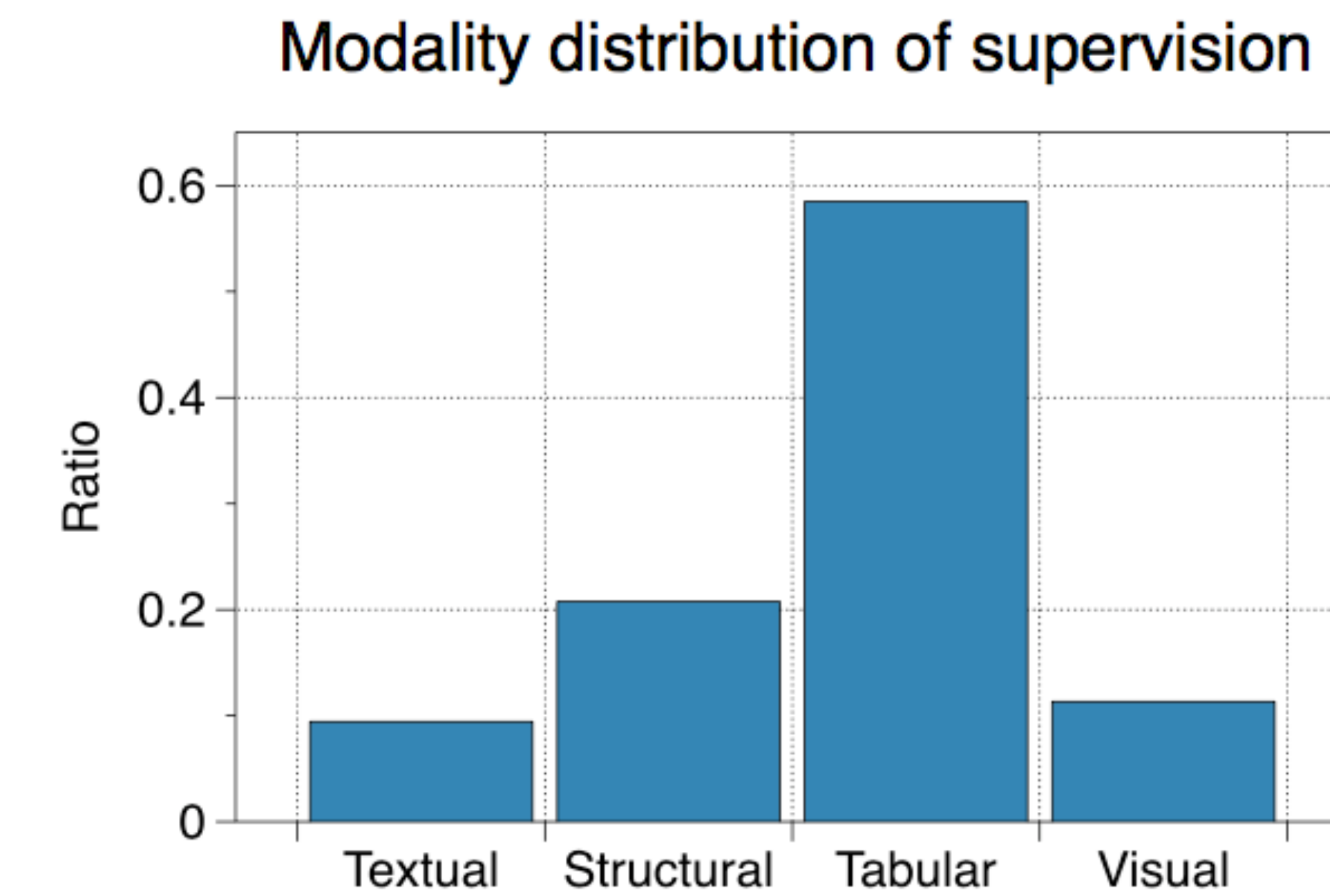
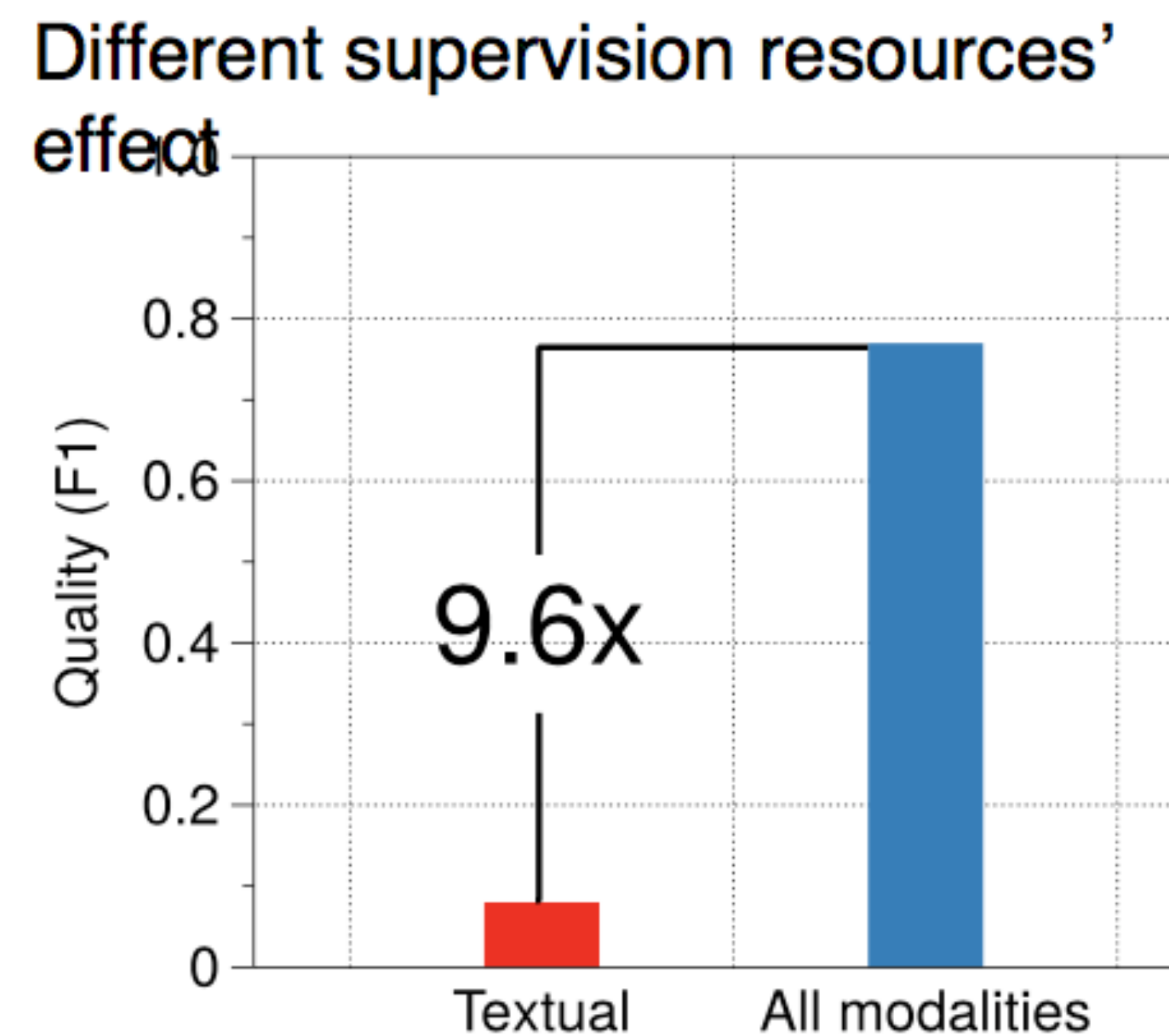
SMBT3094 150 0.15



FONDUE

Multimodal supervision is key to quality

For transistor datasheets...



Users intuitively rely on multimodal information for supervision



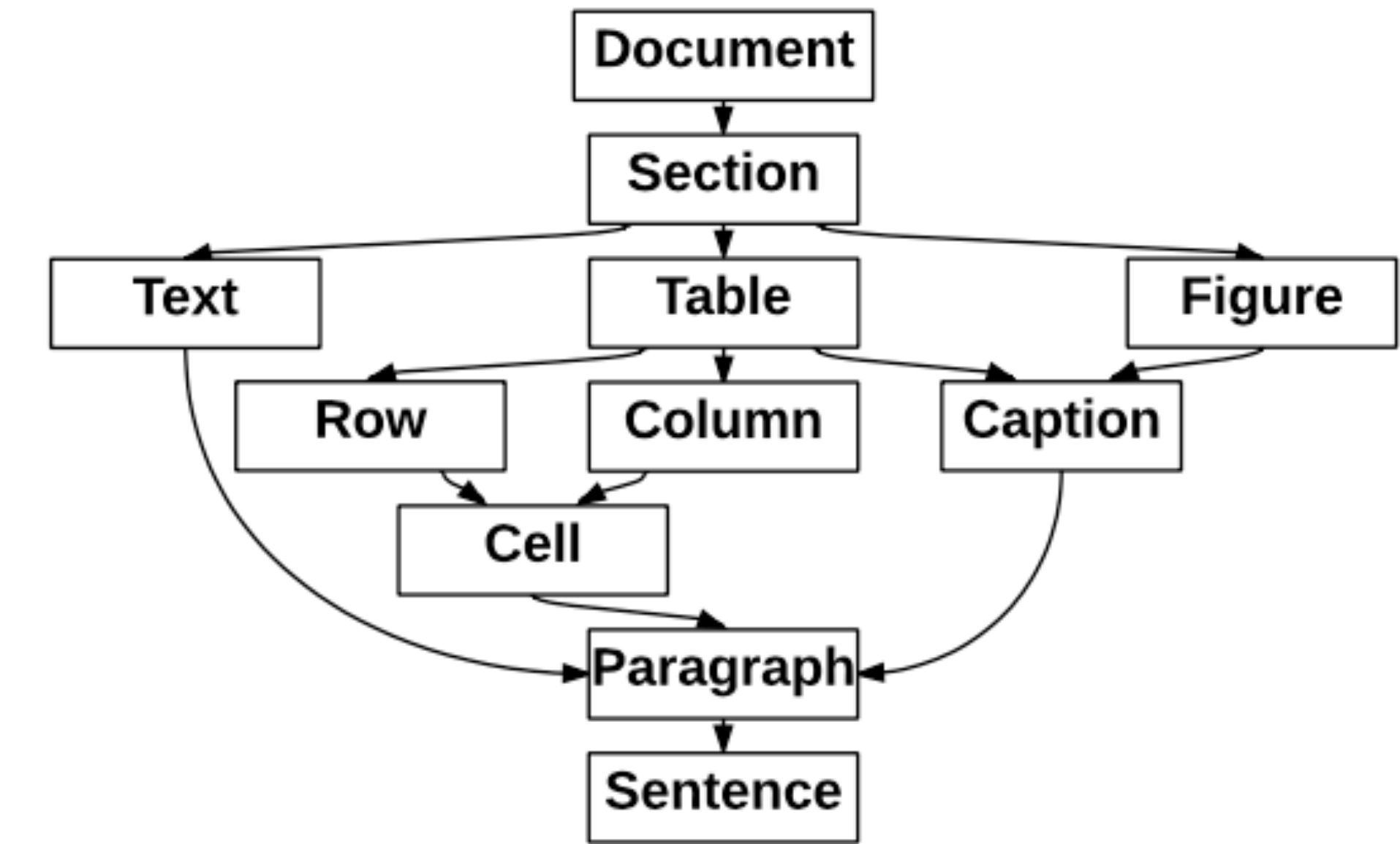
FONDWER

Fonduer's data model

Richly formatted data

SMBT3904...MMBT3904			
NPN Silicon Switching Transistors			
Maximum Ratings			
Parameter	Symbol	Value	Unit
Collector-emitter voltage	V_{CEO}	40	V
Collector-base voltage	V_{CBO}	60	
Emitter-base voltage	V_{EBO}	6	
Collector current	I_C	200	mA
Total power dissipation $T_S \leq 71^\circ\text{C}$	P_{tot}	330	mV
$T_S \leq 115^\circ\text{C}$		250	
Junction temperature	T_j	150	
Storage temperature	T_{stg}	-65 ... 150	°C

Data model



Fonduer automatically parses the richly formatted data into the data model that:

- Preserves structure/semantics across modalities
- Unifies a diverse variety of formats and styles
- Serves as the formal representation in KBC



Weakly Supervised KBC

- Fonduer helps build high-quality KBs from richly formatted data
- Allows users to leverage multimodal signals
- Augments LSTMs with features from each data modality to achieve high quality
- Fonduer is supporting real world applications

From Raw Documents to Fonduer's data model

Table 5

Proposal of ecological groups' (EGs) reassessments of AMBI index, based on Indicator Value (IndVal) coefficient and pollution condition of estuarine areas. Legend: Group 1 (estuaries with undisturbed or low disturbance conditions) and Group 2 (estuaries with medium to high disturbance conditions).

Indicator Value (IndVal) significant	Pollution condition (groups)	EG AZTI list	EG used for this study
40–60	Group 01	IV or V	III
		III	II
	Group 02	I or II	III
		III	IV
60–80	Group 01	IV or V	II
		III	V
	Group 02	I or II	IV
		III	I
80–100	Group 01	IV or V	I
	Group 02	I or II	V

correlation coefficients were calculated using the BIOESTAT v5.0 program (Ayres et al., 2007). Except for Spearman's rank correlation, the level of significance in all statistical analyzes was $\alpha = 5\%$.

3. Results

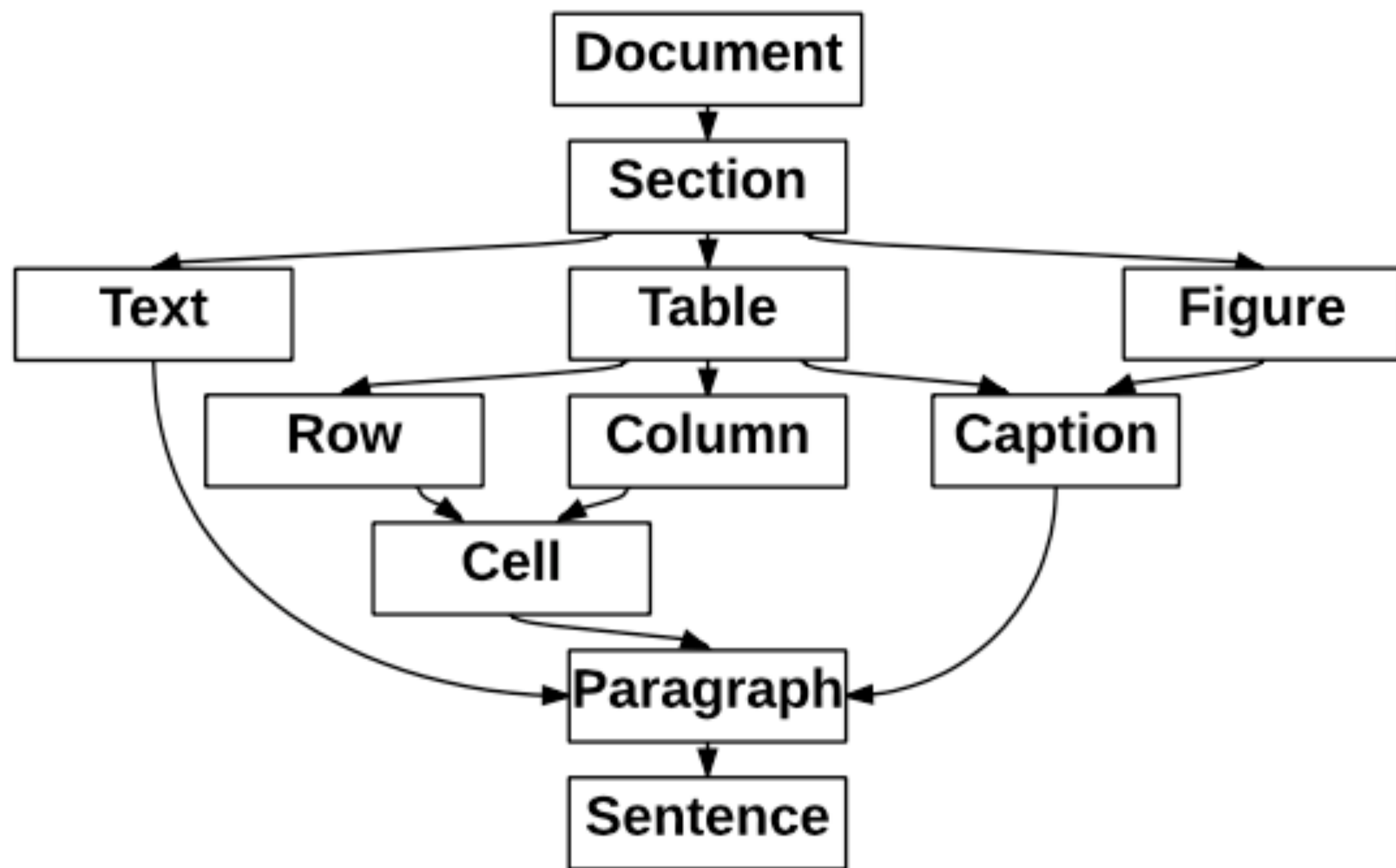
3.1. Environmental data

Water parameters: Mean temperature ranged from 25.7 (± 1.3) (in Mamucabas) to 30.5 (± 1.9) °C (in Marac  pe), with little variation between seasons. Mean salinity values were similar to those obtained in the period of macrofaunal samplings (October 2007), with the majority of the sampling sites situated between polyhaline-euhaline zones. Salinity values ranged from a minimum of 11 (± 5.5) (in Jaboat  o) to a maximum of 33.5 (± 3.7) psu (in Marac  pe) among seasons, excepted for Mamucabas and Pirapama, with low salinity values (oligohaline zones). At most sites, dissolved oxygen levels were found to be outside the normal limits for estuarine systems. On the other hand, only Pina Basin 1 ($3.99 \mu\text{mol l}^{-1}$), Jaboat  o ($6.31 \mu\text{mol l}^{-1}$) and Parati  e ($7.29 \mu\text{mol l}^{-1}$) had higher ammonia-N

However, the majority (82%) was ascribed to an EG based on the classification for the same genus. For the following species, ecological groups were attributed according to the AZTI list for higher taxonomic levels (>family): *Anomalocardia brasiliiana* (I), *Barantolla* sp. (V), *Capitellides* sp. (V), *Fabrisabella* sp. (I), *Megalomma* sp. (I), *Neomediomastus* sp. (V), *Pseudobranchiomma* sp. (I) and *Timarete* sp. (IV). Due to the lack of ecological information for tropical regions, twenty-one taxa remained without classification and were denominated as "not assigned".

Considering the definition of sites into groups using dissolved oxygen and disturbance levels, the IndVal coefficient revealed fifteen significant indicator species/taxa (Table 6). However, based on IndVal scale proposed, only four species had high indicator values (>40%): the polychaetes *Capitella* sp. and *Streblospio* sp., nematodes and the oligochaete *Tectidrilus* sp. In terms of ecological interpretation, *Capitella* sp. and *Tectidrilus* sp. were originally classified as EG_V on the AZTI list. However, the EG of this latter species was changed to EG_{II} based on its presence in unpolluted conditions. Both Nematoda and *Streblospio* sp. [originally considered tolerant (EG_{III})] were associated to sensitive and opportunistic groups by

Data model



Constructing Fonduer's input requires performing document segmentation.

Typical OCR focuses on text only!

Problem: Text-only
segmentation
obscures important
table structure

Table 1. EnKF calibrated biogeochemical parameters in the GENIE-1 model.

Name	Prior assumptions (mean and range ^a)	Posterior mean ^b	Description
$u_0^{\text{PO}_4}$	$1.65 \mu\text{mol kg}^{-1} \text{ yr}^{-1}$ (0.3–3.0)	$1.91 \mu\text{mol kg}^{-1} \text{ yr}^{-1}$	maximum PO_4 uptake (removal) rate (Eq. 3)
K^{PO_4}	$0.2 \mu\text{mol kg}^{-1}$ (0.1–0.3)	$0.21 \mu\text{mol kg}^{-1}$	PO_4 Michaelis-Menton half-saturation concentration (Eq. 3)
r^{POC}	0.05 (0.02–0.08)	0.055	initial proportion of POC export as fraction #2 (Eq. 6)
l^{POC}	600 m (200–1000)	556 m	<i>e</i> -folding remineralization depth of POC fraction #1 (Eq. 6)
$r_0^{\text{CaCO}_3:\text{POC}}$	0.036 (0.015–0.088) ^c	0.022 ^d	$\text{CaCO}_3:\text{POC}$: export rain ratio scalar (Eq. 8)
η	1.5 (1.0–2.0)	1.28	thermodynamic calcification rate power (Eq. 9)
r^{CaCO_3}	0.4 (0.2–0.6)	0.489	initial proportion of CaCO_3 export as fraction #2 (Eq. 11)
l^{CaCO_3}	600 m (200–1000)	1055	<i>e</i> -folding remineralization depth of CaCO_3 fraction #1 (Eq. 11)

^a the range is quoted as 1 standard deviation either side of the mean

^b quoted as the mean of the entire EnKF ensemble

^c assimilation was carried out on a \log_{10} scale

^d Note that the rain ratio scalar parameter is not the same as the $\text{CaCO}_3:\text{POC}$ export rain ratio as measured at the base of the euphotic zone, because $r_0^{\text{CaCO}_3:\text{POC}}$ is further multiplied by $(\Omega - 1)^{\eta}$ to calculate the rain ratio, where Ω is the surface ocean saturation state with respect to calcite (see Sect. 2.1). Pre-industrial mean ocean surface Ω is ~ 5.2 in the GENIE-1 model, so that the global $\text{CaCO}_3:\text{POC}$ export rain ratio can be estimated using the 8-parameter assimilation as being equal to $(5.2 - 1)^{1.28} \times 0.022 = 0.14$.

(Table 1). Because we explicitly resolve the individual “components” (i.e., C, ^{13}C , P, ...) of organic matter, the GENIE-1 model can be used to quantify the effect of fractionation between the components of organic matter during remineral-

(e.g. Zhang et al., 2001, 2003) or by allowing the tracer transport of negative O_2 concentrations (e.g., Hotinski et al., 2001). We treat the remineralization of dissolved organic matter in an analogous manner if O_2 availability is insuffi-

Typical OCR focuses on text only!

**Problem: Text-only
segmentation
obscures important
table structure**

Table 1. EnKF calibrated biogeochemical parameters in the GENIE-1 model.

Name	Prior assumptions (mean and range ^a)	Posterior mean ^b	Description
$u_0^{\text{PO}_4}$	$1.65 \mu\text{mol kg}^{-1} \text{ yr}^{-1}$ (0.3–3.0)	$1.91 \mu\text{mol kg}^{-1} \text{ yr}^{-1}$	maximum PO_4 uptake (removal) rate (Eq. 3)
K^{PO_4}	$0.2 \mu\text{mol kg}^{-1}$ (0.1–0.3)	$0.21 \mu\text{mol kg}^{-1}$	PO_4 Michaelis-Menton half-saturation concentration (Eq. 3)
r^{POC}	0.05 (0.02–0.08)	0.055	initial proportion of POC export as fraction #2 (Eq. 6)
l^{POC}	600 m (200–1000)	556 m	<i>e</i> -folding remineralization depth of POC fraction #1 (Eq. 6)
$r_0^{\text{CaCO}_3:\text{POC}}$	0.036 (0.015–0.088) ^c	0.022 ^d	$\text{CaCO}_3:\text{POC}$: export rain ratio scalar (Eq. 8)
η	1.5 (1.0–2.0)	1.28	thermodynamic calcification rate power (Eq. 9)
r^{CaCO_3}	0.4 (0.2–0.6)	0.489	initial proportion of CaCO_3 export as fraction #2 (Eq. 11)
l^{CaCO_3}	600 m (200–1000)	1055	<i>e</i> -folding remineralization depth of CaCO_3 fraction #1 (Eq. 11)

^a the range is quoted as 1 standard deviation either side of the mean

^b quoted as the mean of the entire EnKF ensemble

^c assimilation was carried out on a \log_{10} scale

^d Note that the rain ratio scalar parameter is not the same as the $\text{CaCO}_3:\text{POC}$ export rain ratio as measured at the base of the euphotic zone, because $r_0^{\text{CaCO}_3:\text{POC}}$ is further multiplied by $(\Omega - 1)^{\eta}$ to calculate the rain ratio, where Ω is the surface ocean saturation state with respect to calcite (see Sect. 2.1). Pre-industrial mean ocean surface Ω is ~ 5.2 in the GENIE-1 model, so that the global $\text{CaCO}_3:\text{POC}$ export rain ratio can be estimated using the 8-parameter assimilation as being equal to $(5.2 - 1)^{1.28} \times 0.022 = 0.14$.

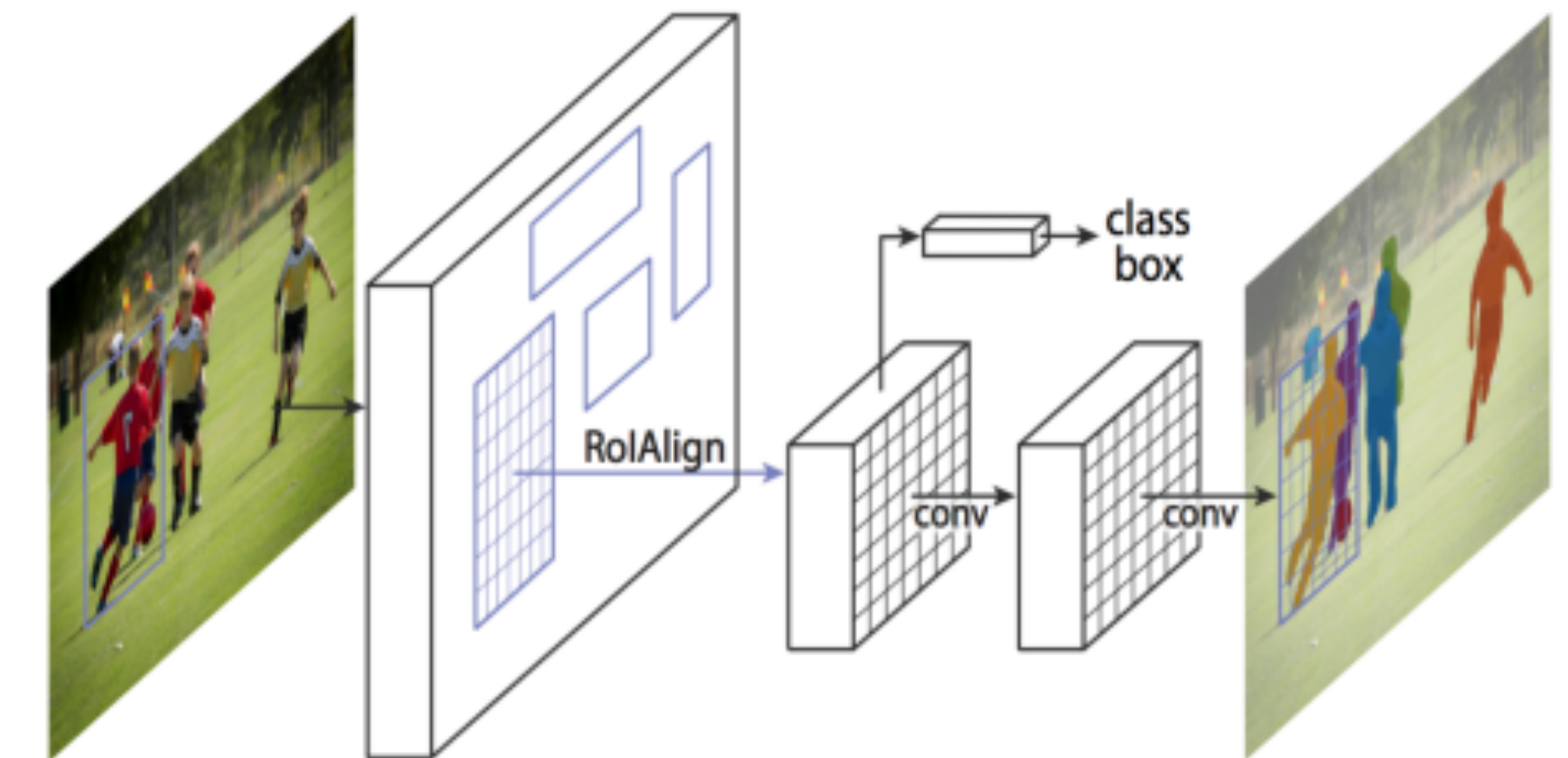
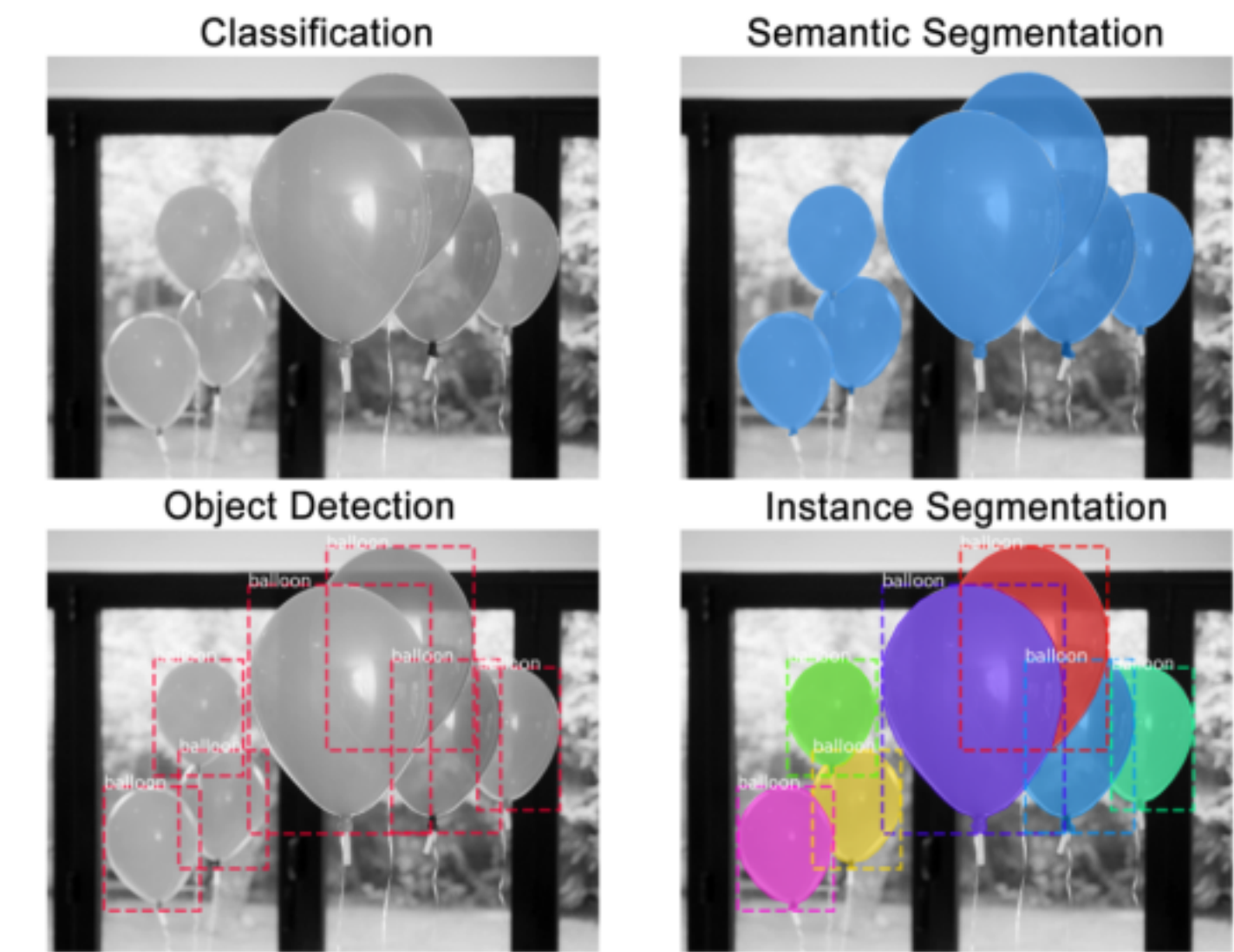
(Table 1). Because we explicitly resolve the individual “components” (i.e., C, ^{13}C , P, ...) of organic matter, the GENIE-1 model can be used to quantify the effect of fractionation between the components of organic matter during remineral-

(e.g. Zhang et al., 2001, 2003) or by allowing the tracer transport of negative O_2 concentrations (e.g., Hotinski et al., 2001). We treat the remineralization of dissolved organic matter in an analogous manner if O_2 availability is insuffi-

**Solution: Cast
document
segmentation as
a vision problem**

Mask-RCNN (He et al. 2018)

- State of the art image segmentation model
- Performs instance segmentation
- Identifies regions of interest (ROI) followed by object detection, classification, and mask detection in parallel
- We set mask to the bounding box with intention to refine bounding box



Mask R-CNN framework. Source: <https://arxiv.org/abs/1703.06870>

Data annotation: In-house labeler

Image tagger Click + drag to create item. Click existing item to adjust.

Save Clear changes [Next image >](#)

Estimating ecological risk in the terrestrial component 249

Table 1. Characteristics of 18 soil samples collected in FSSW-1 and FSSW-2

Parameter	Median	Range
Silt/clay content	36%	13–62%
“Sand” content	57%	34–69%
Organic matter content of “sand”	37%	10–75%
Total organic carbon	10%	1–34%
pH	5.8	5–6.1

The median value for total organic carbon (TOC) was 10% with a range of 1 to 34%; soils closer to the river tended to exhibit higher TOC values. The pH of the soils ranged from 5.0 to 6.1.

Concentrations of chemicals in soils

A 1985 investigation under Superfund [2] revealed elevated concentrations of various pesticides and selected metals such as arsenic in surface soils (Table 2). Highest concentrations occurred in the FSSW-1 area and the lowest in the on-site reference area, FSSW-3. 1,1,1-trichloro-2,2-bis-(*p*-chlorophenyl)ethane (DDT) and its metabolites (herein collectively referred to as DDTR) and chlordane were the chlorinated pesticides found in highest concentrations. The three composite and two hot spot soil samples (DB-3 and DB-12) collected in 1988 for the laboratory bioassays exhibited pesticide levels similar to those seen in 1985 (Fig. 2). Again, DDTR and chlordane were the predominant pesticides. A sample of soil collected in one of the more contaminated areas in FSSW-1 (near DB-3) in the 1989 sampling effort revealed elevated levels of arsenic (700 mg/kg) and total polynuclear aromatic hydrocarbons (63 mg/kg). Thirty-eight samples were analyzed for pesticides in 1989 as part

RESULTS

Site characteristics

The study area consisted of forested and shrubbed swamp/wetland whose soils are comprised of silty-sand, rich in organic matter (Table 1).

Table 2. Historical surface soil concentrations from 1985

Compound	Average concn. (mg/kg dry wt.) [Maximum concn.]		
	FSSW-1 ^a	FSSW-2 ^a	FSSW-3 ^a
Pesticides			
4,4'-DDD	70 [1,100]	4 [28]	1 [12]
4,4'-DDE	10 [47]	1 [5]	1 [2]
4,4'-DDT	61 [630]	2 [10]	1 [4]
Chlordane	143 [1,700]	17 [110]	2 [17]
Dieldrin	4 [32]	1 [1]	
PAHs			
Benzo[<i>a</i>]pyrene	1 [2]	1 [2]	
Fluoranthene	1 [5]		
Total other PAHs	1 [22]		3 [7]
Metals			
Arsenic	80 [1,000]	17 [144]	20 [70]
Beryllium	1 [1]	1 [2]	1 [2]
Cadmium	1 [1]	1 [3]	1 [1]
Nickel	4 [25]	6 [21]	9 [32]
Lead	50 [721]	48 [128]	108 [215]
Silver	1 [4]		1 [1]
Zinc	50 [355]	32 [148]	71 [102]
Dioxin (2,3,7,8-TCDD)	0.003 [0.048]	0.00037 [0.001]	
Number of sampled stations	43	15	9

^aSample location.

Image tagger Click + drag to create item. Click existing item to adjust.

Save Clear changes [Next image >](#)

Page Header Estimating ecological risk in the terrestrial component 249

Table Caption

Table 1. Characteristics of 18 soil samples collected in FSSW-1 and FSSW-2

Parameter	Median	Range
Silt/clay content	36%	13–62%
“Sand” content	57%	34–69%
Organic matter content of “sand”	37%	10–75%
Total organic carbon	10%	1–34%
pH	5.8	5–6.1

Body Text

The median value for total organic carbon (TOC) was 10% with a range of 1 to 34%; soils closer to the river tended to exhibit higher TOC values. The pH of the soils ranged from 5.0 to 6.1.

Section Header

Concentrations of chemicals in soils

Body Text

A 1985 investigation under Superfund [2] revealed elevated concentrations of various pesticides and selected metals such as arsenic in surface soils (Table 2). Highest concentrations occurred in the FSSW-1 area and the lowest in the on-site reference area, FSSW-3. 1,1,1-trichloro-2,2-bis-(*p*-chlorophenyl)ethane (DDT) and its metabolites (herein collectively referred to as DDTR) and chlordane were the chlorinated pesticides found in highest concentrations. The three composite and two hot spot soil samples (DB-3 and DB-12) collected in 1988 for the laboratory bioassays exhibited pesticide levels similar to those seen in 1985 (Fig. 2). Again, DDTR and chlordane were the predominant pesticides. A sample of soil collected in one of the more contaminated areas in FSSW-1 (near DB-3) in the 1989 sampling effort revealed elevated levels of arsenic (700 mg/kg) and total polynuclear aromatic hydrocarbons (63 mg/kg). Thirty-eight samples were analyzed for pesticides in 1989 as part

Section Reader

Section

Body Text

The study area consisted of forested and shrubbed swamp/wetland whose soils are comprised of silty-sand, rich in organic matter (Table 1).

Table Caption

Table 2. Historical surface soil concentrations from 1985

Compound	Average concn. (mg/kg dry wt.) [Maximum concn.]		
	FSSW-1 ^a	FSSW-2 ^a	FSSW-3 ^a
Pesticides			
4,4'-DDD	70 [1,100]	4 [28]	1 [12]
4,4'-DDE	10 [47]	1 [5]	1 [2]
4,4'-DDT	61 [630]	2 [10]	1 [4]
Chlordane	143 [1,700]	17 [110]	2 [17]
Dieldrin	4 [32]	1 [1]	
PAHs			
Benzo[<i>a</i>]pyrene	1 [2]	1 [2]	
Fluoranthene	1 [5]		
Total other PAHs	1 [22]		3 [7]
Metals			
Arsenic	80 [1,000]	17 [144]	20 [70]
Beryllium	1 [1]	1 [2]	1 [2]
Cadmium	1 [1]	1 [3]	1 [1]
Nickel	4 [25]	6 [21]	9 [32]
Lead	50 [721]	48 [128]	108 [215]
Silver	1 [4]		1 [1]
Zinc	50 [355]	32 [148]	71 [102]
Dioxin (2,3,7,8-TCDD)	0.003 [0.048]	0.00037 [0.001]	
Number of sampled stations	43	15	9

Table Note

^aSample location.

Qualitative Results

Prediction
Ground Truth

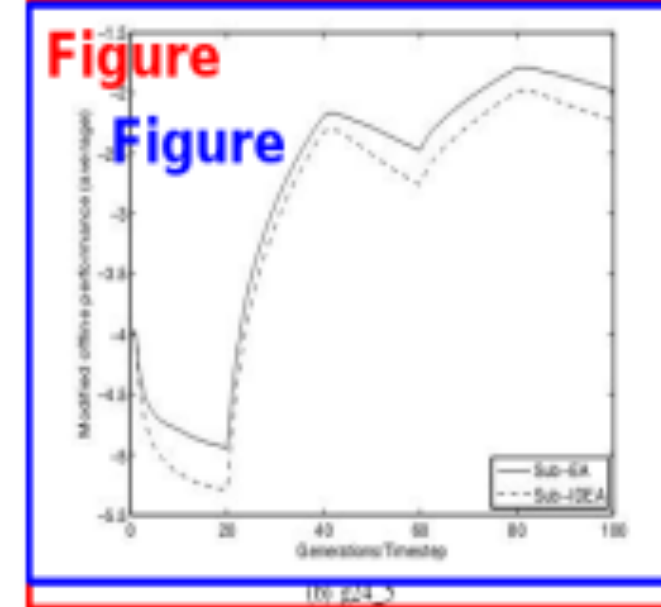
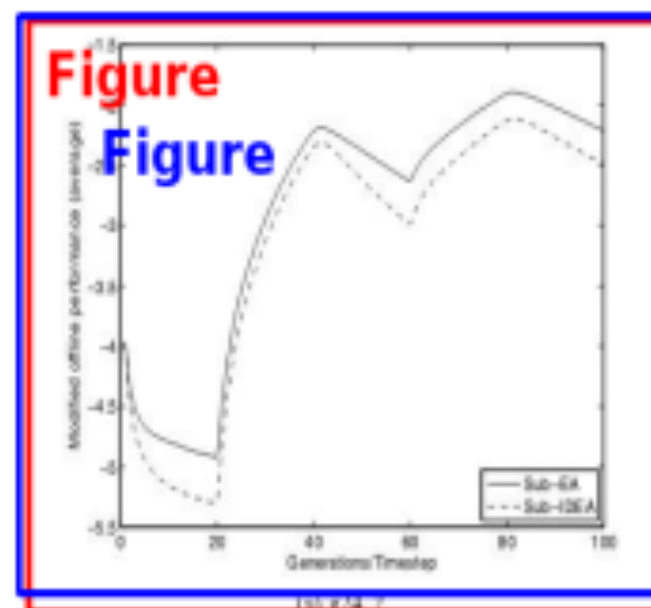


Fig. 5: Modified offline performance of Sub-EA and Sub-IDEA averaged over 30 runs

TABLE IV: Mean best-of-generation values (averaged over 30 runs)

Table	Sub-EA	Sub-IDEA
224.2	-2.2130	-2.4890
224.1	-2.2322	-2.2322

VI. SUMMARY AND FUTURE WORK

This paper highlights the benefits of Infeasibility Driven Evolutionary Algorithm (IDEA) for dynamic, constrained single objective optimization problems. The presence of infeasible solutions allow IDEA to approach the constrained optimum from the infeasible side as well as feasible side of the search space, thereby converging faster than conventional EAs which approach the optimum from feasible side only. The paper provides results of preliminary studies of the algorithm on two dynamic, constrained single objective optimization benchmarks. The results of using IDEA as a sub-evolve mechanism are certainly encouraging for the above problems. Its performance is currently being studied extensively for available constrained dynamic optimization

problems.

The comparison of proposed algorithm has been made with a structurally similar algorithm in order to highlight the benefits of maintaining infeasible solutions for dynamic optimization problems. Currently studies are underway to compare the performance of IDEA with other existing algorithms.

ACKNOWLEDGMENT

The presented work was supported by grants from Defence and Security Applications Research Center (DSARC), Australian Defence Force Academy, University of New South Wales, Australia.

The work of Trung Thanh Nguyen is supported by the Overseas Research Scheme Award (ORS) and the School of Computer Science, University of Birmingham.

The work of Xin Yao is supported by an EPSRC grant (EP/E058884/1) on "Evolutionary Algorithms for Dynamic Optimisation Problems: Design, Analysis and Applications".

REFERENCES

- [1] H. K. Singh, A. Isaacs, T. Ray, and W. Smith, "Infeasibility Driven Evolutionary Algorithm (IDEA) for Engineering Design Optimization," in *Proceedings of 21st Australasian Joint Conference on Artificial Intelligence AI-08*, 2008, pp. 104–115.
- [2] T. Ray, H. K. Singh, A. Isaacs, and W. Smith, "Infeasibility driven evolutionary algorithm for constrained optimization," in *Constraint Handling in Evolutionary Optimization*, ser. Studies in Computational Intelligence. Springer, in press.
- [3] I. Hatrkov and D. Wallace, "Dynamic multi-objective optimization with evolutionary algorithms: a forward-looking approach," in *GECCO '06: Proceedings of the 8th annual conference on Genetic and evolutionary computation*, New York, NY, USA: ACM, 2006, pp. 1204–1208.
- [4] T. Nguyen and X. Yao, "Benchmarking and solving dynamic constrained problems," in *IEEE Congress on Evolutionary Computation (CEC) 2008*, Accepted.
- [5] J. Bräke, "Memory enhanced evolutionary algorithm for changing optimization problems," in *Evolutionary Computation, 1999. CEC 99. Proceedings of the 1999 Congress on*, vol. 3, 1999, pp. 1874–1882.
- [6] S. Baluja, "Population-based incremental learning: A method for integrating genetic search based function optimization and competitive learning," Carnegie Mellon University, Pittsburgh, PA, USA, Tech. Rep., 1994.
- [7] S. Yang and X. Yao, "Experimental study of population-based incremental learning algorithms for dynamic optimization problems," *Soft Computing: A Fusion of Foundations, Methodologies and Applications*, vol. 9, no. 11, 2005.
- [8] S. Yang, "Non-stationary problem optimization using the primal-dual genetic algorithm," *The 2003 Congress on Evolutionary Computation (CEC)*, vol. 3, pp. 2246–2253, December 2003.
- [9] N. Mori, H. Kita, and Y. Nishikawa, "Adaption to a changing environment by means of the thermodynamical genetic algorithm," *Lecture Notes in Computer Science*, vol. 1148, pp. 513–522, 1996.
- [10] P. Moscato, "On evolution, search, optimization, genetic algorithms and martial arts: Towards nematic algorithms," California Institute of Technology, Tech. Rep., 1989.
- [11] T. Ray, A. Isaacs, and W. Smith, "A Memetic Algorithm for Dynamic Multiobjective Optimization," in *Multi-objective Memetic Algorithms*, ser. Studies in Computational Intelligence. Springer, 2008 (in Press).
- [12] S. Yang and X. Yao, "Population-based incremental learning with associative memory for dynamic environments," *IEEE Transactions on Evolutionary Computation*, vol. 12, no. 5, pp. 542–561, Oct. 2008.
- [13] K. Deb, A. Pratap, S. Agarwal, and T. Meyarivas, "A fast and elitist multiobjective genetic algorithm: NSGA-II," *Evolutionary Computation, IEEE Transactions on*, vol. 6, pp. 182–197, 2002.
- [14] K. Deb and S. Agrawal, "Simulated binary crossover for continuous search space," *Complex Systems*, vol. 9, pp. 115–148, 1995.

Table	name	# blocks	# variables	# global avg. block	# generated function terms
Driver "A"	3903	1	1.0	2840	
Driver "B"	4022	2	2.3	2951	
Driver "C"	3925	2	2.0	2860	
Driver "D"	4487	2	2.0	3124	
Driver "E"	3933	4	4.0	2868	
Driver "F"	4519	6	9.2	37365	
Driver "G"	4521	5	13.4	4396	
Driver "H"	6700	18	39.5	14612	
Driver "I"	5429	3	4.3	9744	
Driver "J"	8693	1	1.0	7250	
Driver "K"	4509	7	20.7	29984	

Fig. 3. Measurements from a preliminary investigation of the number of function terms generated for some small test programs. The richer boolean programs that these programs encode contain procedures with parameters and local state, which causes the blocks in the encoding to have varying numbers of variables on entry. The table shows both the number of global variables and the average number of variables per block. The boolean programs can contain unreachable blocks, which explains the fact that the number of function terms is sometimes smaller than the number of blocks.

the program's initial state, are given symbolically (k and m in the running example). If, instead of $\neg A(k, m)$, a complete set of explicit boolean values are used, as in:

$$\neg A(\text{false}, \text{false}) \wedge \neg A(\text{false}, \text{true}) \wedge \neg A(\text{true}, \text{false}) \wedge \neg A(\text{true}, \text{true})$$

then all function-term arguments will also be explicit boolean values, so there are only $N \cdot 2^K$ different function terms, a single exponential.

There is a good reason we don't want to abandon the symbolic initial values in favor of the explicit ones: by using explicit values, we get *at least* 2^K function terms, because that's how many function terms we get for the start block alone. The numbers in Figure 3 show that the symbolic initial values can do better than that.

Interestingly enough, we can adjust the degree to which we use the two argument representations, by using the following simple equality: for any function b , expression e , and lists of expressions E_0 and E_1 , we have:

$$b(E_0, E_1) = (\neg e \wedge b(E_0, \text{false}, E_1)) \wedge (e \wedge b(E_0, \text{true}, E_1)) \quad (12)$$

Thus, if e is an expression other than an explicit boolean value, then the algorithm in Figure 2 can choose the left-hand side of (12) instead of invoking the procedure *Instantiate*. The choice of which one to do would be determined heuristically. A possible heuristic is to use (12) whenever the argument e is "too complicated", as perhaps when the number of variables in e exceeds some threshold, or when e is anything but the symbolic initial value of the program variable corresponding to this function argument. By choosing the latter heuristic, for example, the number of different function terms is $N \cdot 3^K$, a single exponential as in the case of using only explicit boolean values; yet, by using this heuristic, the algorithm begins with just one negated start block function, not an exponential number of them as in the case of using only explicit boolean values.

I have yet to experiment with the symbolic-versus-explicit argument representations in my implementation.

13

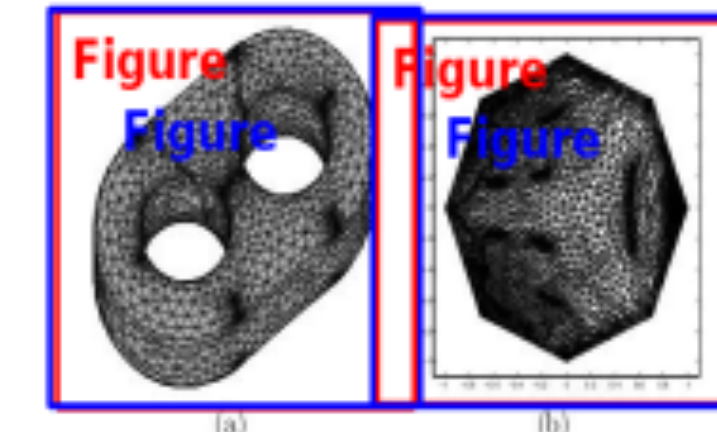


Figure 11: (a)Surface with genus 2 (b)Parameterization on $abo^{-1}b^{-1}cdc^{-1}d^{-1}$

disk P to M then all the 2D-corner vertices $w_1, w_2, \dots, w_{2g-1}$ of P map to the same vertex Ω of the surface mesh M . More precisely, the basepoint Ω is mapped $2g$ times if we deal with genus g . That means we have $2g$ different indices but those $2g$ points all have the same coordinates. Similarly, the points w_1 and w_2 which are portrayed in Fig. 4(b) maps to the same 3D points A of the surface mesh M . For that reason, the point A has to be repeated twice. The vertices of the polygonal disk are chosen as

$$[w_1(\pi/2g), \sin(s\pi/2g)] \quad \text{for all } s = 0, 1, \dots, 2g-1. \quad (20)$$

$$\text{Equation}$$

6 Constrained quadrangulation

In this section, we will describe a way to decompose a surface M into pieces of four-sided domains. In order to facilitate the presentation, we suppose that we have a parametrization \mathcal{P} in disposition and that M is of genus zero and thus the parameter domain is a rectangle.

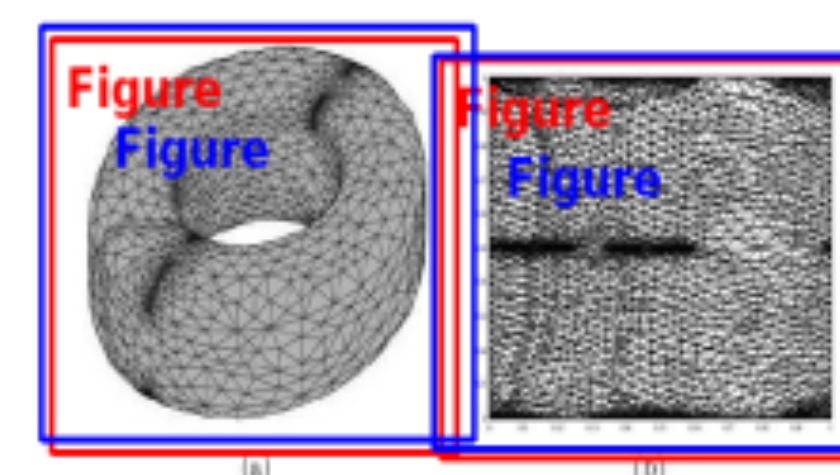


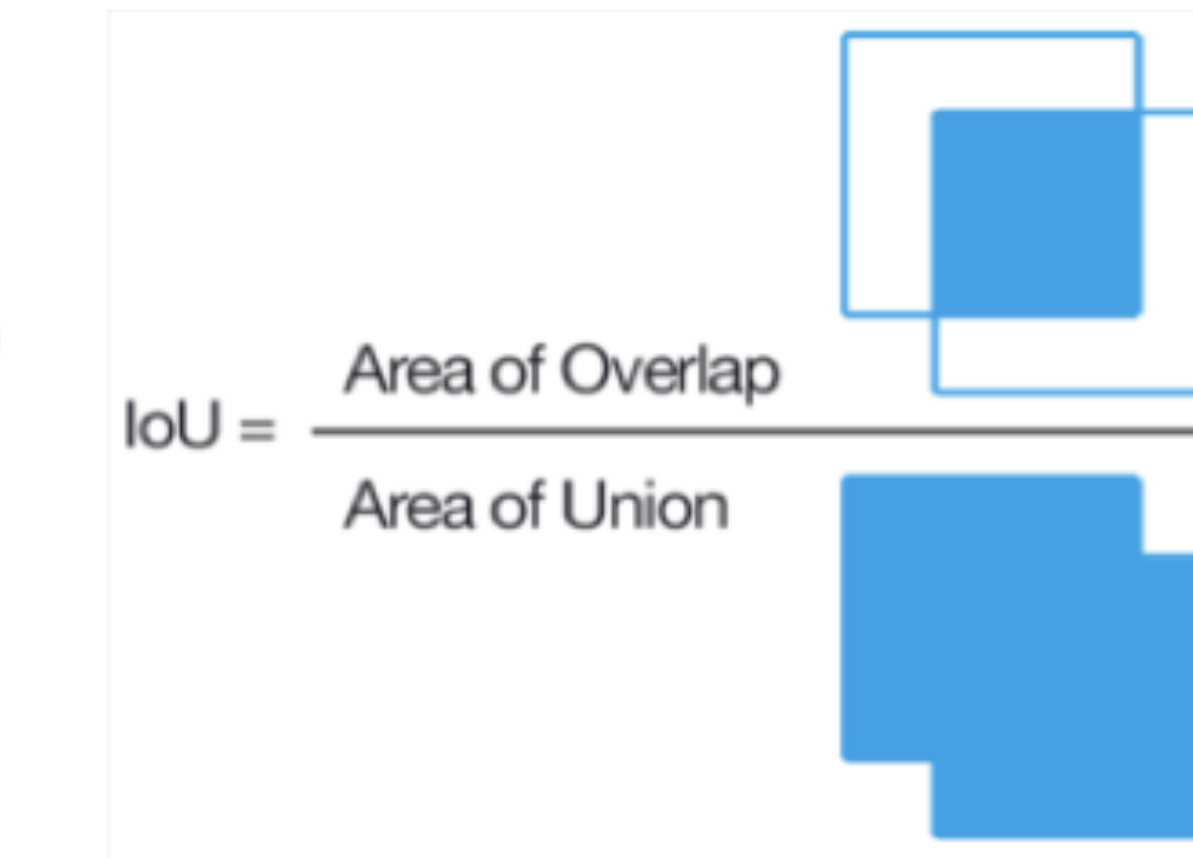
Figure 12: (a)Surface with genus 1 (b)Parameterization on $abo^{-1}b^{-1}$

13

Quantitative Results

$\text{IoU} = \text{TP} / (\text{TP} + \text{FP} + \text{FN})$ (segmentation metric)

Average Precision (AP) -- $\text{TP} / (\text{TP} + \text{FP})$
(classification metric)



Class Specific

Formula AP: 0.723

Formula IoU: 0.750

Figure AP: 0.734

Figure IoU: 0.768

Table AP: 0.888

Table IOU: 0.877

Next Steps: Improve Segmentation

- Multi-modal segmentation
 - Core insight: we are not utilizing the actual text information in the document we're processing
 - IE: If a body text contains the word abstract, it's the abstract
 - Proposed solution:
 - When a region is proposed in the region proposal network, run OCR on the region and pass the text results to the next layer
- Better attention mechanism for document classification
 - Core insight: tradition segmentation is done in a rich pixel environment -- the background corresponds simply to non labelled objects (think a self driving car on the road)
 - Background in a document corresponds to null space. Partitioning null space is a challenge because there are many possible ways to validly partition it
 - Proposed solution:
 - Compensate for a lack of internal ROI info by providing additional context to an ROI
 - Attend to areas directly surrounding the ROI, then feed that output to the head.

Next Steps: OCR within individual segments

Name	Prior assumptions (mean and range ^a)	Posterior mean ^b	Description
$u_0^{\text{PO}_4}$	$1.65 \mu\text{mol kg}^{-1} \text{ yr}^{-1}$ (0.3–3.0)	$1.91 \mu\text{mol kg}^{-1} \text{ yr}^{-1}$	maximum PO ₄ uptake (removal) rate (Eq. 3)
K^{PO_4}	$0.2 \mu\text{mol kg}^{-1}$ (0.1–0.3)	$0.21 \mu\text{mol kg}^{-1}$	PO ₄ Michaelis-Menton half-saturation concentration (Eq. 3)
r^{POC}	0.05 (0.02–0.08)	0.055	initial proportion of POC export as fraction #2 (Eq. 6)
l^{POC}	600 m (200–1000)	556 m	<i>e</i> -folding remineralization depth of POC fraction #1 (Eq. 6)
$r_0^{\text{CaCO}_3:\text{POC}}$	0.036 (0.015–0.088) ^c	0.022 ^d	CaCO ₃ :POC: export rain ratio scalar (Eq. 8)
η	1.5 (1.0–2.0)	1.28	thermodynamic calcification rate power (Eq. 9)
r^{CaCO_3}	0.4 (0.2–0.6)	0.489	initial proportion of CaCO ₃ export as fraction #2 (Eq. 11)
l^{CaCO_3}	600 m (200–1000)	1055	<i>e</i> -folding remineralization depth of CaCO ₃ fraction #1 (Eq. 11)

Extract text modality to construct Fonduers data model

From Raw Documents to Fonduer's data model

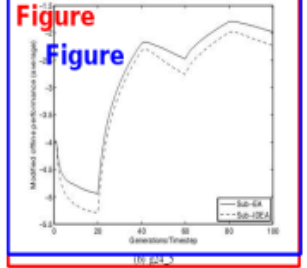
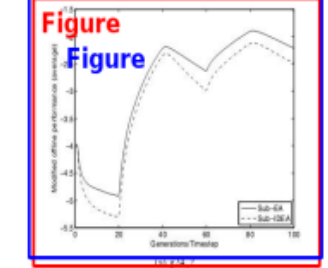
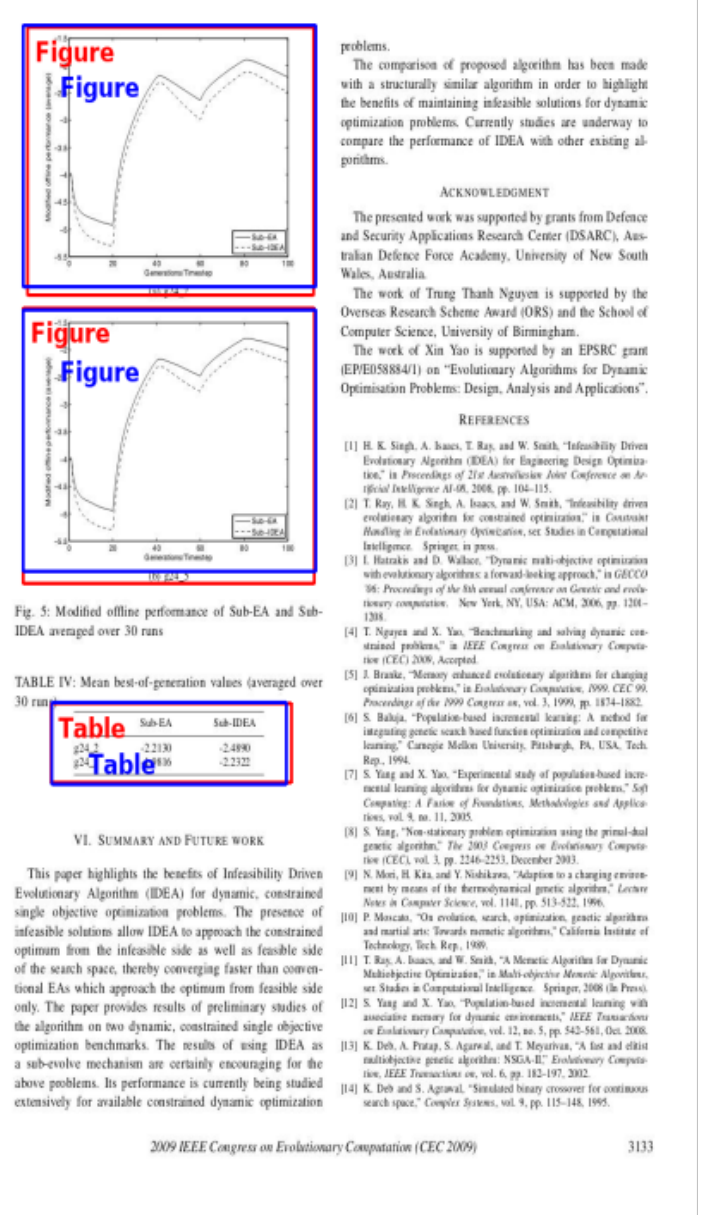


Fig. 5: Modified affine performance of Sub-IDEA and Sub-DEA averaged over 30 runs

Table	Sub-IDEA	Sub-DEA
g2	2.210	2.480

Fig. 5: Modified affine performance of Sub-IDEA and Sub-DEA averaged over 30 runs

Table	Sub-IDEA	Sub-DEA
g3	2.50	2.522

Fig. 5: Modified affine performance of Sub-IDEA and Sub-DEA averaged over 30 runs

VI. SUMMARY AND FUTURE WORK

This paper highlights the benefits of Infeasibility Driven Evolutionary Algorithm (IDEA) for dynamic, constrained single objective optimization problems. The presence of infeasible solutions allow IDEA to approach the constrained optimum from the infeasible side as well as feasible side of the search space, thereby converging faster than conventional EAs which approach the optimum from feasible side only. The paper provides results of preliminary studies of the algorithm on some standard constrained single objective optimization benchmarks. The results of using IDEA as a sub-evolve mechanism are certainly encouraging for the above problems. Its performance is currently being studied extensively for available constrained dynamic optimization problems.

2009 IEEE Congress on Evolutionary Computation (CEC 2009)

3133

Name	Prior assumptions (mean and range ^a)	Posterior mean ^b	Description
$u_0^{\text{PO}_4}$	$1.65 \mu\text{mol kg}^{-1} \text{yr}^{-1}$ (0.3–3.0) yr^{-1}	$1.91 \mu\text{mol kg}^{-1}$	maximum PO ₄ uptake (removal) rate (Eq. 3)
K_{PO_4}	$0.2 \mu\text{mol kg}^{-1}$ (0.1–0.3)	$0.21 \mu\text{mol kg}^{-1}$	PO ₄ Michaelis-Menton half-saturation concentration (Eq. 3)
r^{POC}	0.05 (0.02–0.08)	0.055	initial proportion of POC export as fraction #2 (Eq. 6)
l^{POC}	600 m (200–1000)	556 m	e -folding remineralization depth of POC fraction #1 (Eq. 6)
$r_0^{\text{CaCO}_3:\text{POC}}$	0.036 (0.015–0.088) ^c	0.022 ^d	CaCO ₃ :POC: export rain ratio scalar (Eq. 8)
η	1.5 (1.0–2.0)	1.28	thermodynamic calcification rate power (Eq. 9)
r^{CaCO_3}	0.4 (0.2–0.6)	0.489	initial proportion of CaCO ₃ export as fraction #2 (Eq. 11)
l^{CaCO_3}	600 m (200–1000)	1055	e -folding remineralization depth of CaCO ₃ fraction #1 (Eq. 11)

Name	Prior assumptions (mean and range ^a)	Posterior mean ^b	Description
$u_0^{\text{PO}_4}$	$1.65 \mu\text{mol kg}^{-1} \text{yr}^{-1}$ (0.3–3.0) yr^{-1}	$1.91 \mu\text{mol kg}^{-1}$	maximum PO ₄ uptake (removal) rate (Eq. 3)
K_{PO_4}	$0.2 \mu\text{mol kg}^{-1}$ (0.1–0.3)	$0.21 \mu\text{mol kg}^{-1}$	PO ₄ Michaelis-Menton half-saturation concentration (Eq. 3)
r^{POC}	0.05 (0.02–0.08)	0.055	initial proportion of POC export as fraction #2 (Eq. 6)
l^{POC}	600 m (200–1000)	556 m	e -folding remineralization depth of POC fraction #1 (Eq. 6)
$r_0^{\text{CaCO}_3:\text{POC}}$	0.036 (0.015–0.088) ^c	0.022 ^d	CaCO ₃ :POC: export rain ratio scalar (Eq. 8)
η	1.5 (1.0–2.0)	1.28	thermodynamic calcification rate power (Eq. 9)
r^{CaCO_3}	0.4 (0.2–0.6)	0.489	initial proportion of CaCO ₃ export as fraction #2 (Eq. 11)
l^{CaCO_3}	600 m (200–1000)	1055	e -folding remineralization depth of CaCO ₃ fraction #1 (Eq. 11)

Name	Prior assumptions (mean and range ^a)	Posterior mean ^b	Description
$u_0^{\text{PO}_4}$	$1.65 \mu\text{mol kg}^{-1} \text{yr}^{-1}$ (0.3–3.0) yr^{-1}	$1.91 \mu\text{mol kg}^{-1}$	maximum PO ₄ uptake (removal) rate (Eq. 3)
K_{PO_4}	$0.2 \mu\text{mol kg}^{-1}$ (0.1–0.3)	$0.21 \mu\text{mol kg}^{-1}$	PO ₄ Michaelis-Menton half-saturation concentration (Eq. 3)
r^{POC}	0.05 (0.02–0.08)	0.055	initial proportion of POC export as fraction #2 (Eq. 6)
l^{POC}	600 m (200–1000)	556 m	e -folding remineralization depth of POC fraction #1 (Eq. 6)
$r_0^{\text{CaCO}_3:\text{POC}}$	0.036 (0.015–0.088) ^c	0.022 ^d	CaCO ₃ :POC: export rain ratio scalar (Eq. 8)
η	1.5 (1.0–2.0)	1.28	thermodynamic calcification rate power (Eq. 9)
r^{CaCO_3}	0.4 (0.2–0.6)	0.489	initial proportion of CaCO ₃ export as fraction #2 (Eq. 11)
l^{CaCO_3}	600 m (200–1000)	1055	e -folding remineralization depth of CaCO ₃ fraction #1 (Eq. 11)

Name	Prior assumptions (mean and range ^a)	Posterior mean ^b	Description
$u_0^{\text{PO}_4}$	$1.65 \mu\text{mol kg}^{-1} \text{yr}^{-1}$ (0.3–3.0) yr^{-1}	$1.91 \mu\text{mol kg}^{-1}$	maximum PO ₄ uptake (removal) rate (Eq. 3)
K_{PO_4}	$0.2 \mu\text{mol kg}^{-1}$ (0.1–0.3)	$0.21 \mu\text{mol kg}^{-1}$	PO ₄ Michaelis-Menton half-saturation concentration (Eq. 3)
r^{POC}	0.05 (0.02–0.08)	0.055	initial proportion of POC export as fraction #2 (Eq. 6)
l^{POC}	600 m (200–1000)	556 m	e -folding remineralization depth of POC fraction #1 (Eq. 6)
$r_0^{\text{CaCO}_3:\text{POC}}$	0.036 (0.015–0.088) ^c	0.022 ^d	CaCO ₃ :POC: export rain ratio scalar (Eq. 8)
η	1.5 (1.0–2.0)	1.28	thermodynamic calcification rate power (Eq. 9)
r^{CaCO_3}	0.4 (0.2–0.6)	0.489	initial proportion of CaCO ₃ export as fraction #2 (Eq. 11)
l^{CaCO_3}	600 m (200–1000)	1055	e -folding remineralization depth of CaCO ₃ fraction #1 (Eq. 11)

Name	Prior assumptions (mean and range ^a)	Posterior mean ^b	Description
$u_0^{\text{PO}_4}$	$1.65 \mu\text{mol kg}^{-1} \text{yr}^{-1}$ (0.3–3.0) yr^{-1}	$1.91 \mu\text{mol kg}^{-1}$	maximum PO ₄ uptake (removal) rate (Eq. 3)
K_{PO_4}	$0.2 \mu\text{mol kg}^{-1}$ (0.1–0.3)	$0.21 \mu\text{mol kg}^{-1}$	PO ₄ Michaelis-Menton half-saturation concentration (Eq. 3)
r^{POC}	0.05 (0.02–0.08)	0.055	initial proportion of POC export as fraction #2 (Eq. 6)
l^{POC}	600 m (200–1000)	556 m	e -folding remineralization depth of POC fraction #1 (Eq. 6)
$r_0^{\text{CaCO}_3:\text{POC}}$	0.036 (0.015–0.088) ^c	0.022 ^d	CaCO ₃ :POC: export rain ratio scalar (Eq. 8)
η	1.5 (1.0–2.0)	1.28	thermodynamic calcification rate power (Eq. 9)
r^{CaCO_3}	0.4 (0.2–0.6)	0.489	initial proportion of CaCO ₃ export as fraction #2 (Eq. 11)
l^{CaCO_3}	600 m (200–1000)	1055	e -folding remineralization depth of CaCO ₃ fraction #1 (Eq. 11)

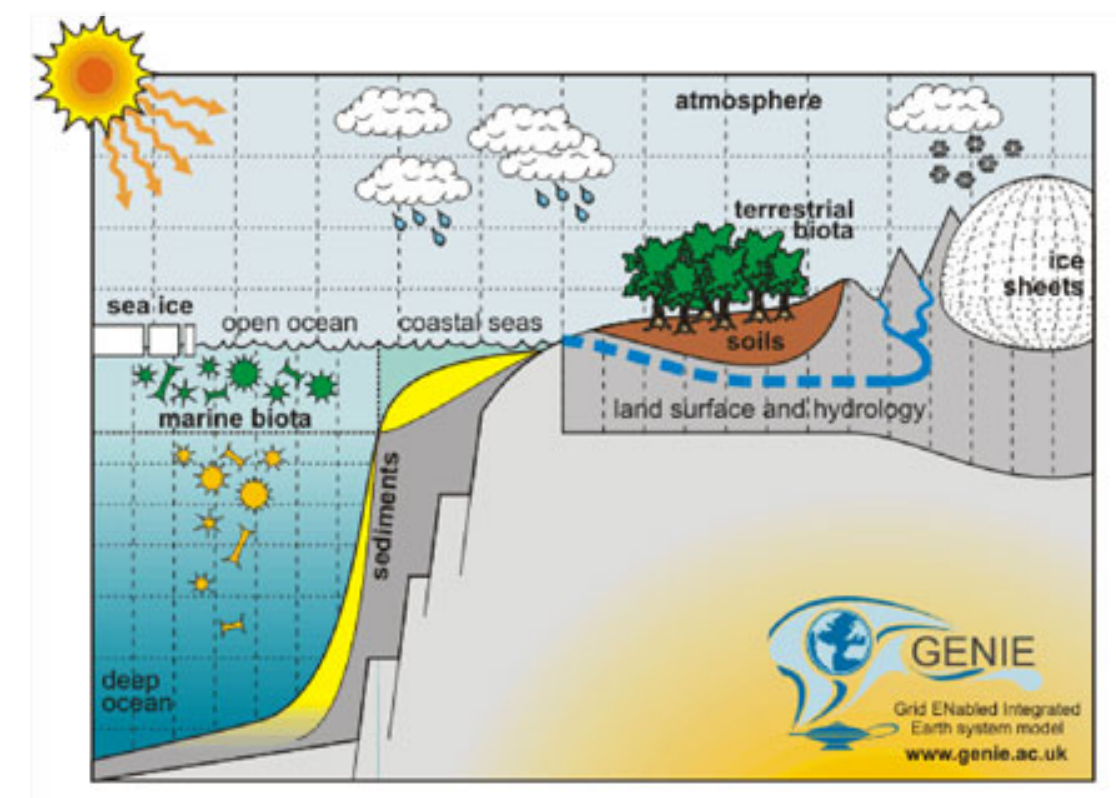
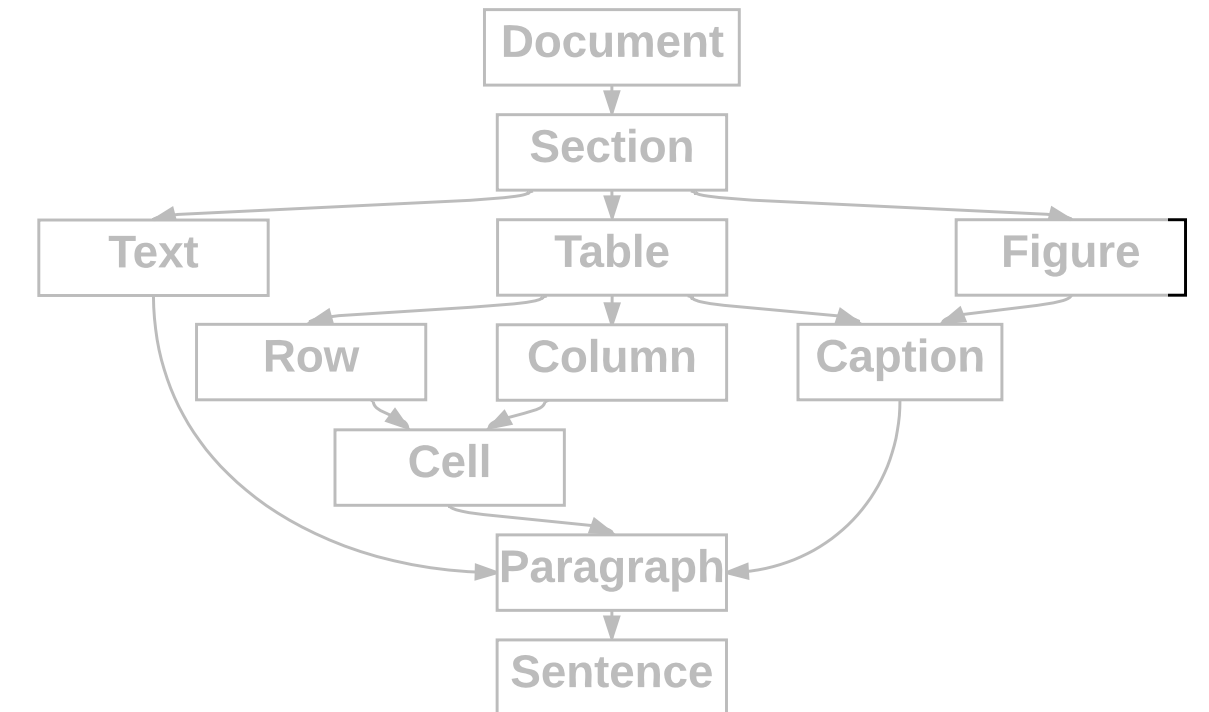
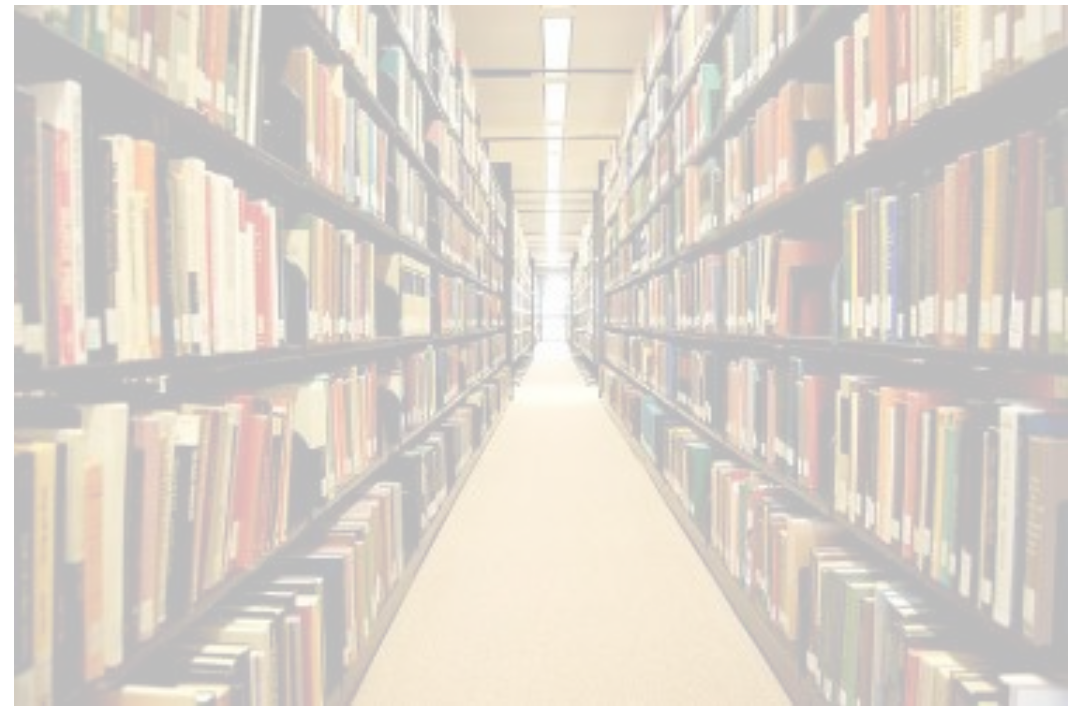
Name	Prior assumptions (mean and range ^a)	Posterior mean ^b	Description
$u_0^{\text{PO}_4}$	$1.65 \mu\text{mol kg}^{-1} \text{yr}^{-1}$ (0.3–3.0) yr^{-1}	$1.91 \mu\text{mol kg}^{-1}$	maximum PO ₄ uptake (removal) rate (Eq. 3)
K_{PO_4}	$0.2 \mu\text{mol kg}^{-1}$ (0.1–0.3)	$0.21 \mu\text{mol kg}^{-1}$	PO ₄ Michaelis-Menton half-saturation concentration (Eq. 3)
r^{POC}	0.05 (0.02–0.08)	0.055	initial proportion of POC export as fraction #2 (Eq. 6)
l^{POC}	600 m (200–1000)	556 m	e -folding remineralization depth of POC fraction #1 (Eq. 6)
$r_0^{\text{CaCO}_3:\text{POC}}$	0.036 (0.015–0.088) ^c	0.022 ^d	CaCO ₃ :POC: export rain ratio scalar (Eq. 8)
η	1.5 (1.0–2.0)	1.28	thermodynamic calcification rate power (Eq. 9)
r^{CaCO_3}	0.4 (0.2–0.6)	0.489	initial proportion of CaCO ₃ export as fraction #2 (Eq. 11)
l^{CaCO_3}	600 m (200–1000)	1055	e -folding remineralization depth of CaCO ₃ fraction #1 (Eq. 11)

Name	Prior assumptions (mean and range^a)	Posterior mean^b	Description

<tbl_r cells="4"

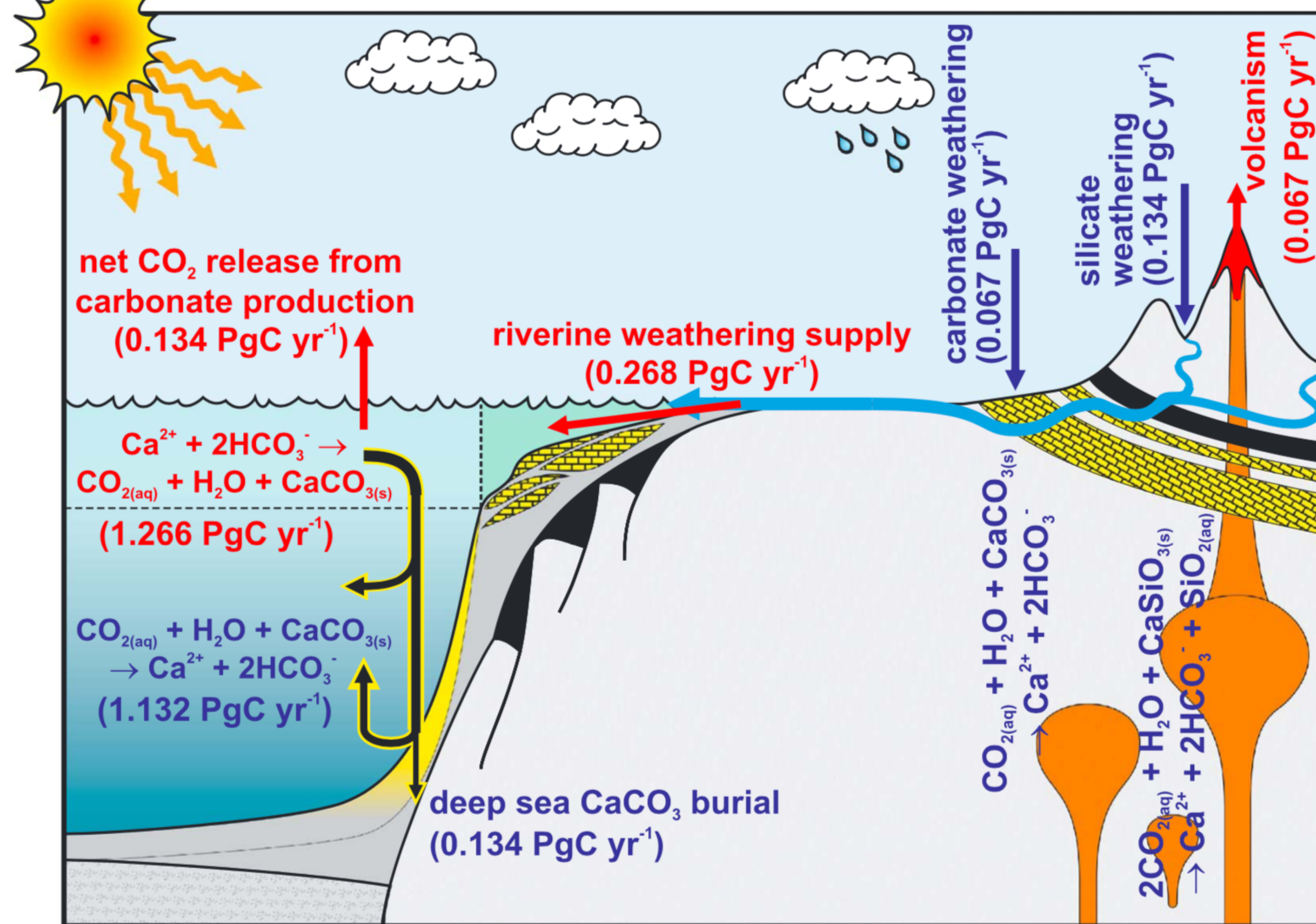
COSMOS: required components

1. Principled, automated access to scientific publications and the computing capacity and infrastructure required to repeatedly analyze them.
2. Models and techniques to represent and capture multi-modal data within publications.
3. Earth system model with parameterizations and predictions that overlap with many different types of empirical data and observations in publications.



GENIE:

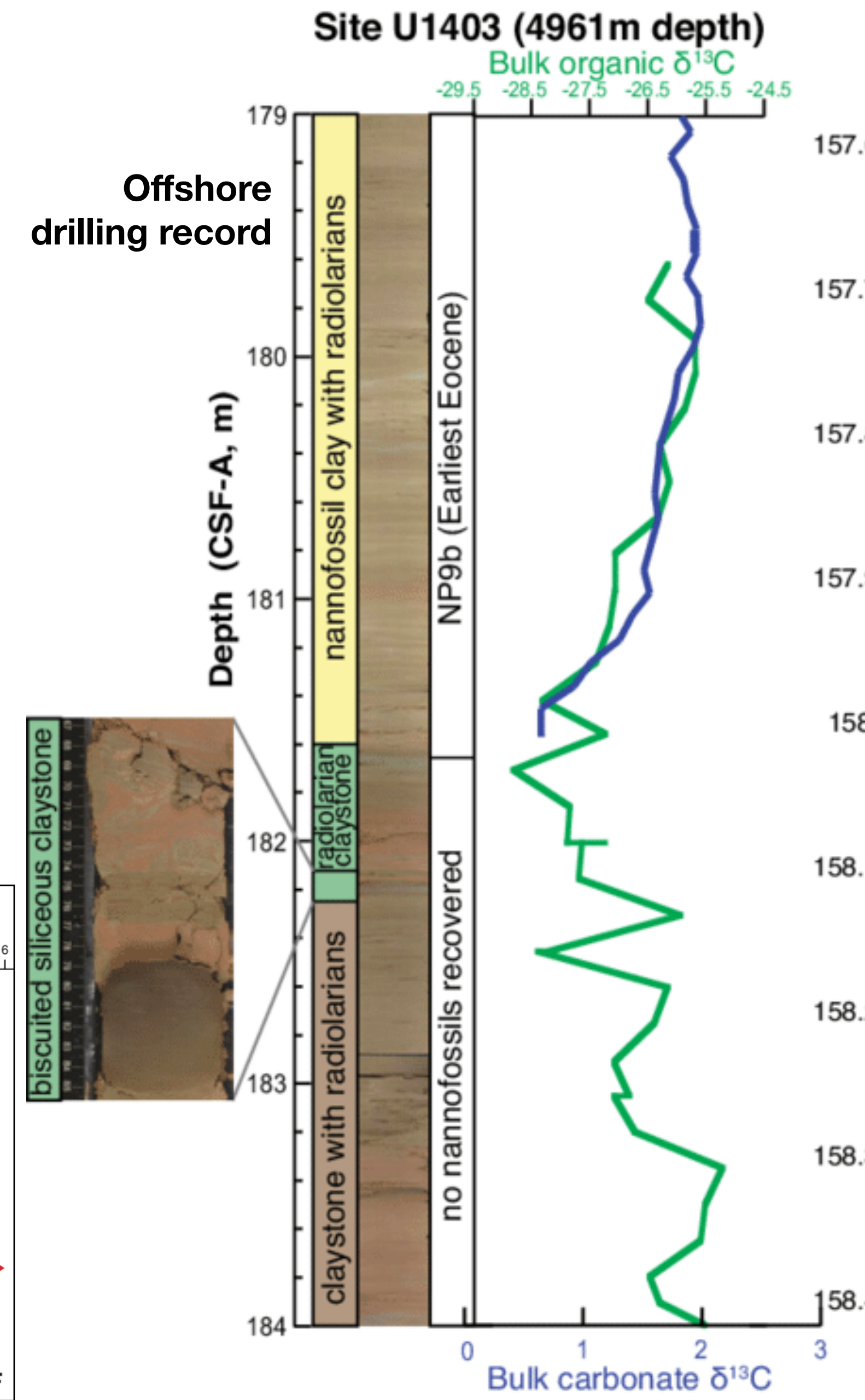
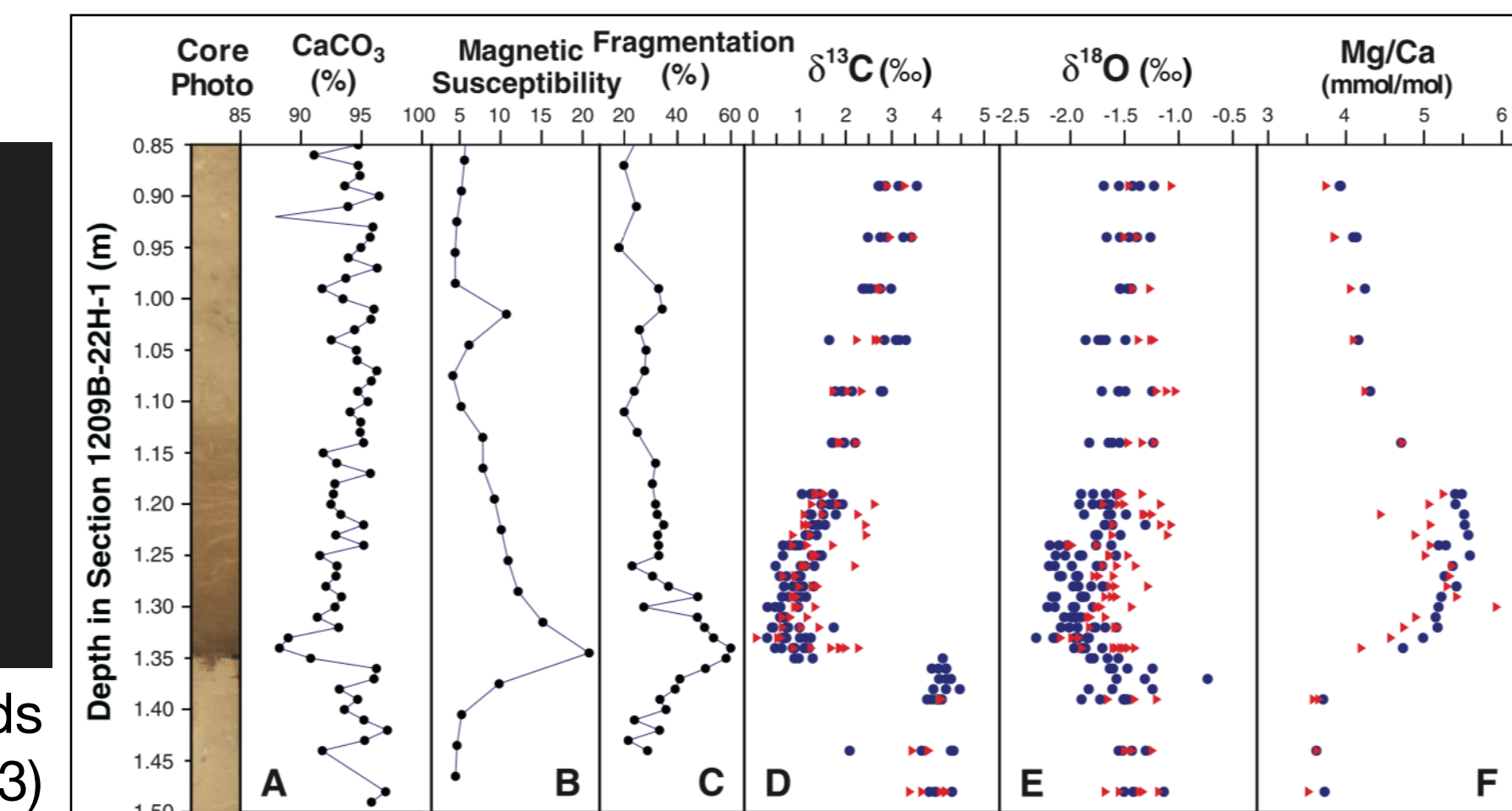
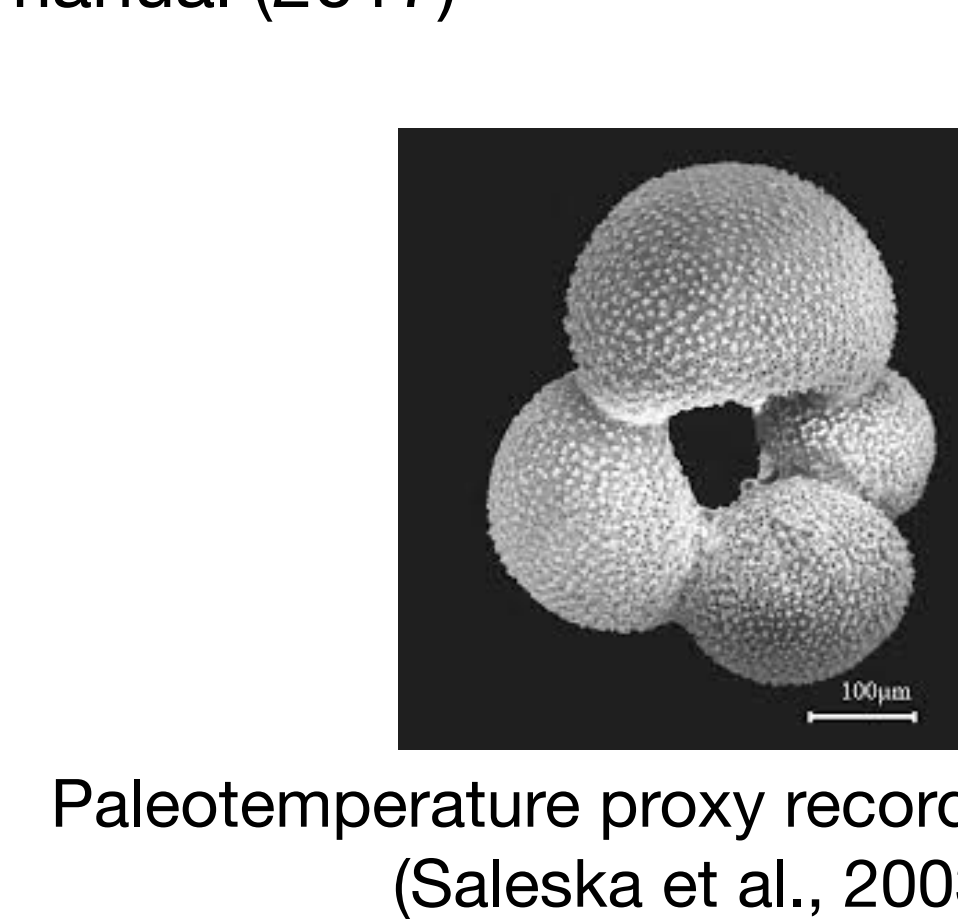
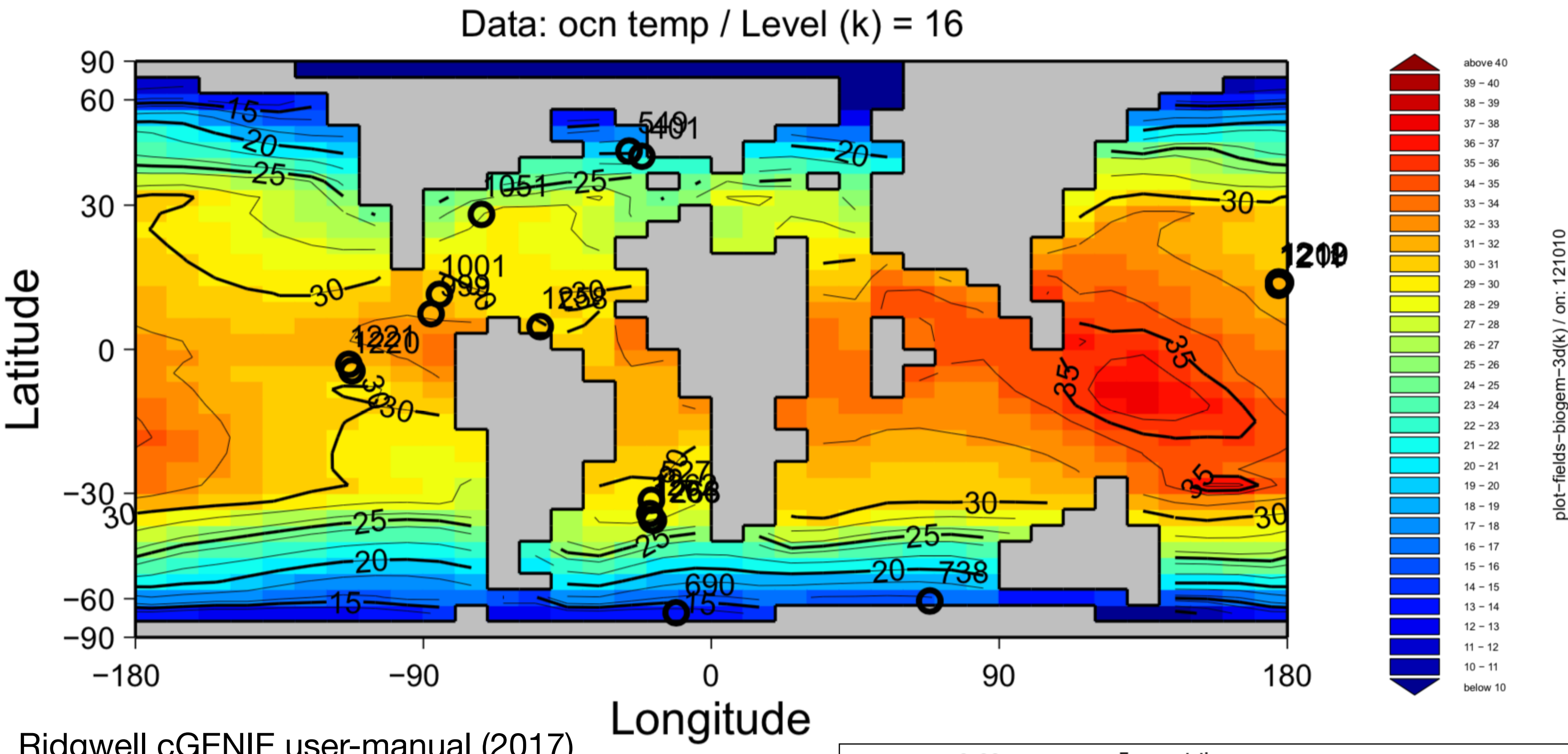
Grid ENabled Integrated Earth system model



- Earth system model of intermediate complexity
 - highly parameterized; processes operating over small spatial and temporal scales aggregated into high-level parameterizations
 - more processes can be modeled and integrated over longer periods of model time, but increased uncertainty
- Includes both first-principle physical and empirical components
- Makes numerous predictions that can be assessed with samples in field.

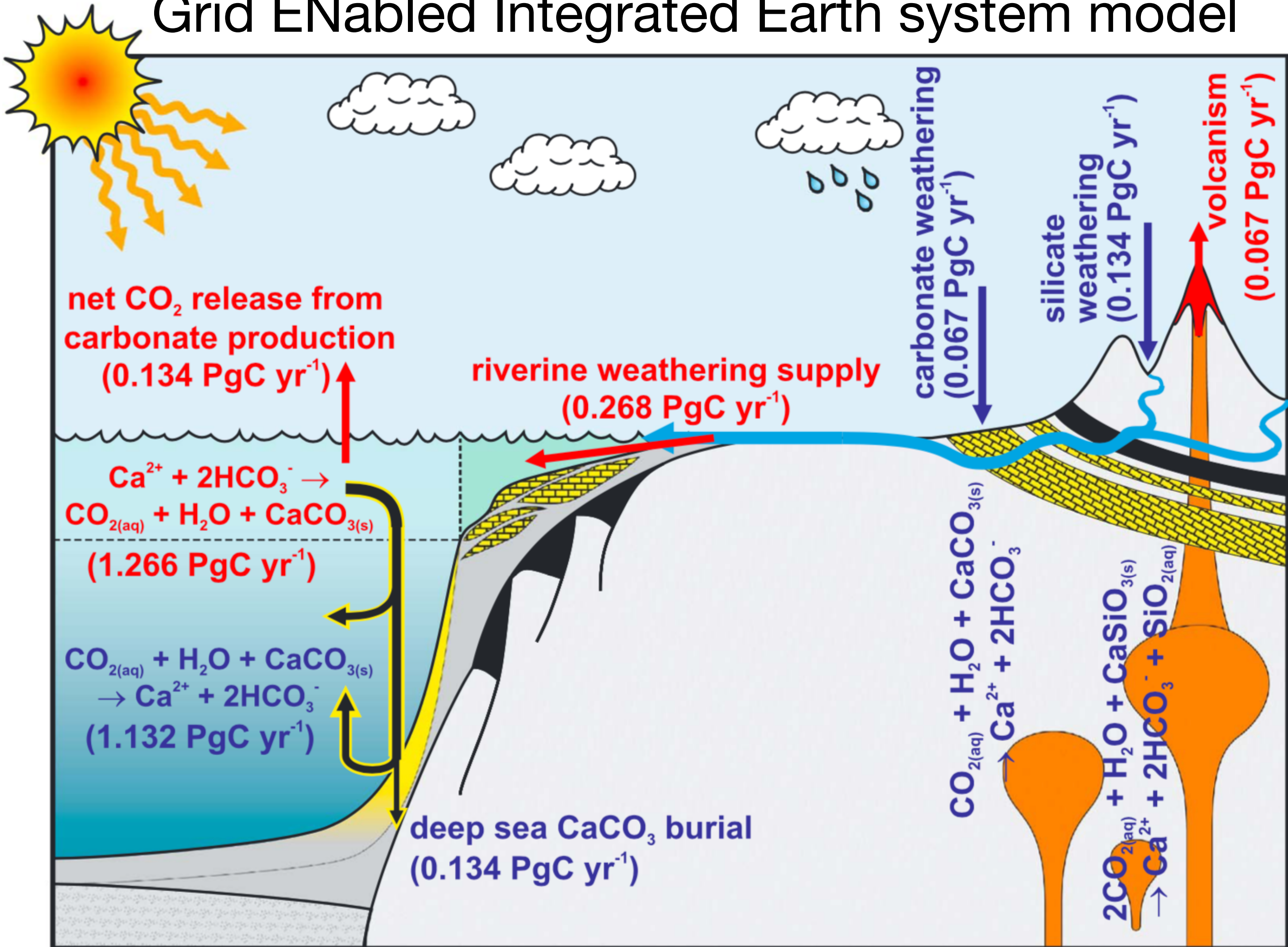
Figure 1. Illustration of the long-term (geological) carbon cycle fluxes. Shown are the long-term fluxes in the GENIE model at steady state. In red are sources of CO_2 to the atmosphere or ocean, and in dark blue are sinks of CO_2 .

Example: cGENIE-predicted sea surface temperature 60 Myr ago



GENIE:

Grid ENabled Integrated Earth system model

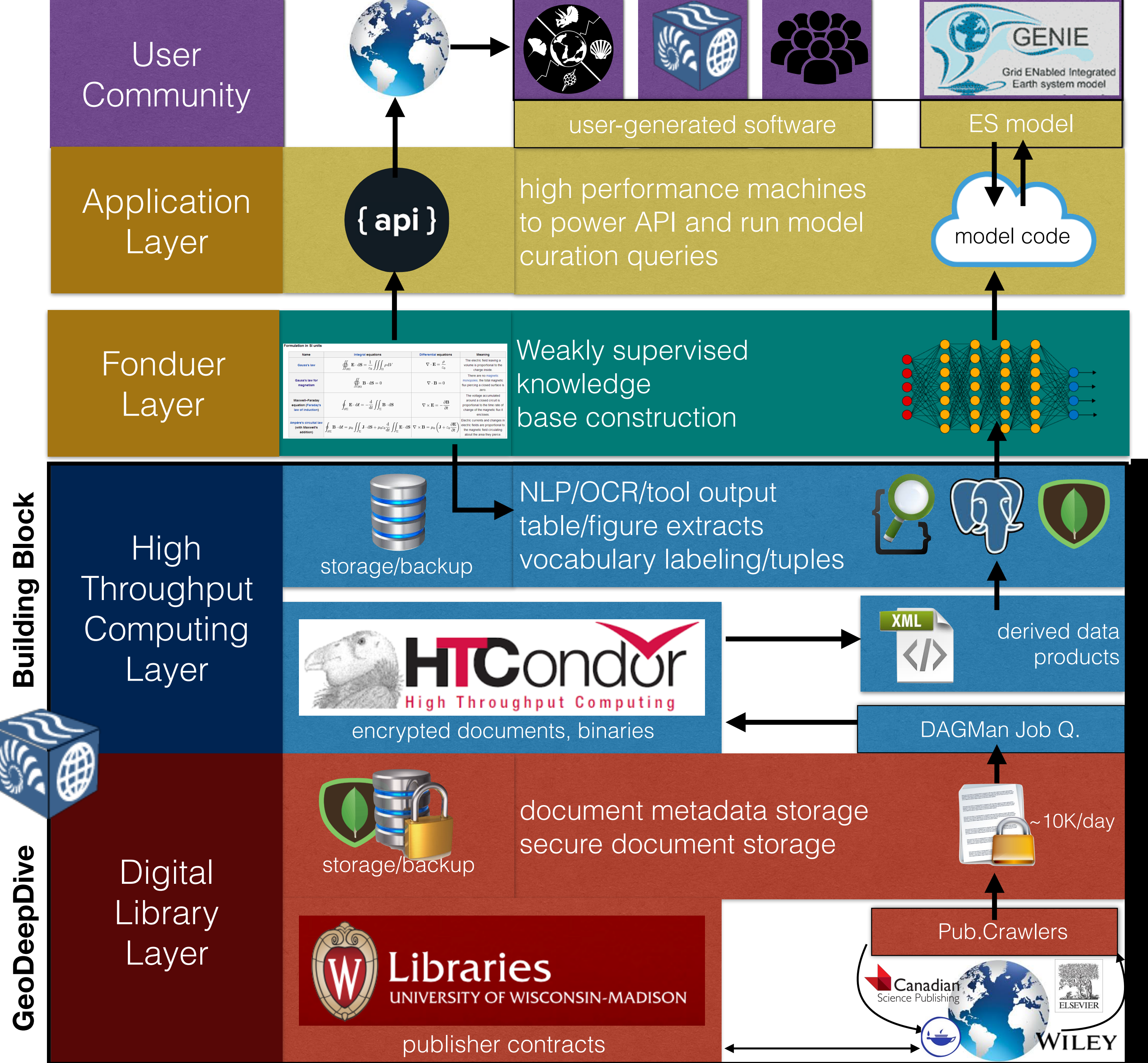


Phase II



Collaborator Seth Finnegan
UC Berkeley

Figure 1. Illustration of the long-term (geological) carbon cycle fluxes. Shown are the long-term fluxes in the GENIE model at steady state. In red are sources of CO_2 to the atmosphere or ocean, and in dark blue are sinks of CO_2 .



ASKE Layer COSMOS

GeoDeepDive Layer